A STUDY OF BIOMASS GASIFICATION SYSTEMS AND HYDROGEN PRODUCTION USING HIGH TEMPERATURE PROTON CONDUCTING CERAMIC MEMBRANE

By

ELANGO BALU

A DISSERTATION PRESENTED TO THE GRADUATE SCHOOL
OF THE UNIVERSITY OF FLORIDA IN PARTIAL FULFILLMENT
OF THE REQUIREMENTS FOR THE DEGREE OF
DOCTOR OF PHILOSOPHY

UNIVERSITY OF FLORIDA

2013

To my Dad

ACKNOWLEDGMENTS

First and foremost, I would like to thank my advisor Dr. Jacob Chung for giving me this opportunity to pursue a doctorate degree. It would not have been possible without his continued support during some of the difficult times i had in my life. So I would like to express my sincere gratitude to my advisor for helping me become not only a better graduate student but a better person overall.

I would also like to thank my committee members Dr. Bill Lear, Dr. Herbert A. Ingley and Dr. S. A. Sherif for their support and valuable inputs that helped me accomplish my goal. A special thanks to Dr. Zhaohui Tong for agreeing to be on my committee on a short notice.

I would like to thank all my friends, especially Dr. T. S. Lee, Dr. Akiko Hiramatsu, Dr. Matthew Camaratta, Uisung Lee, Harsh Khandelwal, Sadagopan Ramesh, Prasanna Venuvanalingam and Aneesh Koka for helping me breeze through my years in Gainesville without a dull moment. Also I would like to thank Dr. Byungwook Lee, Dr. Yoon and Dr. Jianlin Li of Dr. Eric Wachsman's research group for their much valued support during the course of my research.

Finally I would like to express my sincere gratitude to my late dad, who is still and will forever be my source of strength. And also would like to thank my mom and my brother for burdening all the responsibilities of the family on their shoulders and allowing me to concentrate on my research, though this would never do justice to what they all have to go through to support me.

I would also like to thank my funding agencies FESC and FISE.

TABLE OF CONTENTS

page

ACKNOWLEDGMENTS 4

LIST OF TABLES 7

LIST OF FIGURES 9

ABSTRACT 13

CHAPTER

1 INTRODUCTION 15

1.1 Potential of Biomass as a Solution for Future Energy Needs 15
1.2 Biomass Gasification 19
1.2.1 Thermodynamics of Gasification 20
1.2.1.1 Drying 20
1.2.1.2 Devolatisation 21
1.2.1.3 Gasification 21
1.2.1.4 Homogeneous gas phase reactions 22
1.2.2 Air Only Gasification of Biomass 22
1.2.3 Steam Only Gasification of Biomass 24
1.2.4 Integrated Biomass to Power Systems 25
1.3 Hydrogen Separation Membranes 27
1.3.1 Proton Conducting Materials 28
1.3.2 Proton Transport Mechanism 29
1.4 Research Objective 30

2 CONCEPTUAL SYSTEM 36

2.1 Introduction 36
2.2 Description of System Components 37
2.2.1 High-Temperature Gasification Unit 38
2.2.2 Membrane Reactor 38
2.2.3 Surplus Heat Recovery Unit 38
2.2.4 Fischer-Tropsch Catalytic Reactor 39
2.2.5 Hydrogen Combustor 39
2.3 System Characteristics and Efficiencies 40

3 EXPERIMENTAL AND NUMERICAL INVESIGATION OF PORTABLE (PILOT SCALE) PARTIAL OXIDATION/GASIFICATION SYSTEM 45

3.1 Introduction 45
3.2 Portable Gasifier Experimental Setup 45
3.3 Equilibrium Model for Gasification 48

3.4 Results and Discussions 53
3.4.1 Experimental 53
3.4.2 Theoretical Model 55

4 EXPERIMENTAL AND NUMERICAL INVESTIGATION OF HIGH TEMPERATURE STEAM ONLY (BENCH SCALE) GASIFICATION SYSTEM 76

4.1 Bench Scale Gasifier System Experimental Setup 76
4.2 Steam Only Gasification Model 78
4.3 Results and Discussions 80

5 MATERIAL SYNTHESIS AND FABRICATION OF NIO-SCZ82 SUPPORT TUBES AND SCZE721 THIN FILM MEMBRANES 108

5.1 Introduction 108
5.2 SCZ82 ($SrCe_{0.8}Zr_{0.2}O_{3-\delta}$) and SCZE721 ($SrCe_{0.7}Zr_{0.2}Eu_{0.1}O_{3-\delta}$) Powder Synthesis 108
5.3 Support Tube Fabrication 109

6 EXPERIMENTAL STUDY OF MEMBRANE REACTOR 120

6.1 Membrane Reactor Design 120
6.2 Experimental Setup of the Membrane Reactor 121
6.3 Results and Discussions 124

7 CONCLUSIONS 147

LIST OF REFERENCES 156

BIOGRAPHICAL SKETCH 161

LIST OF TABLES

Table		page
1-1	Product gas composition from typical woody biomass gasifiers [11]	33
1-2	Gasification chemical reactions considered dominant during gasifier operation [11]	33
1-3	Properties of different types of hydrogen separation membranes [36]	34
3-1	Experimental conditions and parameters for pilot scale system.	64
3-2	A, B, C, D, E, F, G, H for individual species @ T < 1000 °C from [50]	64
3-3	Average gasifier zone temperature (°C)	72
3-4	Comparison of equilibrium constants calculated @ 1273 K.	72
3-5	20% moisture, 1073 K, No heat added, wood waste, model results	72
3-6	10% moisture, 1073 K, No heat added, wood waste, model results.	73
3-7	Syngas estimated from current model @ 1173 K, No heat added.	74
3-8	Syngas composition from experiments and model comparison	75
3-9	Overall system efficiency	75
4-1	A, B, C, D, E, F, G, and H for individual species @ T > 1000 °C from [50]	87
4-2	Mole fractions from gas analysis run1	103
4-3	Mole fractions from gas analysis run2	104
4-4	Mole fractions from gas analysis run3	105
5-1	Powder proportions required	112
5-2	Support tube mixture	113
5-3	Thin Film membrane Mix	118
6-1	Permeated H_2 concentration vol% measured with mass spectrometer	141
7-1	Case1 with liquid fuel production only	154
7-2	Case2 with hydrogen production only	155

7-3 Effect of membrane reactor on overall system efficiency for both case 1 & 2 .. 155

LIST OF FIGURES

Figure		page
1-1	Prediction of future energy profiles adapted from literature	32
1-2	Proton conducting material matrix showing operating limits [44]	35
2-1	Schematic of concept system with alternate path lines	44
3-1	Schematic of the gasifier mounted on the pilot scale system	60
3-2	Portable pilot scale gasifier system components	60
3-3	Portable pilot scale system..	61
3-4	Load components..	62
3-5	Pictorial representation of K-type thermocouples inside the gasifier.	63
3-6	Temperature distribution inside the gasifier - pyrolysis zone	65
3-7	Temperature distribution inside the gasifier - combustion zone	66
3-8	Temperature distribution inside the gasifier - before throat	67
3-9	Temperature distribution inside the gasifier - after throat	68
3-10	Temperature distribution inside the gasifier - reduction zone	69
3-11	Temperature distributions inside the gasifier in all zones for horse manure	70
3-12	Average temperatures inside the gasifier in all zones for four feedstock	71
4-1	3D-Module stack that was tested and later replaced due to high thermal inertia	85
4-2	Initial bench scale system setup..	86
4-3	Modified bench scale gasifier schematic..	87
4-4	Syngas mole fractions predicted by equilibrium model for woody biomass at 1500°C steam inlet	88
4-5	Syngas mole fractions predicted by equilibrium model for woody biomass at 2000°C steam inlet	89
4-6	Syngas mole fractions predicted by equilibrium model for woody biomass at 2500°C steam inlet	90

4-7 Syngas mole fractions predicted by equilibrium model for woody biomass at 1500°C steam inlet, at lower STBM where solid carbon exists. 91

4-8 Number of moles of syngas produced per mole of feedstock $CH_{1.5}O_{0.67}$, predicted by equilibrium model @ 800°C steam inlet. 92

4-9 Number of moles of syngas produced per mole of feedstock $CH_{1.5}O_{0.67}$, predicted by equilibrium model @ 900°C steam inlet. 93

4-10 Number of moles of syngas produced per mole of feedstock $CH_{1.5}O_{0.67}$, predicted by equilibrium model @ 1000°C steam inlet. 94

4-11 Number of moles of syngas produced per mole of feedstock $CH_{1.5}O_{0.67}$, predicted by equilibrium model @ 800°C, 900°C and 1000°C steam inlet – comparison. 95

4-12 Syngas mole fractions predicted by equilibrium model at 800°C steam inlet for feedstock $CH_{1.5}O_{0.67}$. 96

4-13 Syngas mole fractions predicted by equilibrium model at 900°C steam inlet for feedstock $CH_{1.5}O_{0.67}$. 97

4-14 Syngas mole fractions predicted by equilibrium model at 1000°C steam inlet for feedstock $CH_{1.5}O_{0.67}$. 98

4-15 Syngas mole fractions predicted by equilibrium model at 800°C, 900°C and 1000°C steam inlet comparison 99

4-16 Surface plot of hydrogen mole fractions at varying STBM and steam temperatures from equilibrium model for feedstock $CH_{1.5}O_{0.67}$. 100

4-17 Surface plot of carbon monoxide mole fractions at varying STBM and steam temperatures from equilibrium model for feedstock $CH_{1.5}O_{0.67}$. 101

4-18 Surface plot of methane mole fractions at varying STBM and steam temperatures from equilibrium model for feedstock $CH_{1.5}O_{0.67}$. 102

4-19 Mole fractions calculated from GC analysis, experimental 877°C steam run1 . 103

4-20 Mole fractions calculated from GC analysis, experimental 877°C steam run2 . 104

4-21 Mole fractions calculated from GC analysis, experimental 1000°C steam run3. 105

4-22 Mole fractions predicted by equilibrium model at lower STBM coincides well with the experimental data in the range of 4 to 6. 106

5-1 XRD (X-ray diffraction) peaks for support tube SCZ81 powder prepared after calcination. 113

5-2 Vacuum pot.to bubble out air in tape slurry. 114

5-3 Tape caster.at FISE lab used to fabricate support tube base.. 115

5-4 Finished support tape after tape casting..... 116

5-5 Doctor blade used for adjusting tape thickness.. 117

5-6 Schematic of tape rolling process developed by FISE [59]..... 118

5-7 SEM of sintered tubes. 119

6-1 3-D rendering of quartz reactor..... 130

6-2 Membrane tube enclosed in reactor.. 130

6-3 Schematic of reactor setup during operation 131

6-4 Overall system layout. 132

6-5 Reactor placed inside the furnace.. 133

6-6 Tube placement inside the reactor relative to heating coils with no insulation around interface..... 134

6-7 Membrane tubes Tested..... 135

6-8 Membrane tube exposed to WGS conditons. 135

6-9 SEM Images of Tested Tubes 136

6-10 Setup with new bubbler with heating cartridge and temperature controller 137

6-11 Modified bubbler design with heater cartridge down the middle and insulation jacket 138

6-12 Sintered tubes tested for leaks and pinholes before being used for experiments 139

6-13 Tested tubes with no clear breakage at interface after using insulation inside . 140

6-14 Tested tube with heavy carbon deposit at cold zone out of the heating coils after exposure to WGS atmosphere 141

6-15 Conversion ratio calculated based on experimental data measured and Antoine equation..... 142

6-16 Experimental hydrogen concentration measured in comparison with different permeation factors at 100% WGS conversion. 143

6-17 Experimental hydrogen concentration measured in comparison with different permeation factors at 80% WGS conversion. 144

6-18 Experimental hydrogen concentration measured in comparison with different permeation factors at 60% WGS conversion. 145

6-19 Experimental hydrogen concentration measured in comparison with different permeation factors at 40% WGS conversion. 146

7-1 Schematic of a concept system with alternate path lines 153

7-2 Effect of membrane reactor on overall system efficiency. 154

Abstract of Dissertation Presented to the Graduate School
of the University of Florida in Partial Fulfillment of the
Requirements for the Degree of Doctor of Philosophy

A STUDY OF BIOMASS GASIFICATION SYSTEMS AND HYDROGEN PRODUCTION USING HIGH TEMPERATURE PROTON CONDUCTING CERAMIC MEMBRANE

By

Elango Balu

May 2013

Chair: Jacob Chung
Major: Mechanical Engineering

The need for sustainable alternatives to oil has been of deep concern to many countries around the world, and especially the U.S. due to the rapidly rising cost of oil. As a result, many nations face significant energy security challenges stemming from their dependence on imported oil. To achieve future energy security and independence and in the long run to prepare for the post-oil energy resources, biomass is considered as one of the most important renewable energy resources in a projected sustainable energy future. The key bottleneck for lignocellulosic-derived biofuels is the lack of technology for efficient conversion of biomass in to readily usable fuel products. Current work provides a detailed theoretical and experimental analysis of two (air and steam only) gasification technologies which are carbon neutral that can be used to overcome this hurdle.

This work also examines the use of mixed ion-electron conductors (MIEC) membranes as a significant option to enhance the production of H_2 from biomass feedstock. Currently there are technologies that produce H_2 by using renewable energy sources other than biomass as feedstock but they could not provide a long term solution because of their adverse effects on eco-system. Thin film $SrCe_{0.7}Zr_{0.2}Eu_{0.1}\ O_{3-\delta}$

membranes were developed and supported using NiO-$SrCe_{0.8}$ $Zr_{0.2}$ $O_{3-\delta}$ tubular structure, using Dr. Eric Wachsman's group's work at UF. The main advantage of this membrane setup is that it acts as WGS reactor and also separates the H_2 from the gas stream, thus avoiding the need for two stage reactor setup requiring WGS and H_2 separation independently. The possibility of sequestering the isolated CO_2 stream is also another attribute to such membrane reactors.

The overall objective of this current work is to analyze the air gasification and steam only gasification technology in detail and to investigate the performance of proton conducting ceramic membranes at high temperatures. Current research also analyzed a simplistic model of a concept system, which is a self-sustaining H_2 fuel production system that integrates the gasification technology and the MIEC membrane technology. The proposed system enhances the H_2 produced from the biomass feed stock by carrying out WGS.

CHAPTER 1
INTRODUCTION

1.1 Potential of Biomass as a Solution for Future Energy Needs

U.S. NSF-DOE Workshop report [1] concluded that liquid biofuels produced from lignocellulosic biomass can significantly reduce our dependence on oil, create new jobs, improve rural economics, reduce greenhouse emissions, and ensure energy security. Furthermore, the report emphasized that the key bottleneck for lignocellulosic biomass-derived fuels is the lack of technology for the efficient conversion of biomass into liquid fuels. As a result, new technologies are needed to replace fossil fuels with renewable and sustainable energy resources.

Reliable estimates of renewable and sustainable lignocellulosic forest and agricultural biomass and municipal solid waste (mostly biomass) tonnage in the U.S. range from 1.5 to 2 billion dry tons per year [1] so that these biomass resources could contribute ten times more to our primary energy supply (PES) than they currently do. Another forecast [1] reported that all forms of biomass and municipal solid waste have the potential to supply up to 60% of the total U.S. energy needs.

Lignocellulosic biomass is the fibrous, woody, and generally inedible portion of the plants that are mostly composed of cellulose, hemicellulose and lignin. So, lignocellulosic biomass is non-food based and does not compete with the food crops that are basically cellulosic biomass. Woody biomass in general consists of cellulose, hemicellulose and lignin and hence it is collectively known as lignocellulosic biomass. Cellulose is the most prominent of the 3 components followed by hemicellulose and lignin. Lignin plays the role of the binder in the wood structure and it connects the other two components and holds them together. The ultimate analysis of such feedstock show

that the typical elemental composition consists of C, H, O and some cases there might be traces of sulphur and chlorine is one such element present in horse manure. Researchers have documented the elemental composition and even the lignocellulosic distribution for various woody biomass feedstocks. Several advantages and disadvantages of using woody biomass for such energy generation processes have also been discussed .Most biomass materials are widely available in many parts of the world. As it is abundant, environmentally friendly and renewable, the potential of using biomass to help meet the world energy demand has been widely recognized. Thermochemical gasification is likely to be the most cost effective conversion process. Biomass gasification is one of the highly effective technologies for thermo chemical conversion. Therefore, biomass is considered as one of the most promising energy sources as they do not have a negative impact of food sources.

Studies show that biomass energy has the potential to be ‘‘modernized’’ worldwide [2], that means it can be produced and used efficiently and cost competitively, generally in the more convenient forms of gases, liquids, or electricity. Biomass will play an important role in the future global energy infrastructure for the generation of power and heat, but also for the production of chemicals and fuels. Thermodynamic study [3] found that the hydrogen fuel can be produced from woody biomass gasification coupled with steam-methane reforming and water gas shift reaction in a large-scale industrial plant with an efficiency of 62% that is comparable with those of the existing other process technologies. They also reported that an overall efficiency of 44% can be obtained for power production through a gas-steam combined cycle using woody biomass gasification as the energy source. The U.S. Natural

Resources Defense Council has projected an aggressive plan to make lignocellulosic biofuels. U.S. could produce 7.9 million barrels of oil per day by 2050 or more than 50% of current total oil use in the transportation sector [4].The synthetic biofuels produced by the Fischer-Tropsch process from lignocellulosic materials contain no sulphur, no particulates, no aromatics, and no nitrous compounds, thus making them very clean burning and reducing the production of acid rain. Because it has exactly the same chemical properties as fossil based diesel, it can be blended with regular diesel, stored and distributed using the same infrastructure. Although chemically identical to fossil diesel, it has a higher cetane number and on a gallon basis it contains 22% more energy. In general, the synthetic lignocellulosic diesel has up to 80% less combustion emissions compared to petroleum diesel that include carbon dioxide, carbon monoxide, particulate matter, sulphur oxides, and hydrocarbons [5]. Furthermore, these green biofuels are renewable, carbon-neutral and sustainable.

Therefore, a very promising route to liquid fuels, in particular the synthetic lignocellulosic diesel, is the woody biomass gasification to synthesis gas (syngas: CO + H_2) followed by the Fischer-Tropsch process to convert the syngas to hydrocarbon products. Fischer-Tropsch technology can be briefly defined as the means used to convert synthesis gas containing hydrogen and carbon monoxide to liquid hydrocarbon products [6, 7].

A long-term hydrogen-based economy modeled both qualitatively and quantitatively predicts that the global energy picture would progressively move towards a more sustainable and low emission free system using renewable sources [8]. The model also further predicts the huge positive environmental impact such type of an

economy would have and also sheds light on a very important fact that it is a combination of emerging technologies that will help us achieve this goal rather than one single solution.

Currently there is a lot of interest in a hydrogen economy because of the numerous positives it has to offer. It is not a very easy goal to achieve due to the many technical barriers that has to be overcome, to realize such a fully functional economy. Two technologies very promising for such a transition are the gasification technology and the membrane separation technology.

Figure 1-1 shows the energy profile in the future which tends to a more zero-carbon state because of the infusion of newer clean technologies. Lignocellulosic biomass is the fibrous, woody, and generally inedible portion of the plants that are mostly composed of cellulose, hemicellulose and lignin. So, lignocellulosic biomass is non-food based and does not compete with the food crops that are basically cellulosic biomass. Most biomass materials are widely available in many parts of the world. As it is abundant, environmentally friendly and renewable, the potential of biomass to meet the world energy demand has been widely recognized. Thermochemical gasification is likely to be the most cost effective conversion process. Biomass gasification is one of the highly effective technologies for thermo chemical conversion. Gas separation membrane reactors can help increase the efficiency of producing Hydrogen from renewable sources like steam reformation of natural gas which is the single most popular method of hydrogen production right now, where high temperature steam is used to retrieve hydrogen from methane. But the production of hydrogen from conventional methods like steam reformation of natural gas is cost intensive and so it

could not be viewed as a long term solution [9, 10].Further when the membranes are used alongside other technologies like gasification can also be successfully implemented to sequester the CO_2 produced during the process thus resulting in carbon-neutral systems and lowering the greenhouse gas emissions.

1.2 Biomass Gasification

The thermo chemical conversion of H-C fuel like biomass or coal is a method to produce syngas by partial oxidation of the input feedstock. The main reason for successful gasification applications are because of the fact that it converts the low grade fuel in to gaseous mixture called syngas which is rich in H_2 and CO, also contains H_2O, CH_4, CO_2 and other higher order hydrocarbons. This syngas can be used for a number of applications and processes as fuel that would not be possible with its original form as a raw biomass feedstock. Moreover, since the gasification process is more like a self-regulated cycle, once the initial heat source is provided to start up the reactions and it could go on for a considerable period of time with constant addition of biomass without replacing the heat source. The heating value of syngas produced from normal air gasification is usually in the range of 4-6 MJ/Nm3 and it varies from 12-15 MJ/Nm3 in case of steam only gasification. Table 1-1 gives the typical dry syngas composition obtained from Air only and Steam gasification of biomass.

The low heating value of the syngas in air gasification is usually associated with the moisture content in the biomass which lowers the reaction temperature and also the N_2 that is being supplied along with the oxidizing agent in controlled conditions. This also reduces the temperature of the combustion zone considerably and lowers the range in which gasification reactions occur by diluting the hot zones. This can be drastically improved by using steam only as a gasifying agent thus eliminating the N_2

that dilutes the reaction temperature and it results in almost two-times-higher heating values compared to conventional types. The gasifiers that do not require external heat supply during the course of operation are called auto-thermal and those that require external heat for their continual operation, like the bench scale steam gasifier unit used in this work are named allothermal [12].

1.2.1 Thermodynamics of Gasification

Gasification process involves a lot of complex chemical reactions taking place at the core but over the period of time, these reactions have been studied extensively and the no of reactions that has the major impact on the gasification process has been reduced. The reactions governing the gasification process can be categorized in to different groups as shown below. The presence of gas species like methane, carbon monoxide and especially hydrogen in the product gas composition along with the current technologies, the modern gasifiers are capable of converting almost up to 90 % of the heating value of the feedstock in to synthetic gas [13].

The core of the gasification process can be explained by a series of chain steps namely drying, devolatisation, gasification and homogeneous gas phase reactions. The main reactions in these steps are listed in Table 1-2.

1.2.1.1 Drying

Biomass feedstock inherently contains moisture accumulated over the growth period and the first step of the process is to drive off the moisture in the feedstock by using the heat that is supplied by the combustion reactions that take place in the gasifier. These combustion reactions provide the thermal energy required for other endothermic gasification reactions as well. The heating content of the syngas increases if the feedstock moisture content decreases, meaning there is less energy utilized in

drying the feedstock. So drying of the feedstock before the gasification process is a crucial step in controlling the quality of the syngas.

1.2.1.2 Devolatisation

This process is governed by volatile components produced from the biomass feedstock and low temperature endothermic reactions which are prominent in the temperature range of 300 to 500 ° C.When the process temperature goes to 800 ° C, products formed include Char, hydrogen, carbon monoxide, methane, steam and tar components [14].The gas species formed further interact with other gases as well. The carbon in the char is used for the gasification step.

1.2.1.3 Gasification

The gasification reactions are several orders of magnitude slower than drying and devolatisation. The gasification reactions which convert solid carbon in char to gas phase products are slow because of the limitations in heat and mass transfer, where gas-gas reactions are more rapid than gas-solid reactions, so it is the rate limiting reaction for converting char to synthetic gas. Gasification step takes place alongside the first 2 steps described [15].

The 3 main reactions that govern the gasification process are Boudouard Reaction, heterogeneous Water gas Shift Reaction, and Methanation. The first two are endothermic reactions and are favored by high temperature and low pressure in the gasifier. Hydrogen and carbon monoxide produced during the devolatisation step makes the char gasification reactions very slow. The Methanation reaction is several orders of magnitude slower than the Boudouard and water gas shift.

1.2.1.4 Homogeneous gas phase reactions

After the devolatisation and gasification steps the gases interact with each other and the change in gas composition is best described the homogeneous gas phase reactions. These reactions are very important when there is more emphasis on hydrogen content in the exit synthetic gas. Carbon monoxide and methane react with steam to produce carbon dioxide and carbon monoxide respectively along with hydrogen in both reactions. The presence of catalyst can reduce the equilibrium temperature of the water gas shift reaction.

1.2.2 Air Only Gasification of Biomass

Large scale biomass energy production systems including cellulosic ethanol, gasification, and pyrolysis facilities experience technical and economic hurdles [16]. Compared with these large scale systems, small decentralized and distributed biomass energy production systems could offer advantages including lower capital costs, lower feedstock costs, simplified transportation and logistics, and higher returns for biomass producers. These small-scale distributed systems can directly utilize regional biomass supplies that are practical and economically viable from energy saving consideration. Present research work provides a sound scientific, engineering, and technological solution for converting lignocellulosic biomass, as well as agricultural and forest residues to clean and renewable bio syngas using a pilot-scale downdraft biomass gasification system

Zainal et al. [17, 18] Investigated gasification of four different biomass feedstock namely Wood, Paddy husk, Paper and Municipal Waste. An equilibrium model was used to predict the Syngas composition and it was also used to visualize the variation in the syngas composition especially for H_2, CO and CH_4 with respect to the change in the

moisture content of the feed stock, which in turn shows the trend in the CV of the different biomass materials as a function of the moisture content.

Gautam et al. [19] developed equilibrium model approach to derive an expression that can predict the composition of the H_2, CO and CH_4 in the Syngas based on the C, H, O contents determined by the ultimate and proximate analysis for any type of biomass feedstock .The effect of gasification temperature on the composition of the syngas was also studied using the model. Author also predicted the H_2 and CO contents for most common feedstock available in U.S using the model at 800°C.

Jayah et al. [20] studied gasification in a 80 KW downdraft gasifier using rubber wood, a main source of fuel used in Sri Lanka by the tea industry and also developed a sophisticated model, which takes into account the flow equations and transport phenomena, and conservation laws to calculate the performance of the gasifier by predicting the temperature and concentration of the syngas. The effect of throat angle, a unique feature in the downdraft gasifier, on the temperature distribution in the reduction zone which in turn affects the reaction rate of the gases was considered. The model also predicted the conversion efficiency of the gasifier for varying moisture contents in the feedstock.

Karamkar et al. [21] studied experimentally rice husk gasification. The author also developed an equilibrium model to predict the syngas composition. Although the author used steam as gasifying agent in his work, a similar equilibrium model approach which predicts the maximum achievable yield from the gasification system .The work was based on equilibrium constant method and does not include the complex mathematical formulations associated with the optimization methods.

1.2.3 Steam Only Gasification of Biomass

Umeiki et al. [22, 23] have studied a high temperature gasification process to generate hydrogen-rich fuel gas from woody biomass using steam with temperatures exceeding 1200K. They discovered that both the steam temperature and the molar ratio of steam to carbon (S/C ratio) affected the reaction temperature which strongly affects the gasified gas composition. They also reported that the tar concentration in the produced gas from the high temperature steam gasification process was higher than that from the oxygen-blown gasification processes. The highest cold gas efficiency was found to be 60.4%.

Baratieri et al. [24] presented an equilibrium model (gas–solid), based on the minimization of the Gibbs energy, to estimate the theoretical yield and the equilibrium composition of the gases produced from a biomass thermochemical conversion process. The proposed model has been applied both to partial oxidation and steam gasification processes with varying air to biomass ratio (ER) and steam to carbon (SC) ratio values and different feedstocks; the obtained results have been compared with experimental data and with other model predictions obtaining a satisfactory agreement.

Chang et al. [25] investigated the steam gasification of agriculture waste at temperatures between 600 °C and 1000 °C for the production of bio hydrogen and syngas in a fluidized bed reactor. They also developed a kinetic model to determine the order of the reaction and activation energy. Their results suggested that at the equivalent ratio of 0.2 and at 1000 °C the maximum yield of bio-hydrogen (29.5%) and CO (23.6%) was achieved and the CO_2 concentration at this condition is 10.9% only.

1.2.4 Integrated Biomass to Power Systems

Olgun et al. [26] designed and operated a bench scale, fixed bed, and batch type downdraft gasifier with wood chips and hazelnut shells as the feedstock. They varied the air to fuel ratios to produce a syngas with a high heating value and low pollutants. By analyzing the gas compositions the authors were able to find the optimal system condition to obtain the syngas with the highest lower heating value, which is 0.35 ER or 5.5 MJ/Nm3.

Biomass gasification coupled with an internal combustion engine has also been evaluated by researchers using modeling and simulation approaches. Also, some of the researchers tried to demonstrate the value of an engine application with their gasification systems which produce high quality syngas. Sharma [27 a, b] performed a study using a 75 kWth downdraft gasification system integrated with a 20 kWe internal combustion engine to evaluate the feasibility of this combined operation. Pressure drop, temperature profile, output gas composition and calorific value with respect to the system mass flow rate were investigated. However, the actual experiment using the internal combustion engine was not performed.

Huang et al. [28] introduced a trigeneration system which consists of an internal combustion engine integrated with a biomass gasification unit. This system can offer a combined delivery of heat, electricity and cooling. Modeling and simulation were used to design a commercial building scale trigeneration plant fuelled by a biomass downdraft gasifier. Coronado et al. [29] also tried to increase the total system efficiency with a compact cogeneration system that produces electric energy, and hot and cold water from the wood gasifier. The energy and economic analysis was presented, which concluded that the global efficiency of the system could reach up to 51.42%.

Zabaniotou et al. [30] showed the advantage of a small-scale combined heat and power production system by the experimental result and the chemical equilibrium model analysis so that it could reduce the transportation cost of biomass and provide heat and power where and when a necessity appears. Centeno et al. [31] developed a mathematical model which consists of two separate sub models for the fixed bed downdraft gasifier and the spark ignition internal combustion engine, respectively. These models were validated by comparisons to published theoretical results and experimental data in terms of gas composition and engine power output.

Instead of integrating the gasifier with the engine directly, some researchers used synthesized gaseous mixtures from several pure gases to mimic the syngas to evaluate the possibilities of the conventional engine applications. Mustafi et al. [32] used ‘Powergas’, a synthetic fuel consisting mainly of carbon monoxide and hydrogen to investigate the engine emission and performance. The results indicate that engine power levels were 20% and 30% lower than those burning natural gas and gasoline fuels, respectively, and the carbon dioxide and NOx emissions were found to be higher than those using other fuels. Sahoo et al. [33] varied the chemical composition of the syngas supplied to a diesel engine to check the feasibility. They used two types of pure gases, hydrogen and carbon monoxide to simulate the real syngas, and did the second law analysis for different engine loads.

Finally, some researchers employed combined systems where the biomass gasification system and the internal combustion engine were integrated in series to generate the mechanical power or electricity from the gasification of biomass.

Lin [34] integrated an updraft fixed bed gasifier with a 25 kW Stirling engine, and they successfully generated the shaft power at 24.5 kW. The Stirling engine extracts and converts the heat produced from the solid biomass into electricity automatically. Shah et al. [35] focused on the engine performance and emission of a 5.5 kW spark-ignited engine operated by the syngas produced using a fixed bed, downdraft atmospheric pressure gasifier fed with hardwood chips. Syngas was collected and put in a storage cylinder at a high pressure before supplying it to the engine rather than directly piped to the engine. Results show that even though the power output when using the syngas was lower than that when the gasoline was used, the overall efficiency of the system at the maximum electrical power output on syngas was the same as that on gasoline.

1.3 Hydrogen Separation Membranes

Recently there has been an increase in the research interests of H_2 selective membranes because of the growing need to address the global energy crisis and to move inch closer to the vision of Hydrogen economy. These membranes are mainly grouped under 4 different groups namely metallic type, polymeric type, ceramic type and carbon based.

Dense polymeric membranes are useful at low temperature regime and are commercially available for different applications. The selectivity of these types of membranes is very low and makes it not a viable option for industrial processes where high selectivity is required.

Micro porous ceramic membranes operate at a slightly higher temperature regime but they have stability issues in the presence of H_2O.Since these membranes are more like molecular sieves any water clogging of the pores would result in rapid

drop in performance of the membranes. On the other hand palladium membranes have gained huge popularity because of their high selectivity to hydrogen and this serves to be a very useful attribute in engineering industries. But the main issue associated with Pd membranes is the cost issue and also the effect of CO and H_2S which could deteriorate the membrane, since these gases are very common in process streams.

Porous carbon membranes also operate in terms of molecular sieving and as a result they also inherently have a low selectivity to hydrogen. The good thing is these membranes could operate at a much higher temperature than the previously described types but this comes at a price of technicalities associated with their manufacturing and they are brittle in nature.

The ceramic membranes which are a hybrid of metallic and nonmetallic elements and are also very dense in nature. They have high selectivity and can also operate under very high temperatures making it suitable for use in gasifiers without any protection for thermal degradation. The hydrogen permeation is mainly by the transport of ions across the membrane, the electron conduction can also be increased by adding appropriate metal element to the perovskites mixture. Table 1-3 tabulates the different pros and cons of the types of membranes along with their operating range.

1.3.1 Proton Conducting Materials

Perovskites materials are a group of compounds that are very suitable for the preparation of hydrogen separation membranes. Generally formulated by ABO_3.But in order to be successful in practical applications, the perovskites should have comparable proton and electron conduction. The addition of metal ions to the matrix increases the electronic conductivity of the perovskites, like adding Ni to $SrCeO_3$.

The reason for high selectivity of H_2 in dense ceramic membrane is because the transference number for electron and proton conduction is of the same scale. Usually these perovskites are doped using low-valency cations to facilitate the transport of protons in the presence of water using the mobility of the hydroxyl group that shifts through the oxygen vacancies in the lattice [37, 38].These oxygen vacancies are mainly produced by the act of doping.

Kreuer [39] compared the proton conductivity of various oxides and it is evident that perovskites oxides have the highest proton conductivities. Since the $BaCeO_3$ type oxides have only a small deviation from proper orthorhombic structure, it facilitates the transport of oxygen ions whereas the skewed structure of $SrCeO_3$ inhibits oxygen ion transportation and results in a high proton transference number and serves as a better material to be used for membrane preparation[40, 41].Reports show that $BaCeO_3$ goes through phase change at relatively low temperature whereas $SrCeO_3$ is very stable even at high temperatures up to 1000°C [42, 43].Thus even though $BaCeO_3$ has the highest proton conductivity, $SrCeO_3$ becomes a viable option because of its structural properties. Figure 1-2 shows the proton conductivity of various types of materials.

1.3.2 Proton Transport Mechanism

The transport phenomenon in perovskites materials are mainly explained in terms of either Vehicle mechanism or Grotthus mechanism.

The vehicle mechanism [45] predicts that the proton transport in the perovskites occur as OH_3+ attached to a “vehicle” like H_2O, and also necessitating the continuous movement of unloaded vehicles on the opposite direction The Kroger-vink notations are usually used to explain the vacancies and neutral sites in the crystal structure of the perovskites. The vehicle mechanism is more dominant at high temperature regime.

The Grotthus mechanism can be elaborated by visualizing the fact that a half hydrogen would split in to a proton H^+ and e^- on the outer surface where the partial pressure of hydrogen is high and then these protons latch themselves to the oxygen sites in the structure and thus move from one site to the other. And the electron on the other hand jumps from one cerium ion to the other. Proton transport is terminated when the H^+ ions transferred to the low partial pressure side recombine with the e^- to form the half hydrogen. The major factor that determines this proton hopping between oxygen sites is the bond length, if the bond length is short the proton transfers are heavily favored but if they are longer then they inhibit the proton hopping mechanism.

Recent studies over this transport mechanisms have found that Grotthus mechanism is more likely to occur in the perovskites structures, at relatively lower temperatures where the protons hop from one oxygen site to the other driven by the partial pressure difference on the outside and inside of the membrane [46, 47].

1.4 Research Objective

The energy crisis across the globe has generated a huge interest in hydrogen economy where H_2 could be the baseline fuel for all applications across the board, though that is a very distant possibility from current stand point because of the issues associated with scaling and modifying existing infrastructures. But positively there has been very promising research in this direction and my main objective of this research work is to do a detailed study of a few of these technologies which will help create a sustainable energy future for the people all across the globe.

This research work outlines a sound scientific, engineering, and technology solution for converting lignocellulosic biomass, as well as agricultural and forest residues to syngas, hydrogen and electrical power using gasification systems, a spark-

ignited IC engine and an electric generator, and high temperature ceramic membranes which can further enhance the hydrogen content by making use of the WGS (water gas shift) reaction.

The study is divided into three major parts. The first part focuses on the pilot scale biomass to power integrated system using a traditional air-breathing gasification method from four kinds of biomass feedstock which aims at producing portable electrical power for distributed energy applications. By integrating the syngas production with the power generation, it is possible to operate an independent biomass to energy system for farm communities especially in rural and remote areas where abundant biomass resources, such as wood, agricultural residue or animal waste are widely available.

The second part concentrates on a high-temperature pure steam gasification system biomass for syngas and hydrogen production. Thermo-chemical conversion by air-free, high-temperature superheated steam at >1000 °C offers the technology to convert biomass into a pure synthesis gas which can be converted to pure hydrogen or catalytically reformed into liquid hydrocarbon fuels (biodiesel or green gasoline) and chemicals.

The third part evaluates the high-temperature membrane applications for pure hydrogen production. The key innovation is the use of a novel high temperature membrane reactor developed at the University of Florida by Dr. Eric Wachsman's research group. The main functions of the membrane reactor are to separate hydrogen from the syngas and perform water-gas shift reaction to produce more pure hydrogen and facilitate CO_2 sequestration.

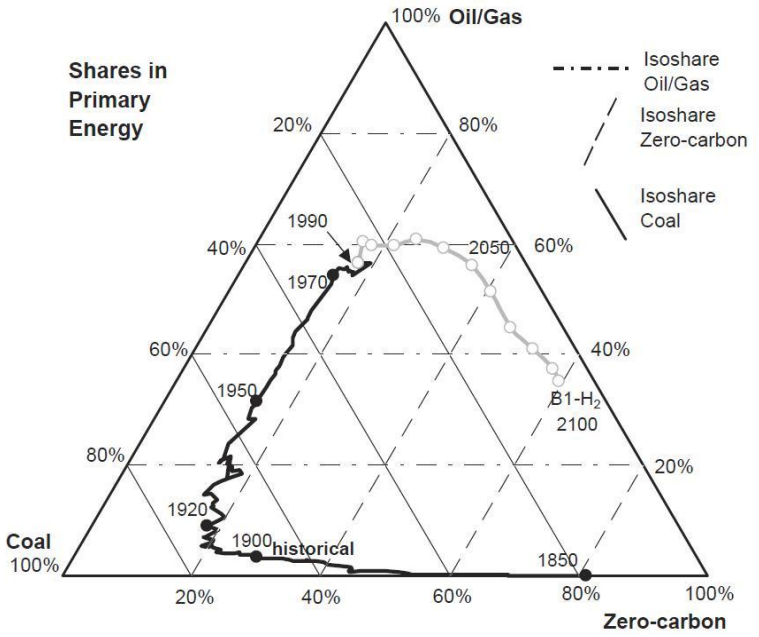

Figure 1-1. Prediction of future energy profiles adapted from literature

Table 1-1. Product gas composition from typical woody biomass gasifiers [11]

Gas comp. %	Air	Steam
H_2	10-20	24-26
CO	15-25	32-41
CO_2	5-15	17-19
CH_4	1-3	11-12
N_2	43-55	-
LHV (MJ/Nm^3)	4-6	12-15

Table 1-2. Gasification chemical reactions considered dominant during operation [11]

Chemical reactions	Enthalpy of reaction [KJ/mol]
Combustion	
$C + ½\ O_2 \longrightarrow CO$	-110.6
$C + O_2 \longrightarrow CO_2$	-393.7
Gasification	
$C + CO_2 \longrightarrow 2\ CO$ (Boudouard)	158.7
$C + H_2O \longrightarrow CO + H_2$ (Heterogeneous water gas shift)	131.4
$C + 2\ H_2 \longrightarrow CH_4$ (Methanation)	-74.9
Homogeneous gas-phase reactions	
$CO + H_2O \longrightarrow CO_2 + H_2$ (Water gas shift)	-40.9
$CH_4 + H_2O \longrightarrow CO + 3\ H_2$ (Methane reformation)	-206.3

Table 1-3. Properties of different types of hydrogen separation membranes [36]

Properties	Dense Polymer	Micro porous Ceramic	Dense Metallic	Porous Carbon	Dense Ceramic
Temperature range	<100 °C	200-600 °C	300-600 °C	500-900 °C	600-900 °C
H_2 selectivity	Low	5-139	>1000	4-20	>1000
H_2 flux(mol/m^2s)	Low	60-300	60-300	10-200	6-80
Stability issues	Swelling, Compaction, Mechanical strength	Stability in H_2O	Phase transition	Brittle, Oxidizing	Stability in CO_2
Poisoning issues	HCl, SO_x, CO_2		H_2S, HCl, CO	Strong adsorbing vapours, organics	H_2S
Materials	Polymers	Silica, Alumina, Zirconia, Titania, zeolites	Palladium alloy	Carbon	Proton conducting ceramics
Transport mechanism	Solution/ Diffusion	Molecular sieving	Solution/ Diffusion	Surface diffusion, Molecular sieving	Solution diffusion (proton conduction)
Development status	Commercially available	Prototype membranes available	Commercially available	Small membrane modules/ Samples available for testing	Small samples available for testing

Material	Optimal conducting temperature (°C)	Proton conductivity (S cm^{-1})
Hydrated sulfonated polymers		
NAFION	<100	5×10^{-2} at 25 °C, 4×10^{-2} at 160 °C
S-PBI	<100	1×10^{-2} at 25 °C
S-PEEK	<100	3×10^{-2} at 25 °C, 4×10^{-2} at 160 °C
Heteropolyacid hydrates		
$H_4SiW_{12}O_{40}\cdot28H_2O$	<100	2×10^{-2} at 25 °C
$H_3PW_{12}O_{40}\cdot29H_2O$	<100	8×10^{-2} at 25 °C
$H_3PMo_{12}O_{40}\cdot29H_2O$	<100	1.7×10^{-1} at 25 °C
Layered hydrates		
$HUO_2PO_4\cdot4H_2O$	<100	5×10^{-3} at 25 °C
α-$Zr(HPO_4)_2\cdot nH_2O$	<100	1×10^{-4} at 25 °C
γ-$Zr(PO_4)(H_2PO_4)\cdot2H_2O$	<100	3×10^{-4} at 25 °C
γ-Zr sulfo phosophonates	<180	1×10^{-2} at 25, 100 °C
Oxide hydrates		
$Sb_2O_5\cdot4H_2O$	<300	3×10^{-4} at 25 °C
$V_2O_5\cdot nH_2O$, $ZrO_2\cdot nH_2O$,	<150	1×10^{-2} at 100 °C
$SnO_2\cdot nH_2O$	<300	4×10^{-4} at 25 °C
$Ce(HPO_4)_2\cdot nH_2O$	<150	1×10^{-3} at 100 °C
Polyphosphate composite		
$NH_4PO_3/(NH_4)_2SiP_4O_{13}$	200–300	8.7×10^{-3} (dry atm), 3.3×10^{-1} (wet atm) at 300 °C.
NH_4PO_3/TiP_2O_7	150–250	2.4×10^{-2} at 250 °C
Layered polyvalent (Zr or Ta) hydrogen phosphate	25 (Ta>Zr)	2×10^{-4} at 25 °C
Sr-doped $La_3P_3O_9$	700	7×10^{-7} to 3×10^{-4} at 300–700 °C
Sr-doped $LaPO_4$	500–925	6×10^{-6} to 3×10^{-4} at 500–925 °C in wet atm
Perovskites		
$BaCe_{0.9}Y_{0.1}O_{3-\alpha}$ (BCY)	500–900	1.8×10^{-2} to 7×10^{-2} at 600–1,000 °C
$BaZr_{0.9}Y_{0.1}O_{3-\alpha}$ (BZY)	500–900	1.6×10^{-3} to 6×10^{-3} at 600–1,000 °C
$Ba_3Ca_{1.18}Nb_{1.82}O_{8.73}$ (BCN18)	500–900	5.5×10^{-4} at 600 °C
Oxo acid salts		
$K_3H(SO_4)_2$	100–200	9.5×10^{-6} to 2.2×10^{-2} at 80–250 °C
$CsHSO_4$		2×10^{-7} to 3×10^{-2} at 110–190 °C
H_3OClO_4		3.5×10^{-4} at 25 °C
Oxo acid composites		
$MeNO_4$–SiO_2 (Me=Rb, Cs)	100–200	1×10^{-6} to 1×10^{-2} at 60–280 °C
$Cs_3(HSO_4)_2(H_2PO_4)$		1×10^{-6} to 1×10^{-2} at 40–180 °C
Pyrochlore		
$(La_{1.95}Ca_{0.05})Zr_2O_{7-\delta}$	500–900	6.8×10^{-2} at 600 °C
$La_2Ce_2O_7$, $Eu_2Zr_2O_7$		7×10^{-7} to 1×10^{-2} at 300–800 °C
Chalcogenides		
$H_2S/(B_2S_3$ or $Ga_2S_3)/(GeS_2$, SiS_2, As_2S_3 or CsI)	200–500	5×10^{-11} to 4×10^{-7} at 60–300 °C

Figure 1-2. Proton conducting material matrix showing operating limits [44]

CHAPTER 2
CONCEPTUAL SYSTEM

2.1 Introduction

The proposed concept system uses high-temperature steam as both the heat source and the gasification agent in an oxygen-starved (air free) environment. The model is created in such a way that of the hydrogen generated from the gasification can be used in the production of the steam. Thus making the model self-sufficient in heat supply and does not require external water. The impact on the environment could be minimized by this type of self-sustained systems. The advanced biomass to hydrogen and liquid fuels conversion process that could be developed with the help of this concept system will help ensure the availability of a highly efficient and clean technology, which is one of the goals of the D.O.E (Department of Energy) for the future. The major goal of the research work presented is to first develop and evaluate a sound idea for converting the biomass to clean energy and then envision an integrated system that would fully accomplish the idea. After that mathematical models and bench-scale systems will be used for the evaluation of the feasibility and effectiveness of the system.

The underlying theme and intended primary contribution of this concept system shown in Figure 2-1 are aimed at providing the engineering community and industry with a breakthrough in the technological capabilities for efficient conversion of lignocellulosic biomass to useful fuels using advancements in membrane technology. The success of proposed concept system thus requires generating innovative ideas on system design, integration and optimization, in addition to a thorough and complete understanding of the individual system components. The models developed and the

outcome of the system designs obtained from this biomass to energy research will undoubtedly prove beneficial for many other energy system projects where innovative ideas play a dominant role. The model of this concept system is developed with a lot of idealizations and assumptions which would be explained in subsequent sections.

2.2 Description of System Components

The heart of the proposed biomass to energy system is the high-temperature steam gasification unit. In an oxygen-starved environment, the gasification unit uses superheated high temperature (1500 °C ~ 2000 °C) steam from a hydrogen combustor as the gasifying medium.

This concept system was modeled as a combination of a gasification driven hydrogen and liquid hydrocarbon fuel production unit that is composed of five major components: a high temperature steam gasifier, a membrane reactor using advancements in proton conduction, a surplus heat recovery unit, a liquid fuel reactor (Fischer-Tropsch synthesis reactor) and a hydrogen combustor as shown in Figure 2-1.

The backdrop under which the concept system model has been developed is explained below. The model does not take in to consideration the energy requirement for the air separator that provides the O_2 for the combustor. Heat loss from the gasifier, combustor and membrane reactor is not considered in calculations. The exit temperature of the combustor is not calculated and steam is assumed to be at 2000°C after mixing with the recycled water. The membrane reactor modeled does not account for the pressure difference in the feed stream and the permeate stream and the power requirement for the compressor to push the recycled hydrogen back to the combustor is neglected. The components of the system are explained in detail.

2.2.1 High-Temperature Gasification Unit

Thermo-chemical conversion by air-free, high-temperature superheated steam at 1500-2000 °C offers the technology to convert biomass into a pure synthesis gas which can be converted to pure hydrogen or catalytically reformed into liquid hydrocarbon fuels (biodiesel or green gasoline) and chemicals. In the model the gasifier has no heat loss and is a continuously fed unit.

2.2.2 Membrane Reactor

The main idea is the integration of a novel high temperature membrane reactor developed at the University of Florida by Dr. Eric Wachsman's group. The main functions of the reactor are to simultaneously separate hydrogen from the syngas and perform water-gas shift reaction to produce more pure hydrogen and facilitate CO_2 sequestration. A key role of the reactor is to separate hydrogen out of the syngas for specific applications. The model reactor assumes no heat loss and pressure loss across the feed/permeate stream, hence the power requirement of a compressor to supply the permeated hydrogen to the combustor is neglected. Also it is assumed that the whole reactor is able to sustain high temperatures without any limitations related to sealing and fittings.

2.2.3 Surplus Heat Recovery Unit

The core of this unit is a heat exchanger that could recuperate the heat associated with the high-temperature exit syngas and transfers heat to desired applications and low-temperature process heat to subsystems could be used in an absorption chiller or a sea water desalination device based on the application/industry. The model assumes that all the watervapour going through the heat exchanger is cooled down and neglects the power requirements of any pump that supplies this

stream back to the gasifier and the effects of back pressure in the case of mixing with the combustor exit is also neglected. The model assumes that there is complete conversion of the CO available in the syngas stream for the base case; this can be varied to see the effect on system efficiency as shown later. Also that the membrane separates all the hydrogen produced by WGS without any loss of pressure across the permeate side. The permeation through the membrane can also be varied and it is taken at complete permeation of available hydrogen on feed side for the base case.

2.2.4 Fischer-Tropsch Catalytic Reactor

In this process, the syngas is catalytically converted to liquid hydrocarbons such as biojet fuel and biodiesel. This could be used as one path for conversion apart from direct production of hydrogen as fuel and the flexibility of the system allows for this to be done. The model assumes no heat loss or energy requirements for this unit and simply calculates the liquid fuel production based on the ratio of available hydrogen and carbon mono oxide at the inlet.

2.2.5 Hydrogen Combustor

This unit is used to provide the super-high temperature steam for the gasification unit. The hydrogen combustor draws the fuel from the syngas produced by the gasification process. Part of the hydrogen produced is recycled based on the operating conditions to make the system self-sustainable in terms of external heat requirements. The combustor material properties and design aspects are not considered in the model, and it is assumed to provide the steam at a specific condition which after mixing with the recycled water becomes steam at 2000°C.

2.3 System Characteristics and Efficiencies

Special characteristics, uniqueness and innovations of the concept system can be summarized as shown in this section.

- The high temperature oxygen-starved (air-free) gasification uses steam at greater than 1500 ^{o}C to gasify the feedstock. Almost all of the carbon is converted to pure fuel gas. As a result, all the tars and char are broken down resulting in minimal contaminants in the exit syngas. The trace amounts of inorganic materials in the biomass are converted into inert vitreous slag – very high environmental benefit.

- Biomass energy brings numerous environmental benefits, like minimizing the CO_2 foot print as biomass systems release only the CO_2 inherently present in the feedstock, by assimilation through photosynthesis and could also help reduce the problems caused by generation/accumulation of municipal solid waste.

- The hydrogen combustor in system that provides the heating agent is modeled as clean combustion process and draws the fuel from the H_2 produced by the gasification process (~30% to 50% of total H_2 produced based on application), so the unit is self-sufficient and there is no need for external heat supply since the energy input for the air separator was neglected as explained above.

- For the proposed system, the model assumes that there is no net water consumption from any external sources apart from the system components, as steam required for gasification is from the hydrogen combustor using part of hydrogen produced and the water condensed from the heat recovery unit.

- The CO_2 produced after the WGS in the membrane reactor could also be further isolated from the reactor exit stream using any commercially available sieve type membranes and could be directly sent for sequestration as shown in the model.

- Due to the high temperature gasifying agent, there is a lot of potential to use different types of biomass sources as feedstock. Other than agricultural and forest biomass, most biomass municipal solid waste could also be included with very minimal modifications to the gasifier.

- This concept system with high-temperature chemical transformation process could provide complete tar cracking and catalyst for WGS reaction, thereby reducing the cost of gasification-based process technology when used in conjunction with membrane technology.

- For applications in the rural and farm infrastructure, the biomass is inherently dispersed and abundant, making the energy costs for harvesting and transporting them prohibitive unless the fuel processing plant is nearby. As the proposed system can be designed at various scales, establishing a network of mobile and

distributed energy (DE) plants would be another advantage of such portable biomass gasification systems.

Based on a mass and energy balance analysis using the chemical reactions presented in the previous chapter, under thermal and chemical equilibrium conditions, the system performances using the operating conditions indicated on the schematic diagrams for the following two cases were estimated.

Case 1: System produces Liquid Bio-fuel production only as net output.

Case 2: System produces H_2 gas only as net output.

For the system calculations, the equations below were used,

$$\text{Gasifier efficiency} = \eta_{gasifier} = \frac{\dot{m}_{syngas} \cdot \text{LHV}_{syngas}}{\dot{Q}_{steam} + \dot{m}_{feedstock} \cdot \text{LHV}_{feedstock}} \quad (2\text{-}1)$$

$$\text{Membrane conversion factor} = \frac{\text{Number of moles of } \text{H}_2^{permeate}}{\text{Number of moles of } \text{H}_2^{total}} * \frac{\text{Number of moles of } \text{H}_2^{total}}{\text{Number of moles of CO}^{syngas}} \quad (2\text{-}2)$$

$$\text{Overall efficiency for concept system} = \eta_{overall} = \frac{\dot{m}_{product} \cdot \text{LHV}_{product} + \dot{Q}_{recovered}}{\dot{m}_{feedstock} \cdot \text{LHV}_{feedstock}} \quad (2\text{-}3)$$

Energy required to heat the steam from 100°C to 2000°C = $\dot{Q}_{steam}$

Mass flow rate of syngas generated and feedstock supplied = $\dot{m}_{syngas}$ and $\dot{m}_{feedstock}$

Lower heating value of syngas generated and feedstock supplied = LHV_{syngas} and $\mathrm{LHV}_{feedstock}$

Total number of moles of hydrogen produced from WGS reaction = H_2^{total}

Number of moles of hydrogen permeating through membrane = $H_2^{permeate}$

Total number of moles of CO available for WGS reaction in syngas stream from gasifier = CO^{syngas}

Rate of heat recovered from heat exchanger = $\dot{Q}_{recovered}$

Mass flow rate of product produced based on syngas path = $\dot{m}_{product}$

Lower heating value of product produced based on syngas path = $\mathrm{LHV}_{product}$

Analysis and calculations to determine the individual component efficiencies will be done in the subsequent chapters, including the air gasification system along with the steam gasification system to show the advantages and versatility of the gasification process in terms of the type of feedstock available. Further the membrane reactor will also be tested under simulated syngas conditions to provide further insight in to the feasibility of using such advanced membrane in the concept system which would enhance hydrogen production in addition to gasification. Based on the results and data obtained from the following chapters, the concept system would be evaluated and the findings are presented in the concluding section. To make the calculations, different state points in the concept system model are labeled. The gasifier exit (a).The point where the exit stream is branched off based on the path chosen (b).The entry to the

membrane reactor is (c).Streams (d) and (e) are the permeated hydrogen and effluent CO_2 line respectively. Stream (d) is split in to (i) and (j) based on the fuel mode selected as the output.(g) and (f) are the line for sequestration of CO_2 after cooling and the water recycled back for the combustor respectively. Finally, (h) represents the hydrogen that is recycled to make the system self-sufficient in terms of heat supplied to the gasifier, depending on the availability and the assumptions made regarding the system components as mentioned earlier.

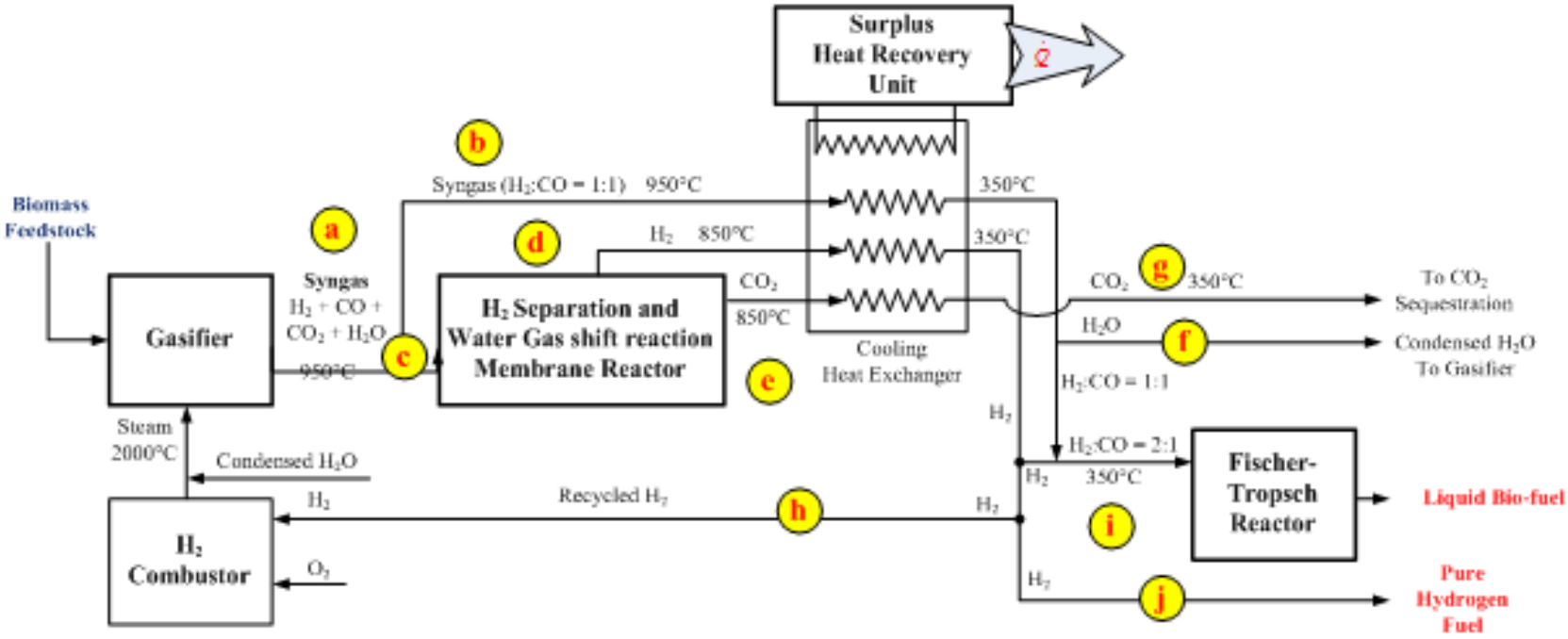

Figure 2-1. Schematic of concept system with alternate path lines

CHAPTER 3
EXPERIMENTAL AND NUMERICAL INVESIGATION OF PORTABLE (PILOT SCALE) PARTIAL OXIDATION/GASIFICATION SYSTEM

3.1 Introduction

This chapter discusses in detail the experimental setups used for the research and also provides a comprehensive list of procedures used in developing the equilibrium model for both the air only (Pilot system) gasifier system. Further, the results from the pilot scale system are also compared with the respective model results for validation

3.2 Portable Gasifier Experimental Setup

The pilot-scale gasification system as shown in Figure 3-1 was designed and built to emphasize on the effectiveness of distributed power generation systems and to demonstrate the feasibility of such gasification systems in real world scenarios, where the biomass resources are widely varying and distributed across the board. Four different feedstock were selected to demonstrate the versatility of the gasifier system. The Imbert design downdraft gasifier [48] has three main sections namely, the top hopper, the combustion and reduction chamber and the bottom ash chamber. The top hopper has a lid that facilitates the loading of the feedstock for operations and the mid-section has five radially arranged nozzles that are connected to a concentric chamber which in turn is connected to the main air intake valve on the outer surface that feeds the air into the gasifier. This design makes the gasifier self-adjusting on its own to compensate for excess coal or excess feedstock in the gasifier and automatically brings the reaction zone in line with the nozzles. The lower half of this section has the reduction chamber that incorporates the hour glass shape and additional thermal insulation, which highly improves the efficiency of the gasifier in breaking down the tar.

The last section of the gasifier has the grate on which all the coal and feedstock are placed. This grate is controlled by a rotary shaker that helps prevent bridging in the reaction zone by constantly letting the ash settle down at the bottom.

The gasifier is connected to a syngas cleaning system given in Figure 3-2. The exit of the gasifier is connected to a cyclone separator which helps in removing any particulates of contents of ash that gets carried along the syngas. After this the syngas enters the cooling tower that lowers the temperature of the gas significantly and makes it more energy dense and in the process it also condenses out tar vapor in the gas stream. The exit of the cooling tower is connected by a 2-way valve to the flare which identifies the quality of the syngas by the flame color and once the flame changes from bright yellow to colorless fumes, the syngas is diverted to the two sets of filters that scrub the syngas clean of almost all the smaller particulates and remaining tars. Then the syngas is ready for use or can be sampled out for gas analysis

To start the gasification process, measured amounts of coal was added to the grate filling it up to the level of the air intake nozzles. This served as the heat source to overcome the thermal inertia of the gasifier and moderate the conditions suitable for gasification and also served as the reduction zone for the gases passing through it during the reaction. The experimental conditions under which tests were conducted are listed in Table 3-1 for all 4 feedstock. Then the coal bed was ignited using a blow torch and the blower attached at the end of the gasifier is started to help pull the air through the gasifier to facilitate the combustion of coal and the variable speed blower settings were adjusted in such a way that it maintains a 5” H_2O pressure differential across the throat of the gasifier, which was determined using the pressure monitor. The gasifier in

the pilot system is equipped with K-Type thermocouples at different zones of the reactor chamber to closely monitor the thermal gradient along the length of the gasifier as the reaction goes on and are continuously monitored using the data acquisition (DAQ) system. Once the coal bed reaches the gasification temperature required, the amount of air flow into the system was controlled with the intake valve to maintain the reactor temperature. Actual system mounted on a trailer is shown in Figure 3-3.

After this the top hopper was opened and measured quantity of feedstock was added and the lid was closed tight. The grate motor was also turned on to prevent any bridging in the reactor. The exit gas temperature was also monitored continuously. When the temperature of the syngas exiting the gasifier reached 250°C, the igniter at the top of cooling tower was turned on to flare the syngas. The color of the flares gives an indication of the quality of gas produced and it is further processed tailoring the needs of the system. The flow rate of the syngas being produced was measured using a gas meter with movable diaphragms. Since it would be difficult to read the rotations of the needle in the meter manually, display was modified using an auto clicker that was connected to the needle using a relay and each rotation of the needle in the meter was recorded as a click in the counter and was used to determine the flow rate.

Pictorial representations of the thermocouple (TC) locations are shown in Figure. 3-5. A similar approach to capture the thermal profile in the downdraft gasifier was used byLv et al. [49] but the sampling rate used was 2-3 min intervals. The clean syngas was allowed to enter the Ford DSG423 engine shown in Figure 3-4.The generator which converts the mechanical power to electrical power was coupled to the engine. This engine was originally developed for the gasoline and the natural gas applications, and

the engine was de-rated to 40 kW at a constant speed of 1800 rpm as a lower rpm engine is more suited for the syngas application. The load bank which was connected to the generator applied variable loads to the engine/generator to measure the output power produced by the engine. The load bank data was recorded after the engine/generator set was started and the engine was loaded in smaller steps until the peak load was achieved.

3.3 Equilibrium Model for Gasification

This section is dedicated to elaborate on the various assumptions and methodology used to construct the model using NIST variables over the temperature range desired. The Air only model was initially developed and was developed further to a steam only model by selecting the constants and the variables accordingly since the original model has been validated by comparison with other existing models.

The thermal-chemical model was tailored specifically to suit the downdraft gasifier, and the choice of the gasifier makes it less intense when it comes to the assumptions that were made to make the model reliable in predicting the syngas composition. To make the process of solving the simultaneous equations using computational methods the following assumptions were made.

- The gasification reactor is in perfect thermodynamic equilibrium.
- In the energy equation there is no heat loss term assuming that the system is perfectly insulated and there is no parasitic influence on the system i.e. the process is completely adiabatic.
- Only C, H, O contents of the feedstock were chosen as in other literatures to validate the model and other mineral contents were not considered because of the negligible amount present.
- The input energy provided by the coal bed to start up the reactions is not accounted for. Although it is not clearly mentioned in any literature why the initial heat provided by the coal bed is not being formulated in the energy equation, this

is justified on the basis that even though there is a significant consumption of coal during the experimental study, it is for heating up the entire system from room temperature to the gasification temperature and there is no perfect insulation of the gasifier ideally which further increases the amount of heat required to bring it up to the operating temperature. When it is modeled as a continuous process then there is no requirement to heat up the system since it is already at the high temperature and the heat required for gasification is provided by the charcoal that is formed from the biomass added thus making the initial charcoal added to serve just as a reducing zone by providing more surface area for the chemical conversion.

- All the Cs (solid carbon) is converted to syngas species and there is no solid carbon left after the gasification and the exit syngas is composed only of H_2, CO, CO_2, H_2O, CH_4 and N_2.Other higher Hydro carbons are neglected. The composition gases are modeled to exhibit ideal behavior irrespective of the high operating temperatures in the gasifier.

- The syngas composition estimated is free of any O2 from the supplied air since the amount of air supplied is constrained using the intake valve, making it a partial oxidation process and all the O2 is consumed during the combustion reaction.

Global Equation:

$$CH_XO_Y + wH_2O + m\left(O_2 + 3.76 \cdot N_2\right) \Rightarrow a_1H_2 + a_2CO + a_3CO_2 + a_4H_2O + a_5CH_4 + m \cdot 3.76\, N_2 \quad (3\text{-}1)$$

The X and Y for the biomass feedstock are determined from the ultimate analysis of the feedstock. There are a total of 6 unknowns in this equation and the equilibrium calculations were carried out with H_2, CO, CO_2, H_2O, and CH_4 as the exit syngas components along with N_2.It is assumed that there is no soot formation and all the biomass is converted to the exit gas composition under a high temperature and there is no tar. The enthalpy changes of the product gas constituents were calculated as a function of the gasification temperature using the fitted values given [50] for corresponding constituents in specific temperature range.

Thus for solving the 6 unknowns, 6 simultaneous equations were formed using the data available from the global equation and the 2 independent reactions. The w is determined using the moisture content in the feedstock

$$w = \frac{MW_{Bio} * MC}{MW_{H_2O} * (1\text{-}MC)} \tag{3-2}$$

$$CH_4 + H_2O \Leftrightarrow CO + 3H_2 \quad \text{Methane reforming} \tag{3-3}$$

$$CO + H_2O \Leftrightarrow CO_2 + H_2 \quad \text{Water gas shift} \tag{3-4}$$

The equations required for the numerical analysis are formulated using the C, H, O balance of the global equation followed by the rate constant equation for the 2 chemical equations considered and finally carrying out the energy balance for the whole system. Terms like, [X] represent the number of moles of species X. ΔG represents the Gibbs free energy minimization as required for each reaction considered.

Carbon Balance:

$$a_2 + a_3 + a_5 - 1 = 0 \tag{3-5}$$

Hydrogen Balance:

$$2 \cdot a_1 + 2 \cdot a_4 + 4 \cdot a_5 - X - (2 \cdot w) = 0 \tag{3-6}$$

Oxygen Balance:

$$a_2 + 2 \cdot a_3 + a_4 - Y - w - (2 \cdot m) = 0 \tag{3-7}$$

The equilibrium constant for methane decomposition can be written in terms of the moles of the participating species,

$$K_1 = \frac{[CO] * [H_2]^3}{[CH_4] * [H_2O]} \tag{3-8}$$

Similarly the equilibrium constant for water gas shift reaction can be written as,

$$K_2 = \frac{[CO_2]*[H_2]}{[CO]*[H_2O]} \tag{3-9}$$

These equilibrium constants are a function of the gasification temperature and they are described by following equations with coefficients given in Table 3-2.

$$C_p^\circ = A + B*t + C*t^2 + D*t^3 + E/t^2 \tag{3-10}$$

$$H^\circ - H^\circ_{298.15} = A*t + B*t^2/2 + C*t^3/3 + D*t^4/4 - E/t + F - H \tag{3-11}$$

$$S^\circ = A*\ln(t) + B*t + C*t^2/2 + D*t^3/3 - E/(2*t^2) + G \tag{3-12}$$

Where, C_p = heat capacity (J/mol*K), H° = standard enthalpy (kJ/mol), S° =standard entropy (J/mol*K), t = temperature (K) / 1000

Using the table values, the ΔH, ΔS, ΔG for the equilibrium reactions were calculated as given below,

$$\Delta H_1 = (3 \cdot h_{H_2} + h_{CO}) - (h_{H_2O} + h_{CH_4}) \tag{3-13}$$

$$\Delta H_2 = (h_{CO_2} + h_{H_2}) - (h_{CO} + h_{H_2O}) \tag{3-14}$$

$$\Delta S_1 = (3 \cdot S_{H_2} + S_{CO}) - (S_{H_2O} + S_{CH_4}) \tag{3-15}$$

$$\Delta S_2 = (S_{CO_2} + S_{H_2}) - (S_{CO} + S_{H_2O}) \tag{3-16}$$

$$\Delta G_1 = \Delta H_1 - (\Delta S_1/1000) \cdot (t \cdot 1000) \tag{3-17}$$

$$\Delta G_2 = \Delta H_2 - \left(\Delta S_2 / 1000 \right) \cdot \left(t \cdot 1000 \right) \tag{3-18}$$

$$K_1 = \exp\left(\frac{-\Delta G_1}{8.3 * t} \right) \tag{3-19}$$

$$K_2 = \exp\left(\frac{-\Delta G_2}{8.3 * t} \right) \tag{3-20}$$

So now, the K values are now written in terms of the unknown values as per definition, and the Gibbs free energy technique is used to set up the variables in terms of the equilibrium constants. The K values are determined using the gasification temperature as input and then the calculated k values are used to solve the set of equations. $\sum nH_{out}$ is the total enthalpy of the product side and $\sum nH_{in}$ is that of the input. Here no external work is taken in to consideration so that would be neglected.

$$K_1 = (a_1^3 * a_2 / a_5 * a_4) \times (4/(a_1 + a_2 + a_3 + a_4 + a_5 + 3.76 * m)^2) \tag{3-21}$$

$$K_2 = a_1 * a_3 / a_2 * a_4 \tag{3-22}$$

$$Q - W = \sum nH_{out} - \sum nH_{in} \tag{3-23}$$

The energy equation can be written in detail as follows, with the reference temperature is 298 K and pressure is 1 atm.

$$\begin{aligned} H^0_{f\,Bio} + w*(H^0_{f_{H_2O}} + H_{vap}) + m*(H^0_{f_{O_2}} + 3.76*H_{f_{N_2}}) &= a_1*\left(H^0_{f_{H2}} + \int_{T_0}^{T_G} C_{p_{H2}}\,dT\right) \\ + a_2*\left(H^0_{f_{CO}} + \int_{T_0}^{T_G} C_{p_{CO}}\,dT\right) &+ a_3*\left(H^0_{f_{CO_2}} + \int_{T_0}^{T_G} C_{p_{CO_2}}\,dT\right) + a_4*\left(H^0_{f_{H_20}} + \int_{T_0}^{T_G} C_{p_{CO_2}}\,dT\right) \\ + a_5*\left(H^0_{f_{CH_4}} + \int_{T_0}^{T_G} C_{p_{CH_4}}\,dT\right) &+ m*3.76*\left(H^0_{f_{N_2}} + \int_{T_0}^{T_G} C_{p_{N_2}}\,dT\right) \end{aligned} \tag{3-24}$$

Owing to the complexities in solving the equations, a mathematical solver Maple was used to carry out the calculations and determine the exit syngas composition. The model was run for all the four different feedstock with their respective properties accounted for. Reliability of the model was also tested by using input conditions from other similar literature works and comparing the results with various models for validation.

3.4 Results and Discussions

This section discusses in detail the results obtained from the gasifier units, both experimental and model results are available for the pilot system. The results are also validated by comparison with other models in literature.

3.4.1 Experimental

The detailed temperature profiles inside the pilot gasifier are shown in Figure. 3-6 through Figure 3-10 for the five zones of pyrolysis, combustion, before throat, after throat and reduction with all the four different feedstock included for comparison. The legends have been placed at certain distance percentage on the temperature curve to make it very readable, since the data points were collected at a sampling rate of 1 second.

A general trend found on all the temperature history profiles is the oscillations. The main reason for the oscillations is the self-regulating nature of the downdraft gasifier mentioned above. The oscillations are believed to be attributed to the alternating sequence between the air intake flow and the flu gas flow. First the cycle starts when the air flow must be cranked up to facilitate the combustion and the production of flue gas that then rises up to the pyrolysis zone. The flu gas then recirculates back down once it loses heat to the feedstock for pyrolysis and as it

reenters the combustion zone it retards the intake air flow. As a result, the combustion slows down and so do the flu gas production that will cause the flu gas flow rate to decrease and the air flow to increase to support more combustion and that starts a new cycle.

The pyrolysis zone profiles given in Figure 3-6 show a very high peak at 1000 seconds for the cardboard feedstock, this may be because of the low density nature of the feed stock which tends to form localized pockets filled with air in the gasifier which when exposed to the reaction zone as gasification progresses will release a lot of heat because of the sudden inclusion of the oxidizing agent. Although other feedstock also shows similar isolated high peaks but they are all lower than that of cardboard because of their inherently high density distributions in the hopper with lower number of air pockets.

In Figure 3-7, the combustion Zone temperature profiles display some large fluctuations which were captured because of the high sampling rate. The reasons for such high fluctuations in this zone are explained [49] but the author actually shows a fairly smooth profile with minimal fluctuations in the combustion zone in their results which they attribute to a low sampling rate. Usually a low sampling rate damps out the jumps in the combustion zone especially. This is the zone where all the heat required for the gasification reaction is produced and hence the temperatures are the highest among all five zones.

Figure 3-8, Figure 3-9 and Figure 3-10 basically represent the 3 zones that make up the space between the throat of the gasifier and the grate which is primarily the region where all the tar cracking and reformation reactions take place. The average

temperature peaks in this region drop to 800 °C from 1100 °C and it is mainly because of the endothermic nature of the reactions that take place in the reduction zone.

Figure 3-11 shows the temperature history curves for all the five zones in the gasifier using horse manure as the feedstock and it can be seen clearly from the profiles that the reaction zones near the throat are more stable with much smaller fluctuation amplitudes and frequencies than the combustion and pyrolysis zones, which is attributed to the fluctuations in heat releases due to interaction with O2 trapped in the hopper section, and the average temperature in the reduction process is 850 °C which is high enough to crack tar and facilitate shift and reformation reactions.

The time-averaged temperatures in all the zones for the four feedstock are plotted in Figure 3-12 and tabulated in Table 3-3, where Zones 0, 1, 2, 3, and 4 represent pyrolysis, combustion, before throat, after throat and reduction zones, respectively. Generally the combustion zone, as expected, has the highest temperature, followed by before the throat zone, after the throat zone and reduction zone. The pyrolysis zone has the lowest temperature. The trends shown in Figure 3-12 are consistent and similar with those given by [26]. It clearly shows that all the four feedstock display almost similar trends in all the 5 zones. Table 3-3 summarizes the average temperature values in all different zones for each feedstock.

3.4.2 Theoretical Model

In order to check the validity of the current model developed specifically for pilot gasifier, the model predictions were compared to other well-known models widely used in the literature and the results are tabulated below .For making the comparisons easier the models used by the corresponding authors have been named as follows.

1. Model 1 GasifEq [51]

2. Model 2 GasEq [52]
3. Model 3 ChemEq [53]
4. Model 4 Predicted [18]
5. Model 5 SynGas model [54]
6. Model 6 Cycle-Tempo model [54]

The current model used the chemical properties from [50] whereas the other authors have used values from different sources [55]. Since the equilibrium constant is very sensitive to the coefficients, any slight change in the chemical composition of syngas is attributed to the use of different standards for calculating them, which is clearly shown in Table 3-2.

The gasifier output gas compositions predicted by current model at 1073K with moisture contents of 10% and 20% under no-heat condition for wood waste are given in Table 3-5 and 3-6 that also list the results from other models for comparison. Although the syngas compositions predicted by current model is in accordance with other literature values, the variations in the syngas composition shown in Table 3-5 and 3-6 are mainly due to the following reasons: the type of independent reactions chosen for solving the model and the enthalpy of formation of wood. For the enthalpy of formation, it was taken to be 149.752 KJ/mol [51] in their model whereas a value of 118.050 KJ/mol was used in [18, 54], which is due to the error in using the enthalpy of formation of water vapor instead of liquid water as explained by these authors. But current model calculated the enthalpy of formation for the different feed stock based on their compositions. Complete methodology is explained by Balu et al. [58].Table 3-5 and Table 3-6 compares the model predictions with other known models in literature and it is in good agreement as listed.

Now using the experimental input conditions for four different feedstock materials and using the ultimate analysis to determine the heat of formation and number of moles

of water from the moisture content of each feedstock, the current model was applied to predict the syngas compositions and the details of the volumetric composition and the heating values of the syngas are listed in Table 3-7.

Table 3-8 provides a comparison between experimental data analyzed using HP 5890 GC and those predicted by current equilibrium model for the hydrogen volume percent in the syngas. The differences between the two sets of results are explained below.

The assumptions listed in the start of the Numerical analysis may not take place totally in the experiment especially the equilibrium and adiabatic conditions that usually result in a higher hydrogen volume fraction.

The model prediction is based on the reactor temperature of 1173 K while the actual gasifier has variations both in space and in time as shown.

As a result of the temperature variations, some tar would form in the experimental gasifier due to low temperature spots while no tar formation was assumed in the model.

The deviation between the values from the model and experiment is relative large for the cardboard that may be due to its much lower density and an inaccurate ultimate analysis. The lower density feedstock tends to entrain more air due to local pockets. The ultimate analysis values selected from the literature may not fit directly to the type of cardboard used.

All the models in the literature under estimated the CH_4 content in the syngas because the models do not take in to account the amount of CH_4 produced from cracking of tar and other volatiles which is basically the case in an actual gasifier.

With considerations given to the differences between the model assumptions and the actual experimental conditions and also the experimental uncertainties, the agreement shown in Table 3-8 between the experiment and the model is reasonably good except for the cardboard. Based on the relatively close comparisons, the current pilot-scale distributed energy gasification system would be capable of delivering efficiencies as discussed in literature.

The overall system efficiency is calculated using the following methods, by determining the individual component efficiencies to start with. The overall system efficiencies can be calculated using Eq. 3-27.The results from the current research are listed in Table 3-9 for the four different types of feedstock. Martínez [56] reviewed integrated systems of syngas production by downdraft gasification coupled with power generation using internal combustion engines. They compared the performances and the efficiencies of systems for a wide range of power capacities. One of the results discussed in the review has a similar system scale to that in the current research except that a diesel engine was used is also listed in Table 3-9 for comparison purposes. Both the engine rpm and the power level are similar between the current work and [56]. It can be seen that the overall system efficiencies of the current research compare well with Martinez et al. [56]. As mentioned above, Henriksen et al. [57] worked on the integrated gasification-engine system that generated 15 kWe to 20 kWe of electricity with wood chips. In addition to the engine efficiency, a 25% efficiency for the overall system that is included. It is clearly indicated in Table 3-9 that the overall efficiencies found in the current research are comparable to those reported in the literature for the gasification to power systems of similar power levels and scales. While among the four representative

feedstock, the pine, red oak and horse manure all produced similar overall system efficiencies that can be classified in a single category of woody biomass. As to the cardboard feedstock which can represent the general category of paper and paperboard materials in the municipal solid waste produced the lowest overall efficiency that is basically resulted from the lowest heating value of cardboard generated syngas.

$$\eta_{gasifier} = \frac{Calorific\ value\ of\ syngas\ \ per\ mol}{Calorific\ value\ of\ 1\ mol\ of\ \ feedstock} \tag{3-25}$$

$$\eta_{engine} = \frac{P_{measured}}{(Q_{LHV} \cdot \dot{m}_{syngas})\eta_{gen}} \tag{3-26}$$

$\eta_{gen}, \eta_{engine}$ is the efficiency of the generator and engine respectively. The efficiency of the generator was assumed at 95% in the current work. The efficiency for the overall integrated system, $\eta_{overall\ system}$ can be estimated by the following equation,

$$\eta_{overal\ system} = \eta_{gasifier} \cdot \eta_{engine} \cdot \eta_{gen} \tag{3-27}$$

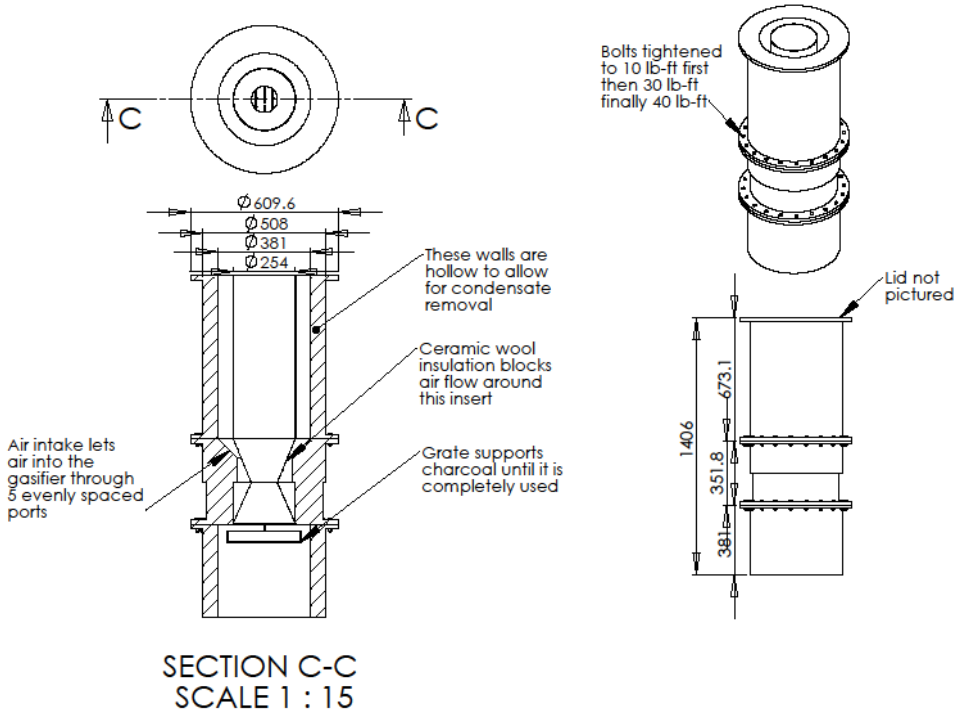

Figure 3-1. Schematic of the gasifier mounted on the pilot scale system

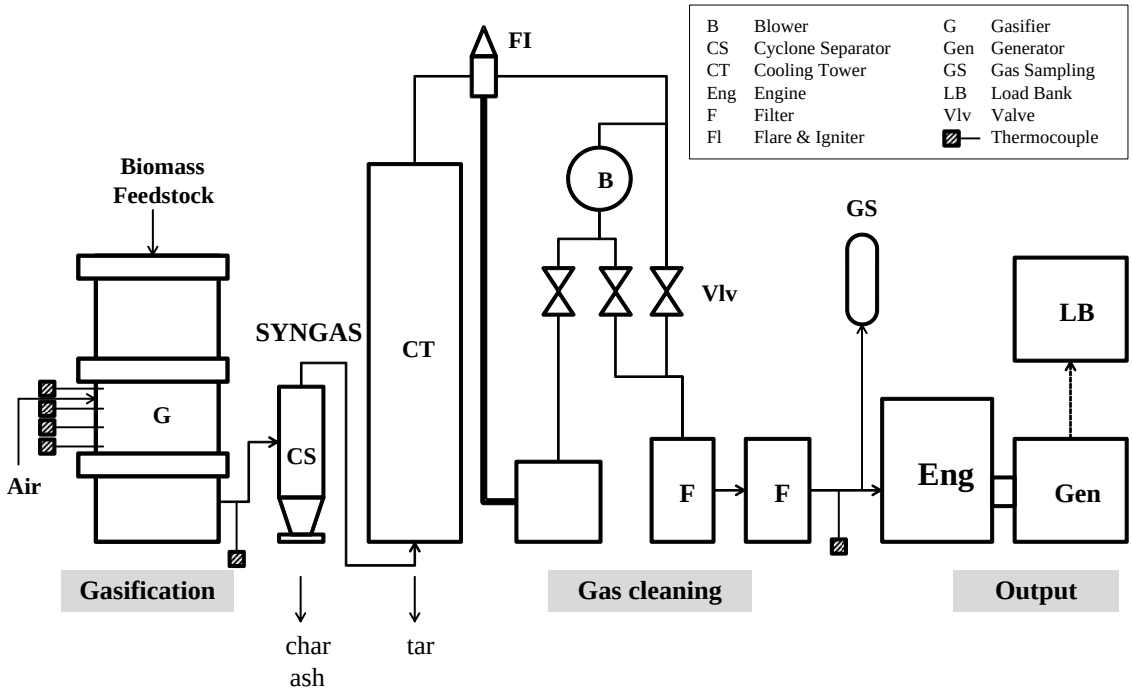

Figure 3-2. Portable pilot scale gasifier system components

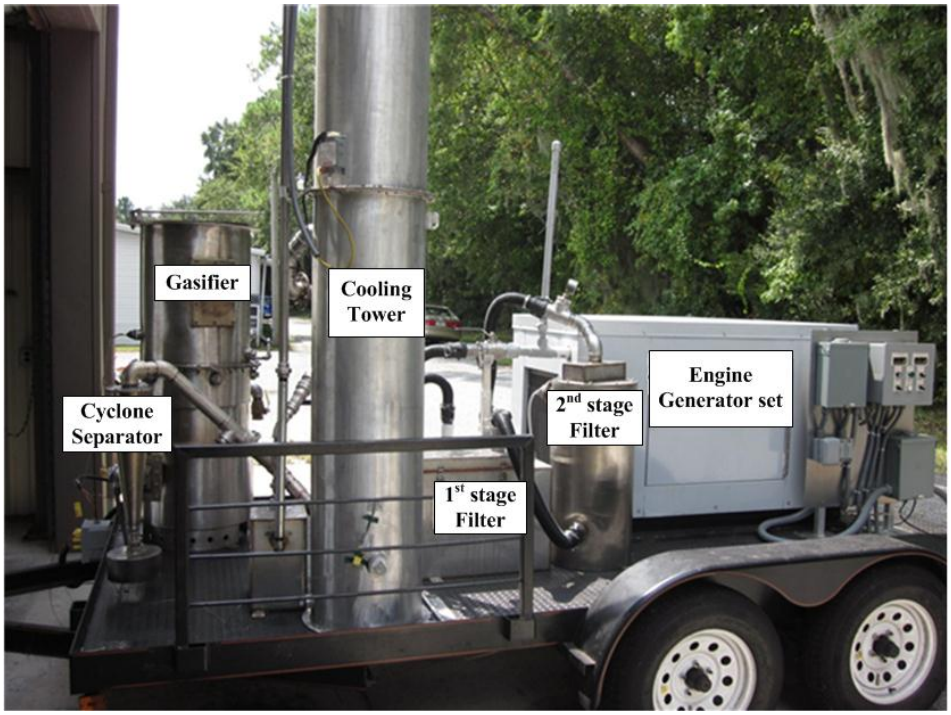

Figure 3-3. Portable pilot scale system. Photo courtesy of Elango Balu.

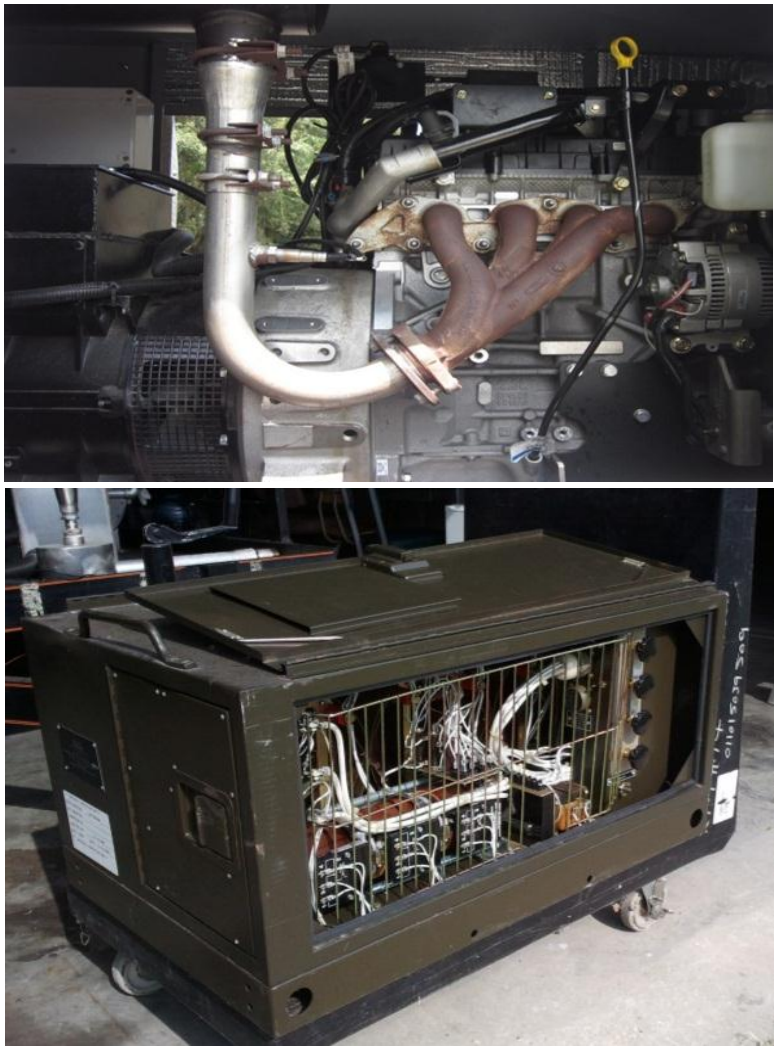

Figure 3-4. Load components A) Engine B) Load bank. Photo courtesy of Elango Balu.

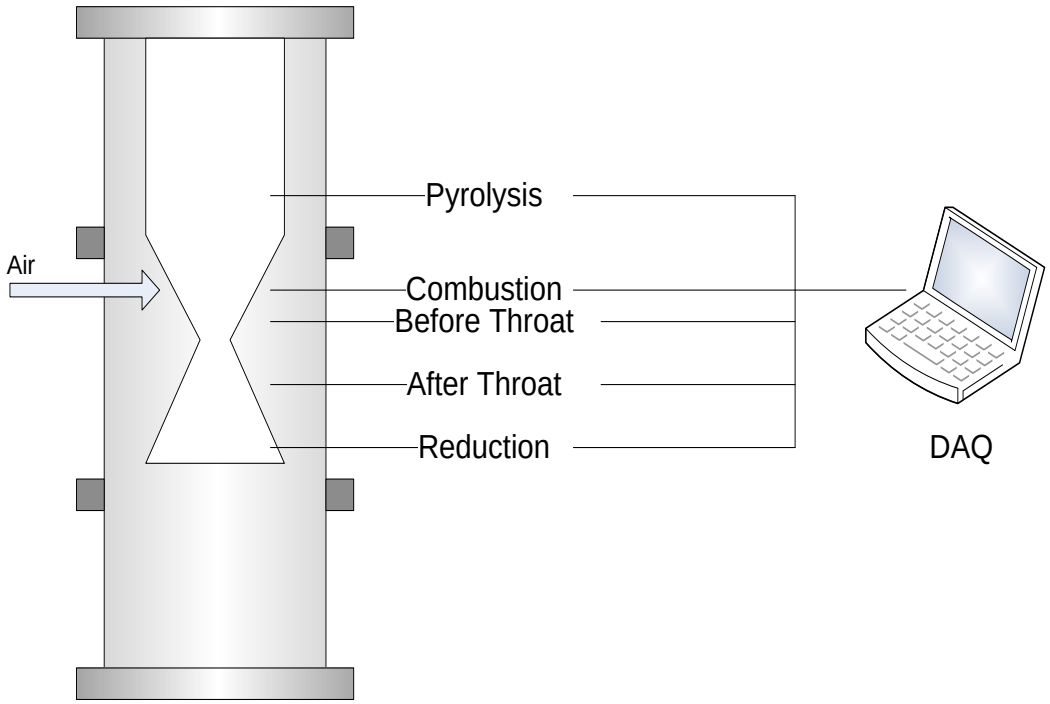

Figure 3-5. Pictorial representation of K-type thermocouples inside the gasifier.

Table 3-1. Experimental conditions and parameters for pilot scale system.

	Pine	Horse manure	Red oak	Card board
Test condition				
Ambient temperature [°C]	28.6	29.1	28.7	29.6
Relative humidity [%]	83.6	84.8	81.7	81.7
Moisture content[%]	12.2	18.33	14.8	12.6
Ultimate analysis [wt %] [60][61]				
C	52.7	48.6	49.6	48.6
H	6.1	5.8	6.62	6.2
O	41.2	44.3	43.8	45
N	~	0.9	~	0.11
S	~	0.14	~	0.13
HHV [KJ/Kg]	20721	19370	20230	18450
LHV [KJ/Kg]	19388	18140	18728	17097
Feedstock Loading [kg]	7.11	8.55	5.86	5.96
Charcoal Loading [kg]	2.04	1.91	2.08	1.94
Air Feed Rate [m^3/hr]	1290	1235	1326	1891
Syngas data				
Syngas flow rate [m^3/min]	0.57	0.65	0.68	0.71

Table 3-2. A, B, C, D, E, F, G, H for individual species @ T < 1000 °C from [50]

Species	H_2	CO	CO_2	$H_2O_{(g)}$	CH_4	$H_2O_{(l)}$
A	18.5631	25.56759	24.99735	30.092	-0.70303	-203.606
B	12.2574	6.09613	55.18696	6.832514	108.4773	1523.29
C	-2.8598	4.054656	-33.6914	6.793435	-42.5216	-3196.413
D	0.26824	-2.6713	7.948387	-2.53448	5.862788	2474.455
E	1.97799	0.131021	-0.13664	0.082139	0.678565	3.855326
F	-1.1474	-118.009	-403.608	-250.881	-76.8438	-256.5478
G	156.288	227.3665	228.2431	223.3967	158.7163	-488.7163
H	0	-110.527	-393.522	-241.826	-74.8731	-285.8304

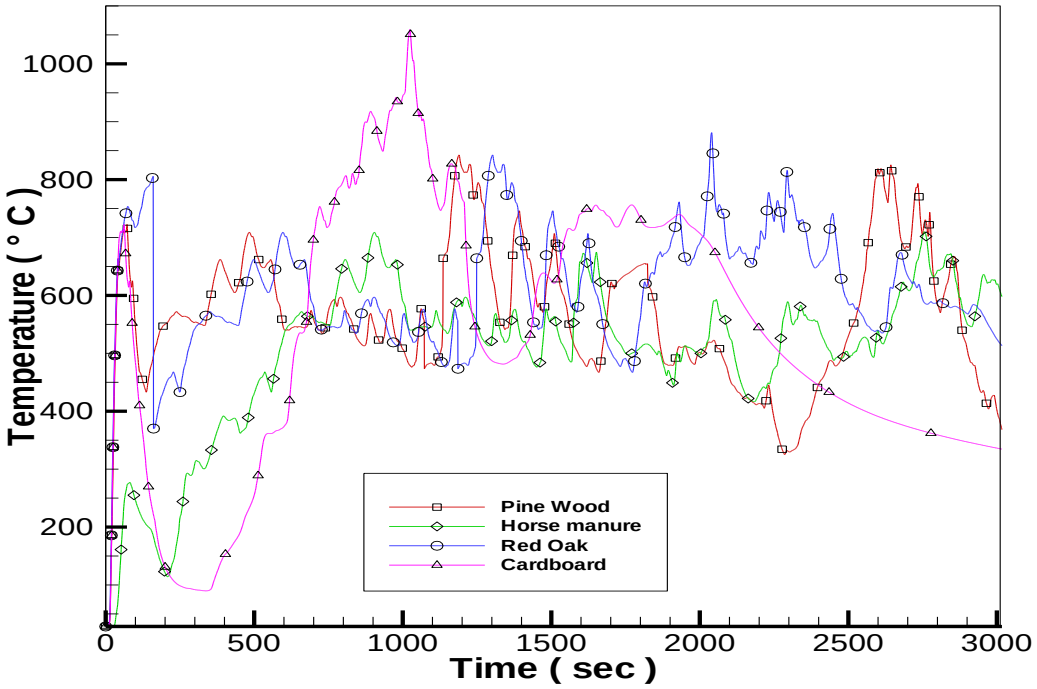

Figure 3-6. Temperature distribution inside the gasifier - pyrolysis zone

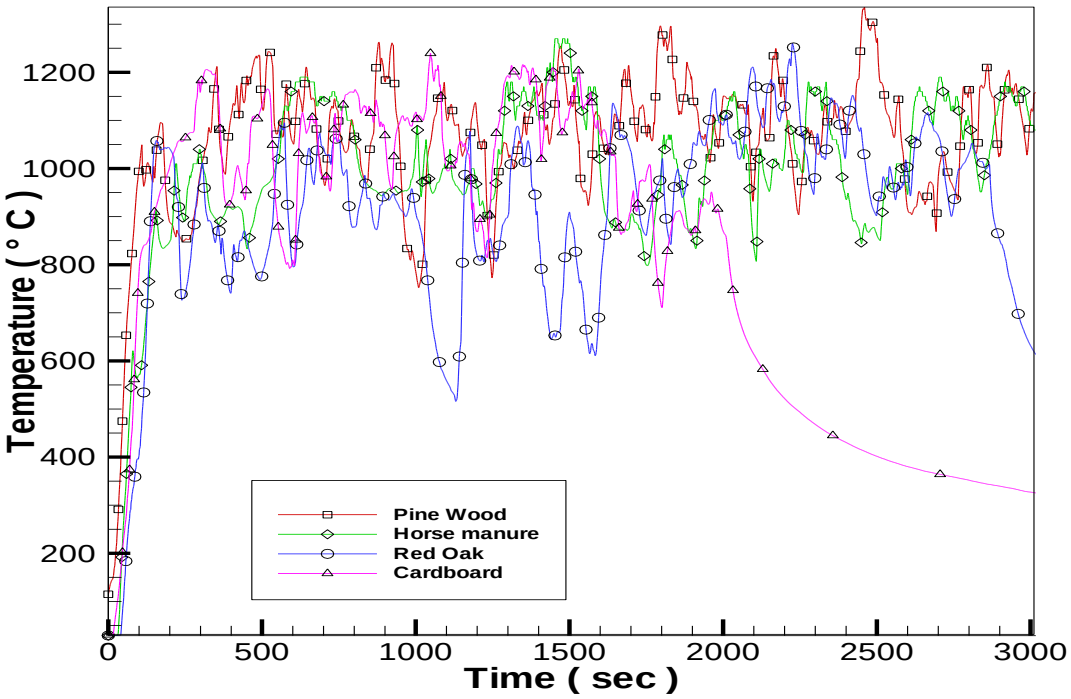

Figure 3-7. Temperature distribution inside the gasifier - combustion zone

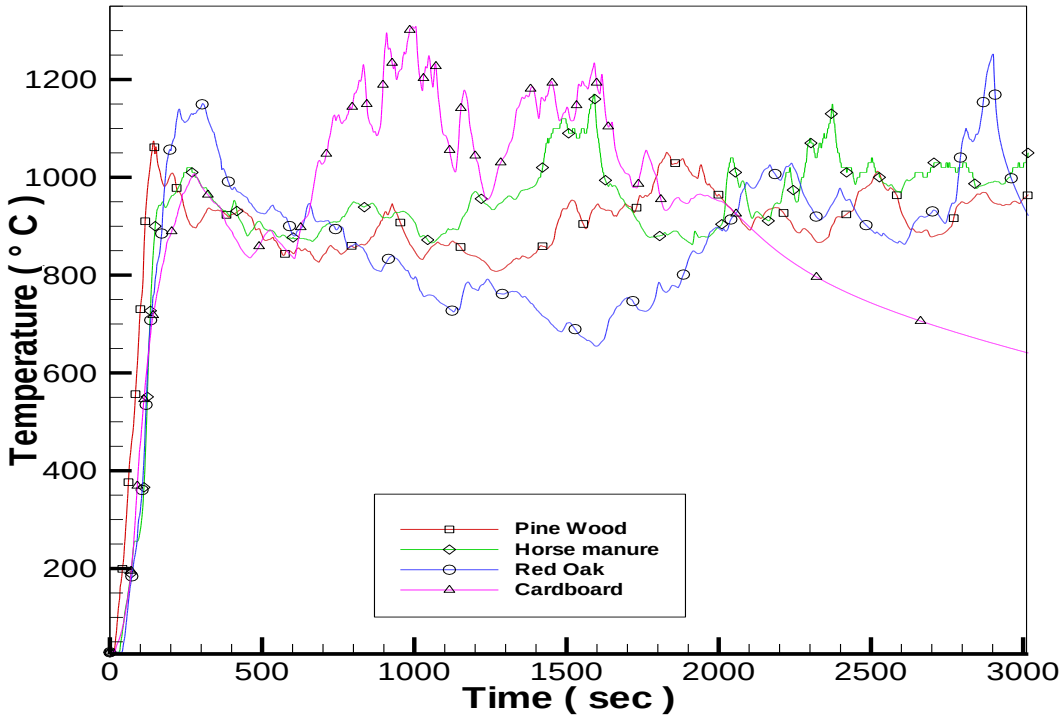

Figure 3-8. Temperature distribution inside the gasifier - before throat

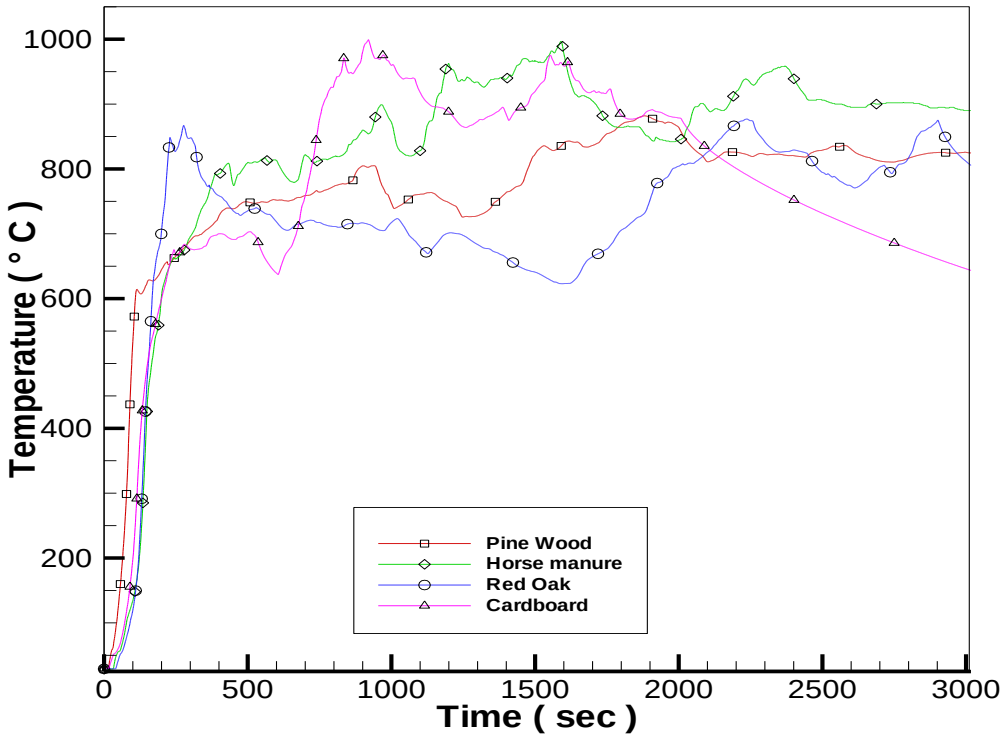

Figure 3-9. Temperature distribution inside the gasifier - after throat

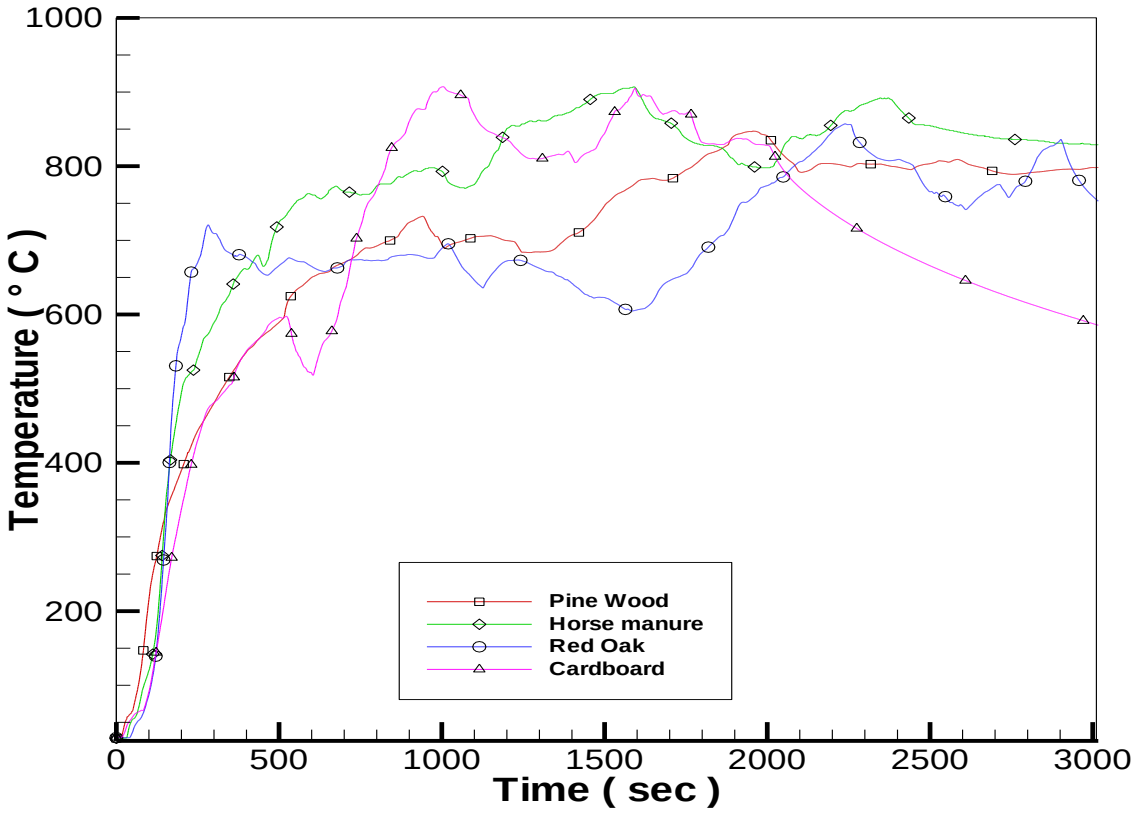

Figure 3-10. Temperature distribution inside the gasifier - reduction zone

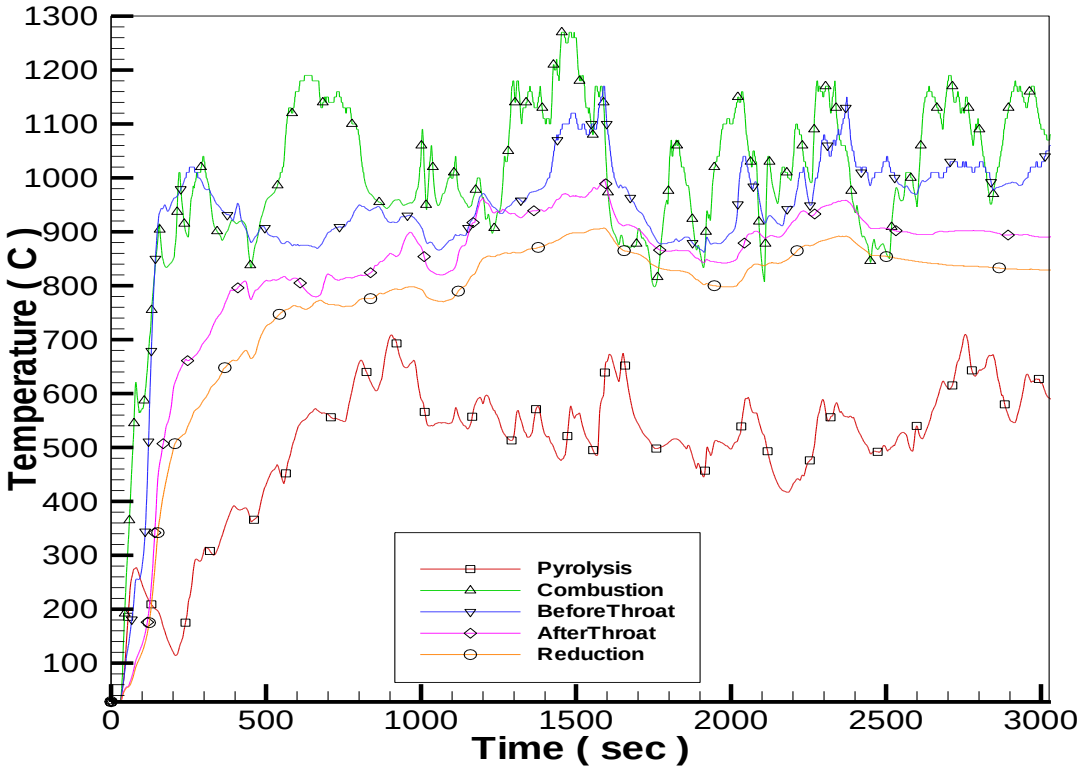

Figure 3-11. Temperature distributions inside the gasifier in all zones for horse manure

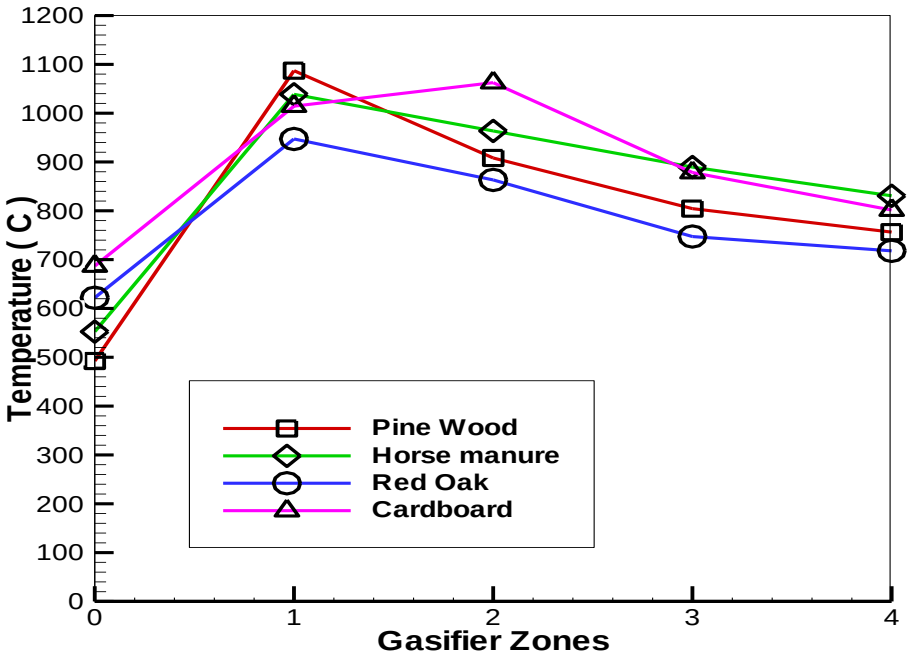

Figure 3-12. Average temperatures inside the gasifier in all zones for four feedstock

Table 3-3. Average gasifier zone temperature (°C)

		Pine	HM	Red Oak	CB
Pyrolysis	Zone:0	492.43	552.57	621.97	686.99
Combustion	Zone:1	1087.11	1038.57	947.12	1014.35
Before Throat	Zone:2	908.20	963.52	863.24	1062.54
After Throat	Zone:3	804.51	889.63	747.38	878.43
Reduction	Zone:4	756.34	830.71	717.96	801.54

Table 3-4. Comparison of equilibrium constants calculated @ 1273 K.

Reactions	Model 1	Model 2	Model 3	Current Model
$CO+H_20 = CO_2+H_2$	0.558	0.607	0.568	0.604
$CH_4+H_2O = CO +3H_2$	8835	8861	8624	9250.85
$C+H_20 = CO +H_2$	94.71	82.71	82.55	95.61

Table 3-5. 20% moisture, 1073 K, No heat added, wood waste, model results

Gas Comp. % v/v	Model 1	Model 4	Current Model
H_2	18.44	21.06	20.13
CO	17.46	19.61	18.52
CO_2	13.13	12.01	12.79
CH_4	0.00	0.64	0.02
N_2	50.96	46.68	48.53
Total	100	100	100

Table 3-6. 10% moisture, 1073 K, No heat added, wood waste, model results.

Gas Comp % v/v	Model 1	Model 5	Model 6	Current Model
H_2	19.8	20.06	21.4	18.52
CO	23.45	19.7	23	20.78
CO_2	9.16	10.15	9.74	11.12
CH_4	0.01	0.00	0.01	0.02
N_2	47.57	50.1	45.31	49.56
Total	100	100.01	99.56	100

Table 3-7. Syngas estimated from current model @ 1173 K, No heat added.

Feedstock	Species	N	MW g/mol	Vol %	M	Wt %	Species LHV MJ/Kg	Syngas LHV MJ/Kg
Pine	H_2	0.7011	2	20.20	1.40	1.76	120.00	2.11
	CO	0.6842	28	19.71	19.16	23.98	10.10	2.42
	CO_2	0.3157	44	9.10	13.89	17.39		0.00
	H_2O	0.4117	18	11.86	7.41	9.28		0.00
	CH_4	9E-05	16	0.00	0.00	0.00	50.00	0.00
	N_2	1.3583	28	39.13	38.03	47.60		0.00
		3.47		100.00	79.90	100.00		4.53
Horse	H_2	0.6909	2	21.90	1.38	1.93	120.00	2.32
	CO	0.7326	28	23.22	20.51	28.71	10.10	2.90
Manure	CO_2	0.2673	44	8.47	11.76	16.46		0.00
	H_2O	0.3207	18	10.16	5.77	8.08		0.00
	CH_4	0.0001	16	0.00	0.00	0.00	50.00	0.00
	N_2	1.1437	28	36.25	32.02	44.82		0.00
		3.16		100.00	71.45	100.00		5.22
Red	H_2	0.748	2	22.17	1.50	1.97	120.00	2.37
	CO	0.721	28	21.37	20.19	26.64	10.10	2.69
Oak	CO_2	0.2788	44	8.27	12.27	16.19		0.00
	H_2O	0.3681	18	10.91	6.63	8.74		0.00
	CH_4	0.0001	16	0.00	0.00	0.00	50.00	0.00
	N_2	1.2576	28	37.28	35.21	46.46		0.00
		3.37		100.00	75.80	100.00		5.06
Cardboard	H_2	0.6452	2	18.57	1.29	1.58	120.00	1.89
	CO	0.6688	28	19.25	18.73	22.91	10.10	2.31
	CO_2	0.3311	44	9.53	14.57	17.83		0.00
	H_2O	0.4065	18	11.70	7.32	8.95		0.00
	CH_4	7E-05	16	0.00	0.00	0.00	50.00	0.00
	N_2	1.4225	28	40.94	39.83	48.73		0.00
		3.47		100.00	81.74	100.00		4.21

Table 3-8. Syngas composition from experiments and model comparison

	Pine		Horse Manure		Red Oak		Cardboard	
	H_2	CH_4	H_2	CH_4	H_2	CH_4	H_2	CH_4
Experimental Value Volume %	15	5	20	3	17	1.5	11	3
Model Prediction Volume %	20.2	0	21.9	0	22.1	0	18.5	0

Table 3-9. Overall system efficiency

Authors	Feedstock	Engine Type	Engine rpm	Power [kWe]	Overall Efficiency %
Current work	Pine	SIICE*	1800	11.76	24.8
Current Work	Red Oak	SIICE	1800	13.10	21.2
Current Work	Horse Manu	SIICE	1800	10.14	22.3
Current work	Cardboard	SIICE	1800	9.60	17.6
Martínez et al. [56]	Wood	Diesel	1500	12-16	21-24
Henriksen et al. [57]	Wood Chips	Diesel	NA	15-20	25

CHAPTER 4
EXPERIMENTAL AND NUMERICAL INVESTIGATION OF HIGH TEMPERATURE STEAM ONLY (BENCH SCALE) GASIFICATION SYSTEM

4.1 Bench Scale Gasifier System Experimental Setup

The bench scale steam gasifier system shown in Figure 4-2 was designed and built by the current research group for carrying out gasification experiments using high temperature steam. The basic design based on the flow of the gas path is an updraft gasifier where the steam and the biomass are fed from the bottom and the resultant syngas rises up and exits at the top. Fig 4-3 shows the initial gasification setup that was tested and gasifier itself is made of a set of modules which can be assembled to vary the volume of the gasifier. The picture shows a two module set. This setup was modified with cylindrical shorter tubes to account for the amount of time it took to get the module stacks to consistent temperature and the time taken to fill the internal volume with the low flow rate of steam produced from the steam generator. Figure 4-1 shows a 3-D drawn module set just for illustration purposes demonstrating the provision for the grate placement and the steam injector. The modules were designed in such a way that the hollow stainless steel chamber is fitted on the inside with concentric high and low density alumina to withstand extremely high temperatures. This also played a significant role in modifying the design since it took a lot of steam and time to heat through the insulation and provide a steady gasification temperature inside the chamber. But this setup proved to be very energy intensive and time consuming to bring the temperature in the chamber close to the conditions needed for experiments.

The gasifier exit is connected to a gas cleaning system consisting of the gas cooling coil and the liquid condensate collector where the steam and other particulates would settle down after being cooled down in the cooling coil. At the end of the cooling

coil is the gas sampling and exhaust port controlled by a valve to allow the respective operation to be carried out. Gas samples were collected using sampling bags with vacuum pulled in it, to ensure fast retrieval of syngas and contamination issues while analyzing the gas composition because nitrogen and carbon monoxide have the same peaks at 28.

Since this steam gasifier needs external heat supply in the form of steam, the system contains a steam generator and a super heater to provide the necessary gasifying agent. The steam generator is capable of producing 1Kg/hr of steam at 1300 °C when operating at full power. The water reservoir equipped with a pump provides the water supply to the steam generator which produces steam and then it is further superheated in the ceramic super heater furnace. The control system allows precise control of the amount of steam being supplied and the temperature at which it is introduced in to the gasifier.

The final stage of preparing the steam gasifier is under way and to make this system a continuously operated system a feeder screw system is implemented to introduce the feedstock in to the gasifier as a controlled operation. Further the feed screw should be tested by measuring the amount of feedstock introduced in to the gasifier chamber to control the amount of turns on the screw required to match the desired amount of feedstock. This continual feed screw when developed fully would give us a very good source of data to validate the modeling which assumes continuous gasification process.

The startup would be with initiating the steam generator and once there is steam generation at the required rate, the super heater is turned on to heat the steam to the

desired temperature and is introduced in the gasification chamber. Once the chamber is heat treated, feedstock would be introduced in the lower module using the feed screw. Thermocouples mounted on the modules continuously record the temperature distribution in the gasifier using a data acquisition panel (DAQ).

Once gasification reactions takes place, the syngas produced moves up the gasifier and is further cooled down in the cooling coil allowing any particulates/tar and steam to condense and collect in the collector. And sampling bags would be used to collect syngas for analysis at different time intervals to study how the composition evolves over the course of gasification in the chamber.

4.2 Steam Only Gasification Model

The steam gasification model is further improved than the previous model, in this case instead of assuming the gasification temperature, the temperature at which the gas components exit the gasifier are determined along with the volumetric composition of gas species. All these are calculated based on the temperature of the steam that is being supplied to the gasifier and the STBM (Steam to Biomass Ratio).

$$CH_XO_Y + wH_2O + m\left(H_2O_{steam}\right) \Rightarrow a_1H_2 + a_2CO + a_3CO_2 + a_4H_2O + a_5CH_4 \quad (4\text{-}1)$$

So in this case the equilibrium constant described in the previous section are compiled as a function of the gasification temperature and similarly the enthalpy of the individual gas species in the exit are also compiled as a function of the gasification temperature that is determined based on the equilibrium reaction calculations. The equilibrium constants would remain the same since the same equations are chosen for this model as well but the expression would differ as shown below because of the

absence of air. C balance would be the same but the mole balance of H and O will be different because of the absence of air and the addition of steam on the input side.

Carbon Balance:

$$a_2 + a_3 + a_5 - 1 = 0 \quad (4\text{-}2)$$

Hydrogen Balance:

$$2*a_1 + 2*a_4 + 4*a_5 - X - 2*w - 2*m = 0 \quad (4\text{-}3)$$

Oxygen Balance:

$$a_2 + 2*a_3 + a_4 - Y - w - m = 0 \quad (4\text{-}4)$$

The equilibrium constant for methane decomposition can be written in terms of the moles of the participating species,

$$K_1 = \frac{[CO] * [H_2]^3}{[CH_4] * [H_2O]} \quad (4\text{-}5)$$

Similarly the equilibrium constant for water gas shift reaction can be written as,

$$K_2 = \frac{[CO_2]*[H_2]}{[CO]*[H_2O]} \quad (4\text{-}6)$$

$$K_1 = (a_1^3 * a_2 / a_5 * a_4) \times (4/(a_1 + a_2 + a_3 + a_4 + a_5)^2) \quad (4\text{-}7)$$

While expanding K1 would not have the moles of nitrogen since there is steam only on the input side. And further the energy equation would also be modified to suit the steam gasification conditions.

$$H^0_{f\,Bio} + w*(H^0_{f_{H_2O}} + H_{vap}) + m*(H^0_{f_{steam}}) = a_1*\left(H^0_{f_{H2}} + \int_{T_0}^{T_G} C_{p_{H2}}\,dT\right)$$
$$+ a_2*\left(H^0_{f_{CO}} + \int_{T_0}^{T_G} C_{p_{CO}}\,dT\right)$$
$$+ a_3*\left(H^0_{f_{CO_2}} + \int_{T_0}^{T_G} C_{p_{CO_2}}\,dT\right)$$
$$+ a_4*\left(H^0_{f_{H_20}} + \int_{T_0}^{T_G} C_{p_{CO_2}}\,dT\right)$$
$$+ a_5*\left(H^0_{f_{CH_4}} + \int_{T_0}^{T_G} C_{p_{CH_4}}\,dT\right) \quad (4\text{-}8)$$

The methodology to solve the equations are similar to the previous model but with these modified equations the constants for calculating the equilibrium constants also varies accordingly since the Air gasification model operated in temperatures lower than 1000 °C.In steam gasification model the constants are chosen in the range of 1000 °C and above to suit the high temperature regime in steam gasification and the constants could also be modified to account for steam at lower temperatures than 1000°C . Table 4-1 lists the constants chosen for calculating the parameters needed for the calculations at high temperatures above 1300°C.

4.3 Results and Discussions

In this section, the results obtained from the equilibrium model and the experiments would be analyzed in details and the comparisons would also be shown to establish the consistency of the model in predicting the gas composition.

First, the results of the model at very high temperatures are discussed to show the potential of high temperature steam gasification. Figure 4-4 through Figure 4-7 shows clearly that when the temperature of the gasifying agent, steam is increased the

STBM (steam to biomass) ratio at which there is no solid carbon exists goes down. The models were developed to handle even the presence of solid carbon at lower STBM for different gasification temperatures. But since at high gasification temperatures the solid carbon is fully converted to gas components after a certain STBM, the range of values were chosen such that there is no solid carbon in the product side. As we increase the steam temperature the dry gas composition of hydrogen also increases but the trend is much evident at 1500 °C and 2000 °C As we increase the steam temperature the dry gas composition of hydrogen also increases but the trend is much evident at 1500 °C and 2000 °C but there is not much of a clear difference in the maximum concentration of hydrogen when the temperature is further increased.

The very high temperature models were used only to see the trend in the increase in the gasification temperature but once the bench scale unit was fully modified the models were run based on the experimental conditions as input to simulate the actual gasification process more closely. The model is also evaluated for 3 different steam inlet conditions, at 800 °C, 900 °C and 1000 °C to make sure the model is able to predict the gas compositions in the operating range of the gasifier since using the furnace at full temperature poses serious risk of damaging the heating coils over a prolonged period of time.In each case the composition of the product gas was calculated and the results have been compiled and compared with each other to understand the evolution/decay of different gas species with respect to STBM as the inlet temperature is varied and the results from the lower steam temperature rang has been compared with experimental values. Similar to the molar values, the mole fraction of the gas species is also plotted for the different inlet temperatures of the steam used for gasification. And it is clear from

the fact that the production of hydrogen flattens out with increase in the STBM as the entire available CO and CH_4 are converted to hydrogen and resulting in the production of CO_2 from WGS and MGS reactions.

It is evident from the Fig 4-8 through Fig 4-10 that the H_2 moles increases with steam temperature for the same STBM and as a result more H_2O is converted to H_2 and it could be seen in the drop in moles of H_2O for the same STBM as steam temperature increases from T1 to T3

Similar to the H_2 moles, the no of moles of CO and CO_2 also increases with steam inlet temperature for the same STBM, indicating that the heating content of the syngas would be increased significantly due to the production of more H_2 and CO as we increase the inlet steam conditions for the same STBM. The air gasification model did not take in to consideration the presence of Solid carbon and as a result always underestimated the amount of CH_4 in product gas. This is because tar cracking leads to the production of CH_4 and this model captures this aspect very well. As seen in Fig 4-10, that compares the moles for all three inlet conditions, the methane concentration drops down once the solid carbon goes to zero, indicating the fact that the amount of methane produced from tar cracking diminishes as the source vanishes after a certain STBM in all 3 cases and the STBM at which solid carbon vanishes decreases with temperature due to the high heat content available for cracking. This is show in Fig 4-10, where the solid carbon ceases to exist after STBM ~ 1.3 in all three cases.

From the analysis it is clear that higher steam inlet temperature and higher STBM results in improving the H_2 and CO content in the product gas. And also eliminates the

presence of solid carbon which might not be suitable in many applications where purity of product gas is a top priority.

Fig 4-12 through Fig 4-14 shows the mole fractions (dry) of the gas species for the three inlet steam temperatures over a varying STBM.In this it is very clear to see the concentrations of the combustible gas components and as expected the amount of H_2 flattens out after a certain STBM in each case, since there is only a certain amount of feedstock to be gasified at each point in the process. Fig 4-15 compares the dry mole fractions for all three inlet conditions for the same STBM range and the advantage of higher steam temperature can be seen at lower range of STBM.

Fig 4-16 shows the surface plot of the hydrogen mole fractions calculated from the equilibrium model and clearly predicts the increase in hydrogen production with increase in STBM and steam temperature. Similarly the increase in CO production at lower STBM with respect to the increase in steam inlet temperature is also captured by the equilibrium model as shown in Fig 4-17.As discussed in previous chapter, the methane concentration is always under estimated due to the omission of solid carbon in the equilibrium calculations but, in this steam model the tar cracking is also considered and hence the amount of methane produced from this tar cracking is also estimated. This can been seen clearly in Fig 4-18 which shows higher concentrations of methane at lower STBM and steam temperature and drops off as the steam temperature and STBM increases, indicating that the production of methane decays after the conversion of all solid carbon in the gasifier, which usually happens at higher STBM and steam inlet temperatures.

Further the experiments were also conducted using the setup to validate the model consistency. The woody biomass .was tested in two different runs to give a considerable sample size for comparison purposes and in the first run 3 gas samples were collected to be analyzed using the GC and in run 2 6 samples and in run3 8 samples were collected to closely mimic the continuous evolution of gas species in the reactor.

Fig 4-19 shows the concentrations of the gas species collected from the 3 gas samples during the course of gasification. The data points were curve fit to show the trend in the evolution/decay of different species and the LHV of each sample is also plotted simultaneously to show the advantage of using steam gasification as compared to that of air gasification, where the LHV was in the range of 4-5 MJ/Nm3 and in case of steam only gasification it could be 2-3 times that value.

Fig 4-20 shows the concentrations and LHV of the 6 samples collected during run2 and is also similar to run 1 in terms of species evolution/decay over the course of gasification. Fig 4-21 shows the plot of gas concentrations from the exit syngas collected over the course of the process in 8 different samples. Here the data points look far off the curve fit due to the fact that there were two instances when the feedstock was introduced and it could be seen that from samples 1 t04 and 4 to 8 the trend is similar to the previous two experimental runs with one feedstock cycle. The values of these are also listed in Table 4-2, Table 4-3, and Table 4-4.

To compare the results of the model and experimental runs, the mole fractions (dry) from the model results for all inlet conditions of steam were plotted for lower range of STBM as the experimental STBM values calculated were in this lower range. Fig 4-22

shows the concentrations in the lower STBM range and they match very well with the experimental results in terms of composition for all the individual species the difference in the values of CO and CO_2 between the model and experimental results is because of the fact that model assumes perfect equilibrium and most CO/CH_4 is converted to H_2 .Whereas in experimental state this is not entirely true and there is still CO/CH_4 left in the gas stream and thus the concentrations from the gas samples have lower H_2 in turn. The consistency of the two approaches can be further validated by plotting the LHV values of the model results as in Fig 4-23 and it can be seen that the experimental and model result agree in the lower range of 4-6 STBM , where the LHV is approximately between 8-10 MJ/Nm^3 as calculated from the GC analysis.

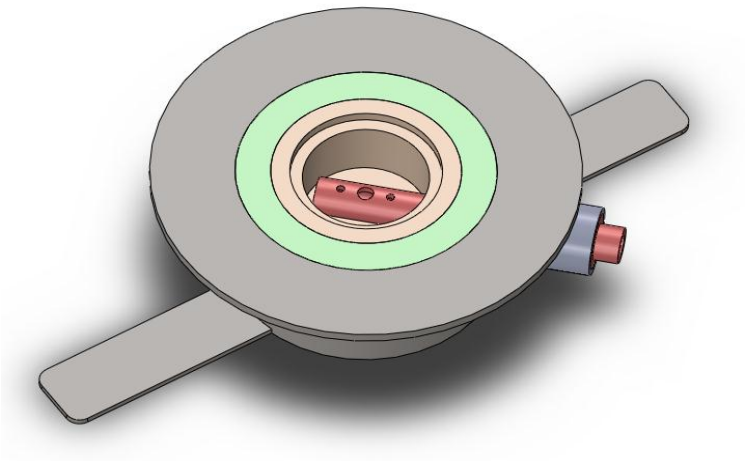

Figure 4-1. 3D-Module stack that was tested and later replaced due to high thermal inertia

Figure 4-2. Initial bench scale system setup. Photo courtesy of Uisung Lee.

Figure 4-3. Modified bench scale gasifier schematic. Photo courtesy of Uisung Lee.

Table 4-1. A, B, C, D, E, F, G, and H for individual species @ T > 1000 °C from [50]

Species	H_2	CO	CO_2	$H_2O_{(g)}$	CH_4	$H_2O_{(l)}$
A	18.5631	35.1507	58.16639	30.092	85.81217	-203.606
B	12.2574	1.300095	2.720074	6.832514	11.26467	1523.29
C	-2.8598	-0.205921	-0.492289	6.793435	-2.114146	-3196.413
D	0.26824	0.01355	0.038844	-2.53448	0.13819	2474.455
E	1.97799	-3.28278	-6.447293	0.082139	-26.42221	3.855326
F	-1.1474	-127.8375	-425.9186	-250.881	-153.5327	-256.5478
G	156.288	231.712	263.6125	223.3967	224.4143	-488.7163
H	0	-110.5271	-393.5224	-241.826	-74.8731	-285.8304

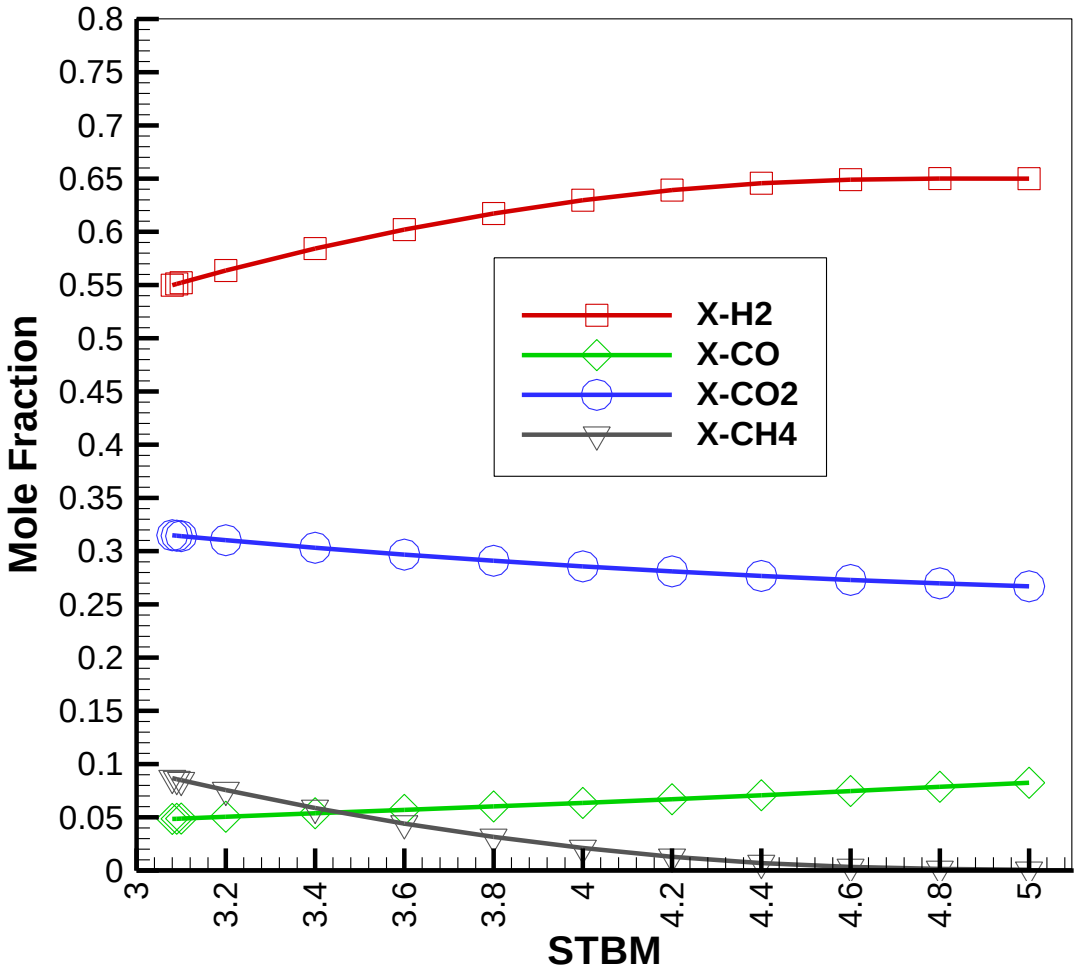

Figure 4-4. Syngas mole fractions predicted by equilibrium model for woody biomass at 1500°C steam inlet

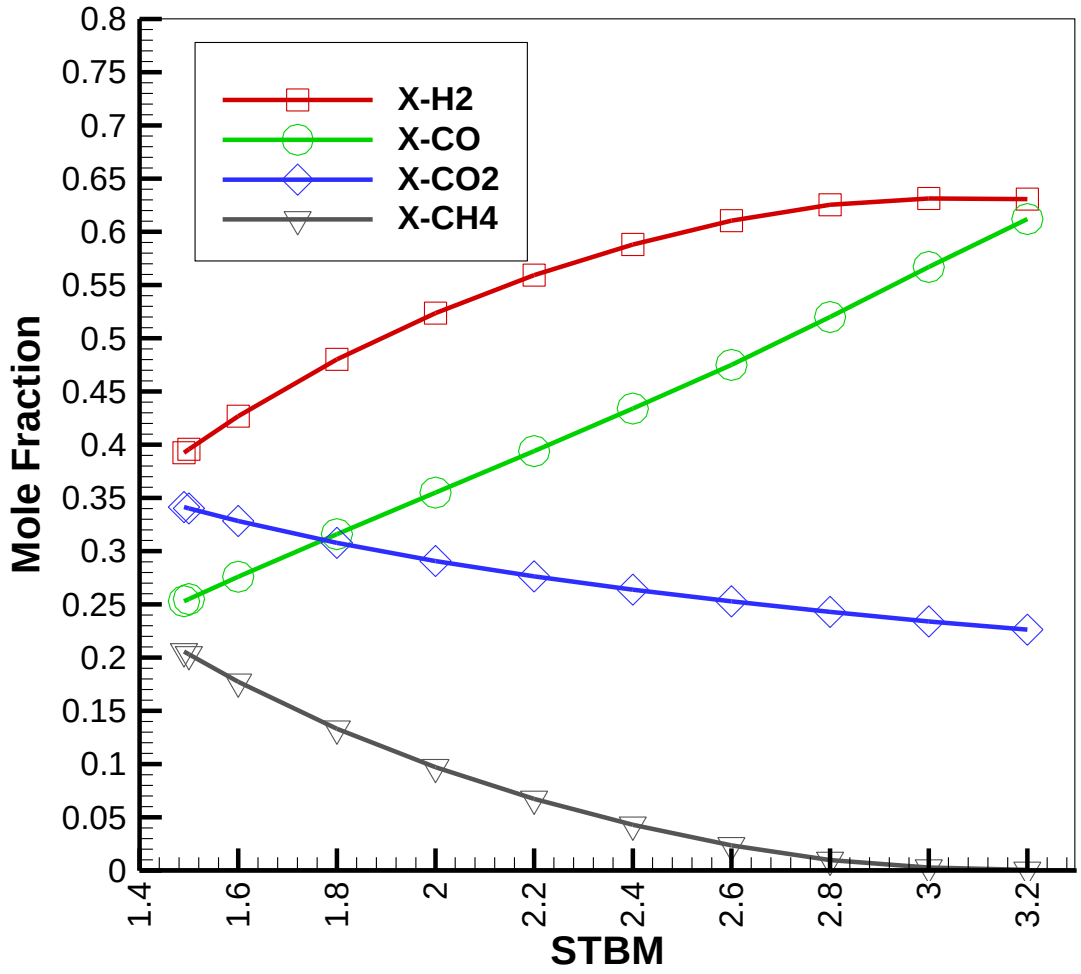

Figure 4-5. Syngas mole fractions predicted by equilibrium model for woody biomass at 2000°C steam inlet

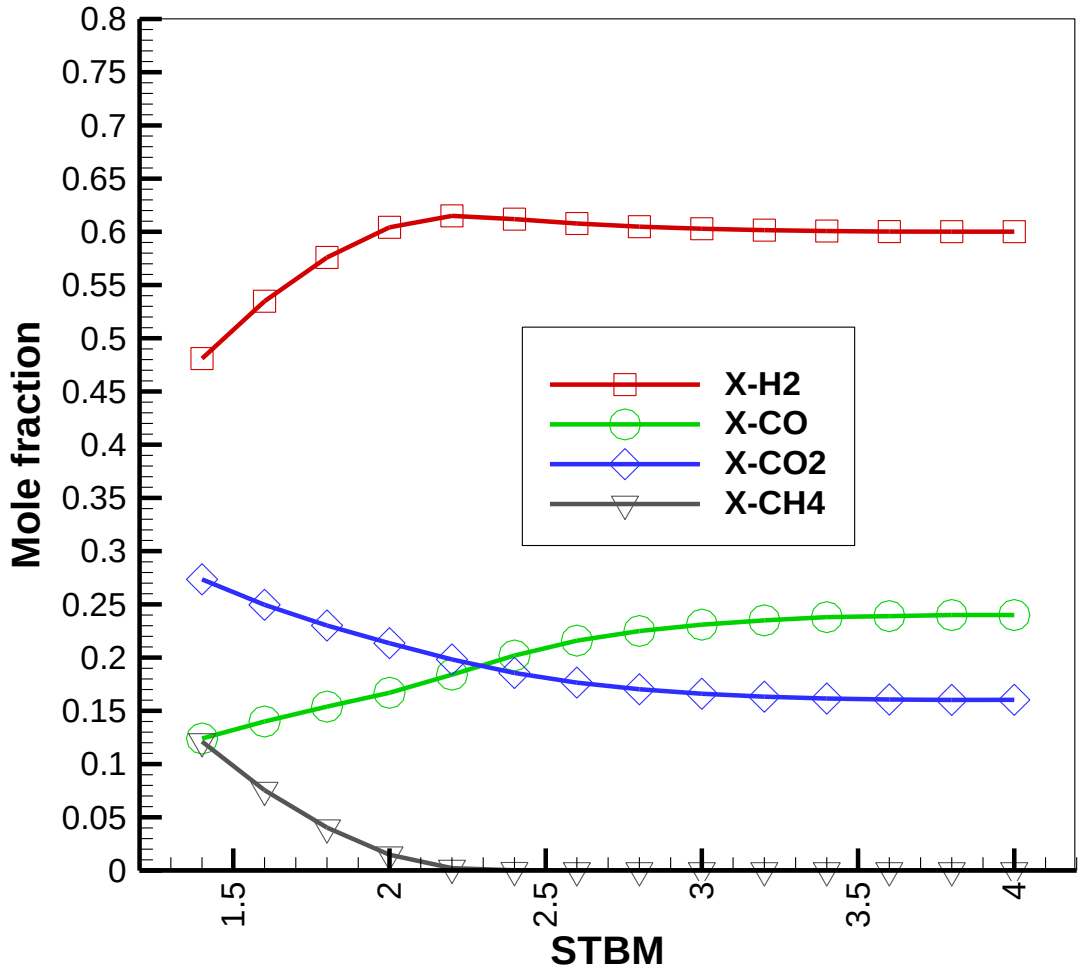

Figure 4-6. Syngas mole fractions predicted by equilibrium model for woody biomass at 2500°C steam inlet

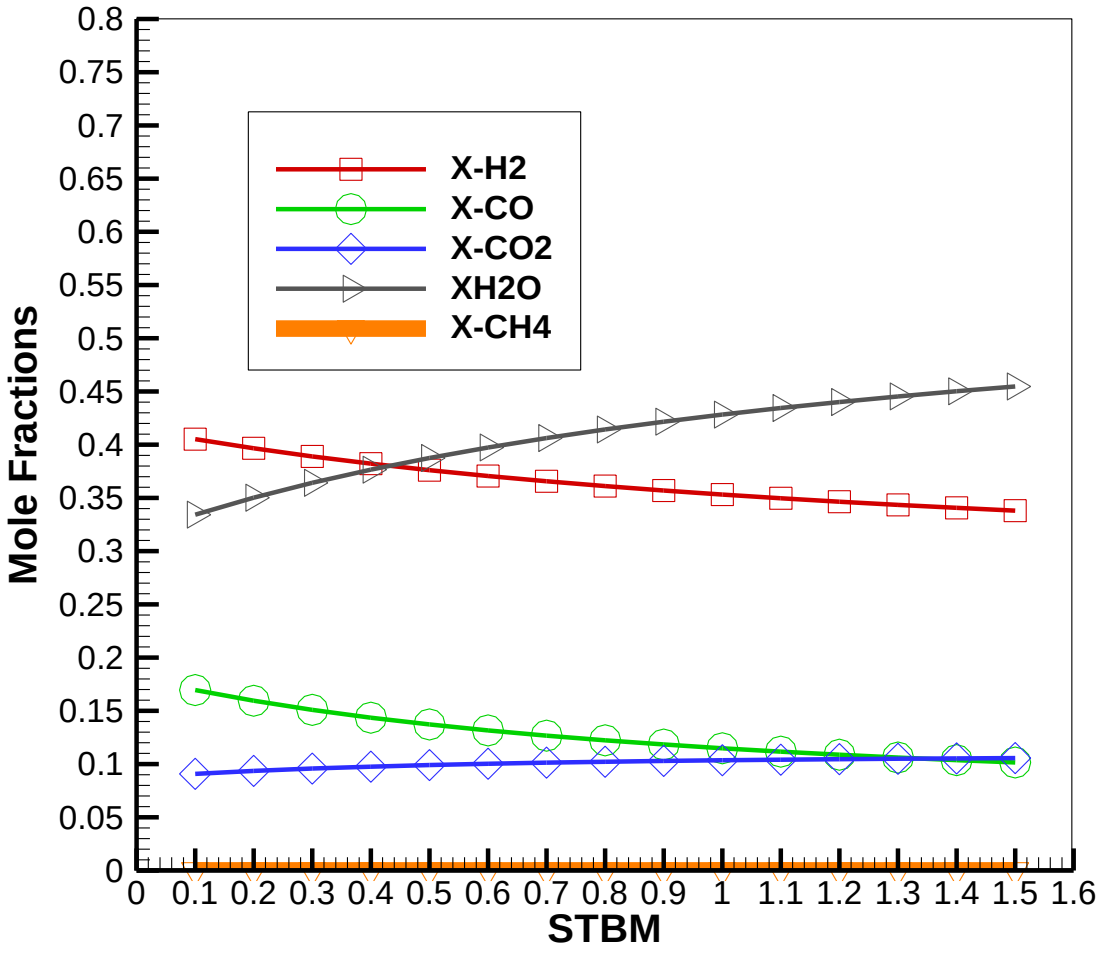

Figure 4-7. Syngas mole fractions predicted by equilibrium model for woody biomass at 1500°C steam inlet, at lower STBM where solid carbon exists.

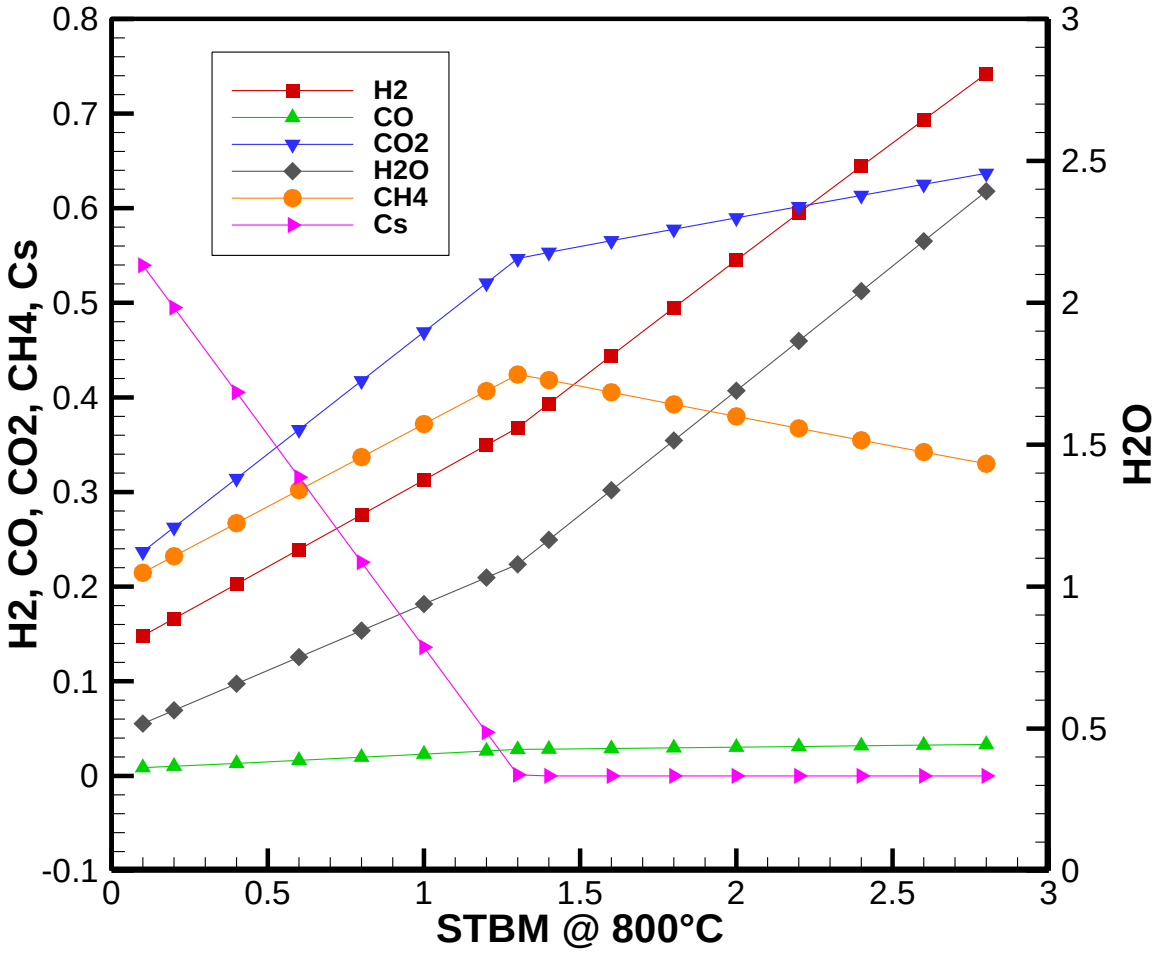

Figure 4-8. Number of moles of syngas produced per mole of feedstock $CH_{1.5}O_{0.67}$, predicted by equilibrium model @ 800°C steam inlet.

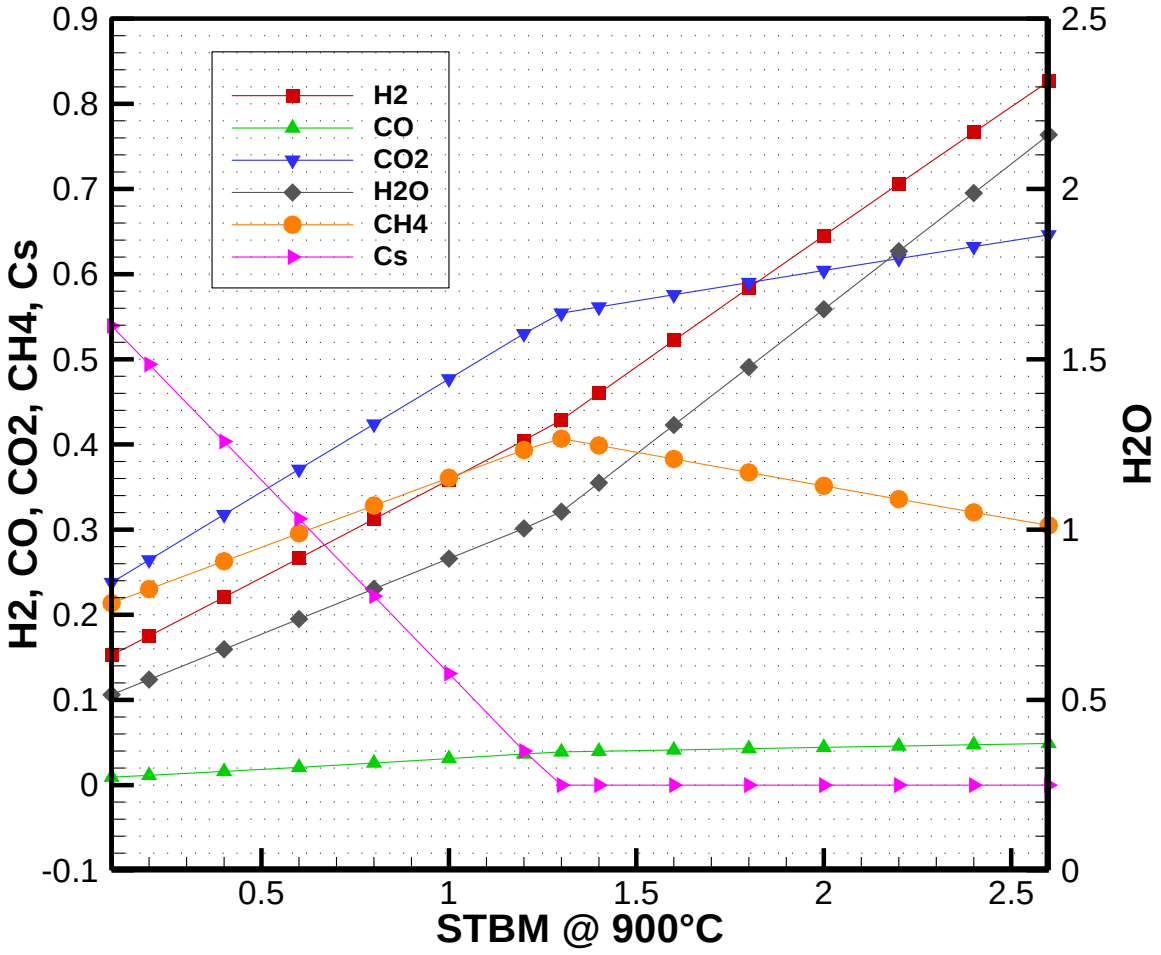

Figure 4-9. Number of moles of syngas produced per mole of feedstock $CH_{1.5}O_{0.67}$, predicted by equilibrium model @ 900°C steam inlet.

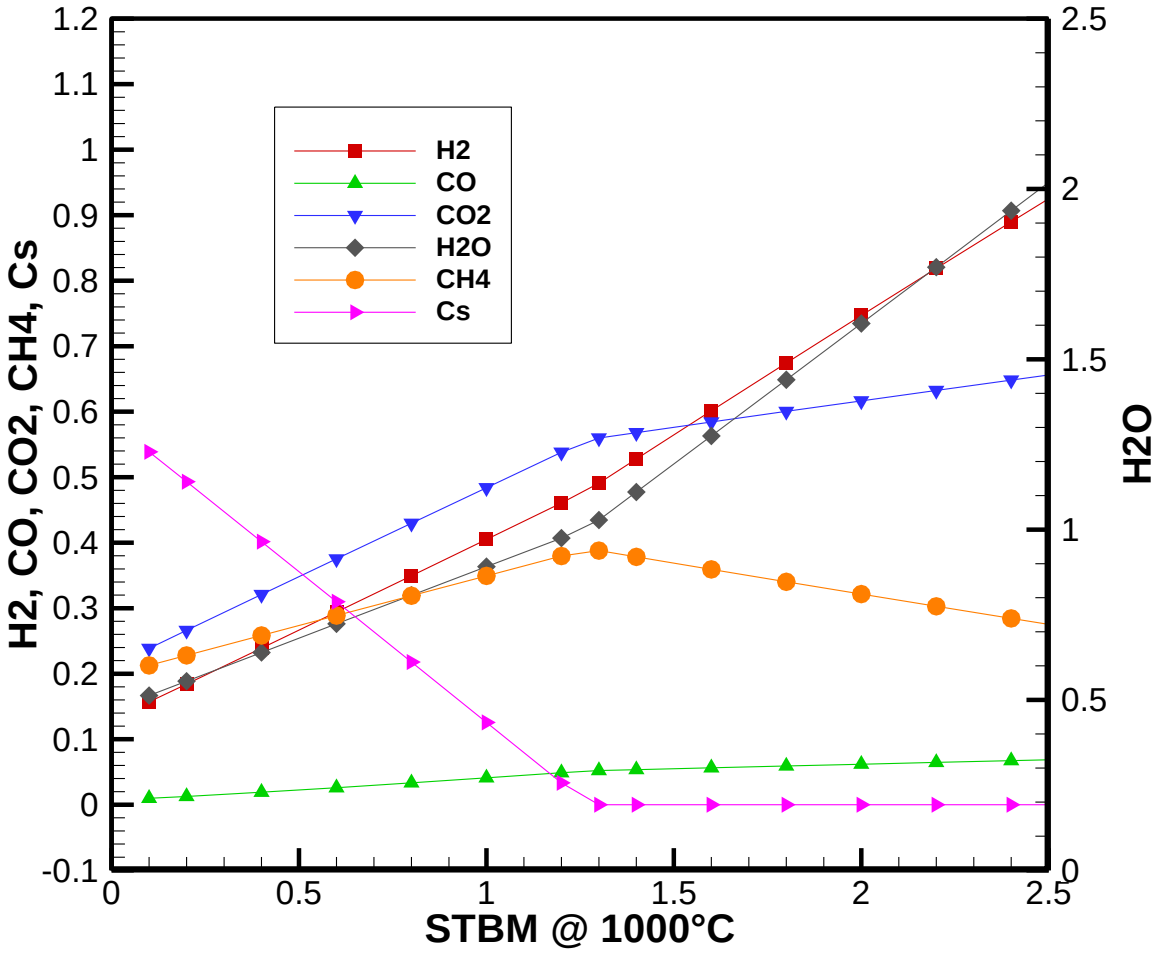

Figure 4-10. Number of moles of syngas produced per mole of feedstock $CH_{1.5}O_{0.67}$, predicted by equilibrium model @ 1000°C steam inlet.

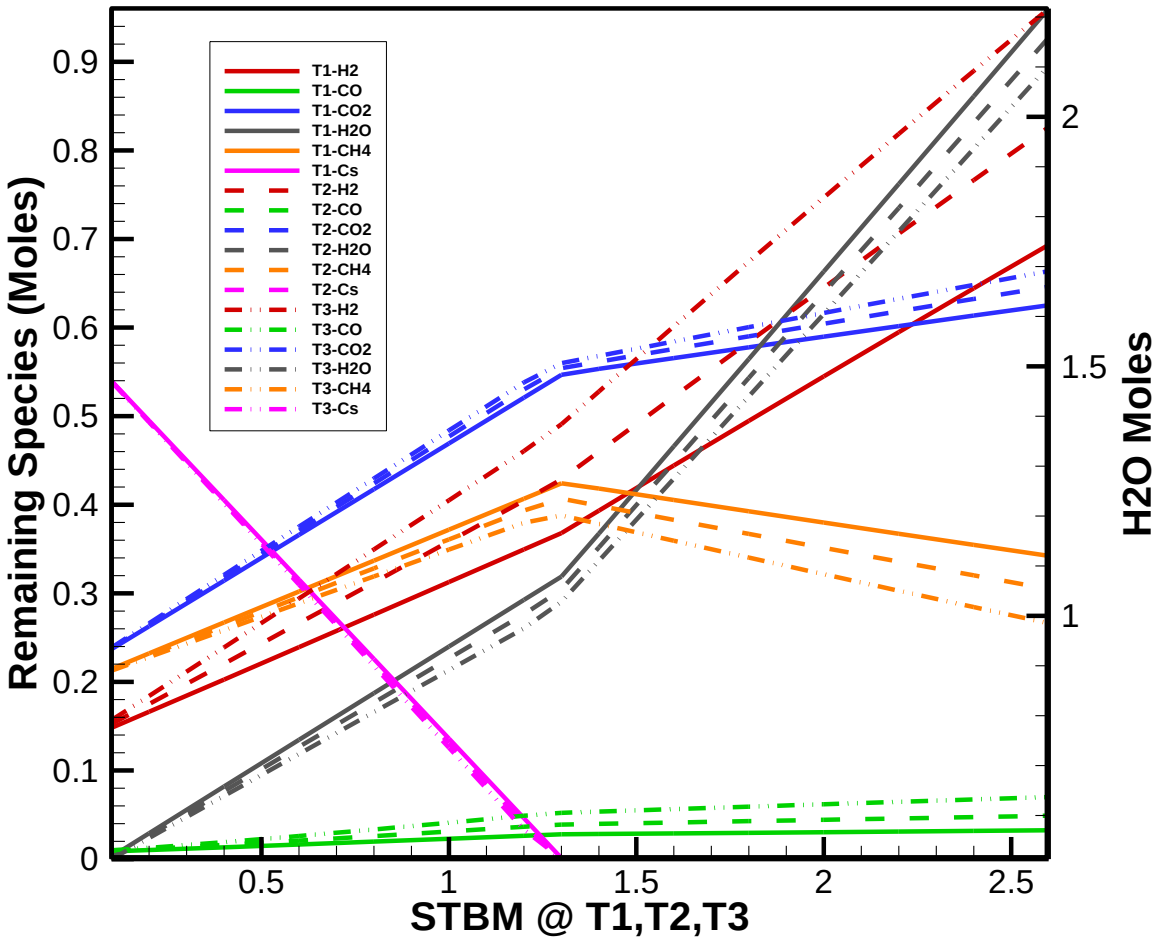

Figure 4-11. Number of moles of syngas produced per mole of feedstock $CH_{1.5}O_{0.67}$, predicted by equilibrium model @ 800°C, 900°C and 1000°C steam inlet – comparison.

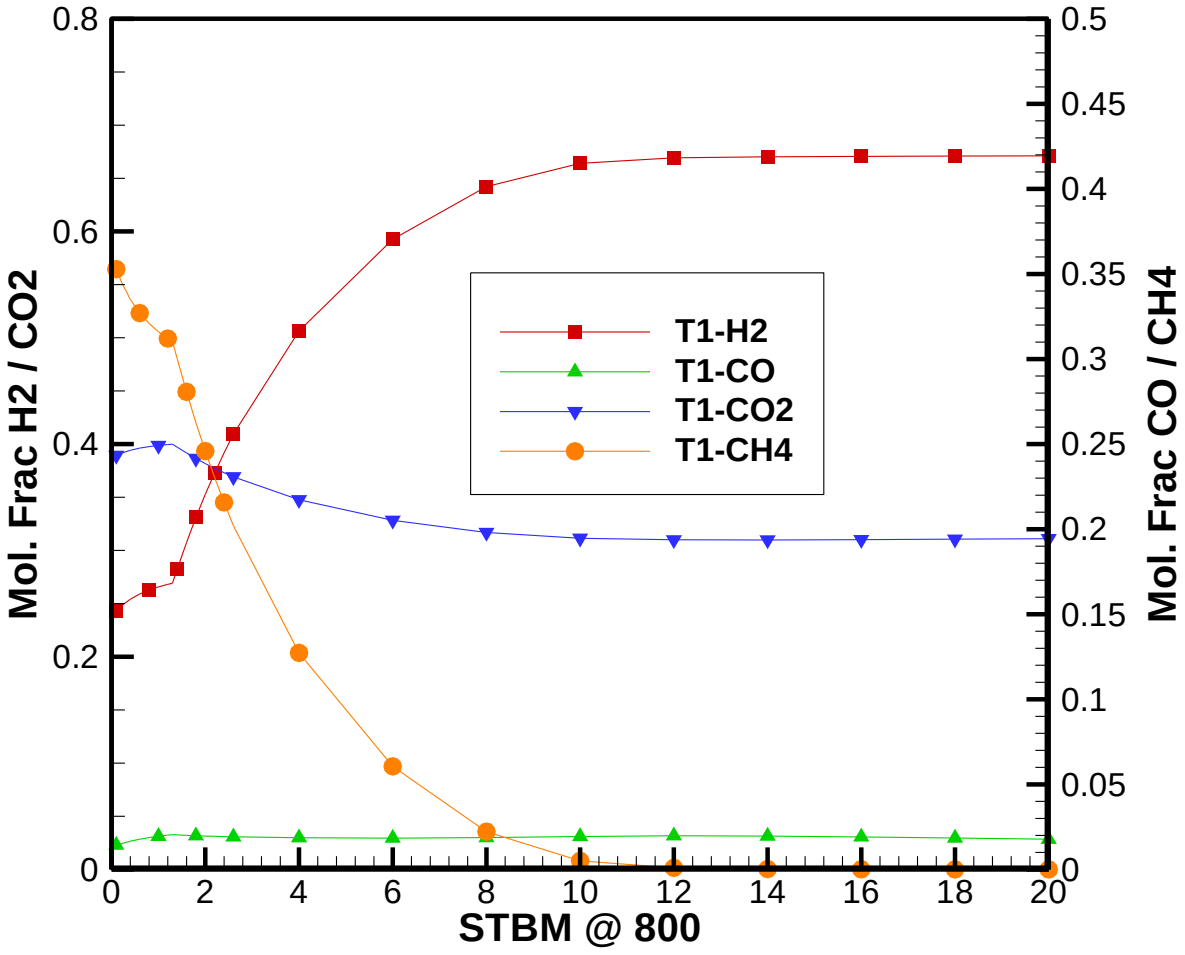

Figure 4-12. Syngas mole fractions predicted by equilibrium model at 800°C steam inlet for feedstock $CH_{1.5}O_{0.67}$.

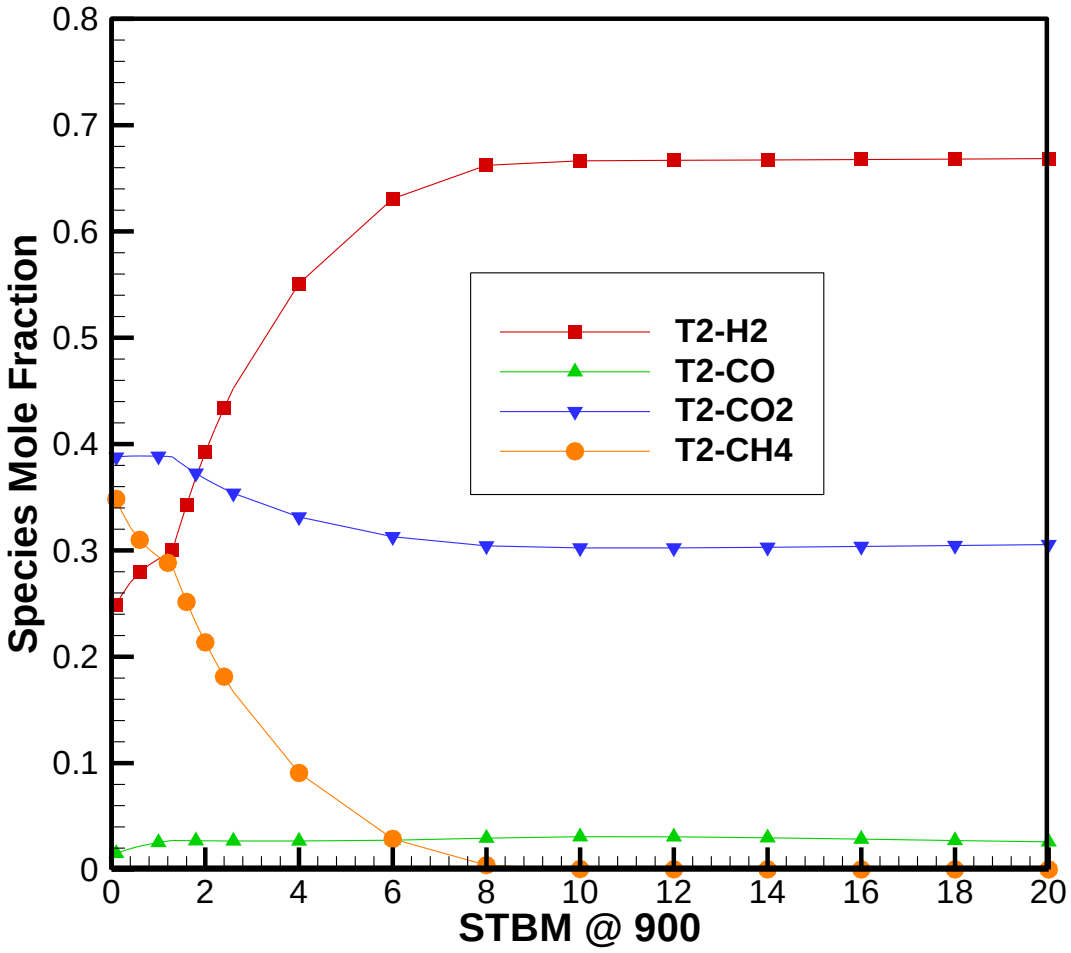

Figure 4-13. Syngas mole fractions predicted by equilibrium model at 900°C steam inlet for feedstock $CH_{1.5}O_{0.67}$.

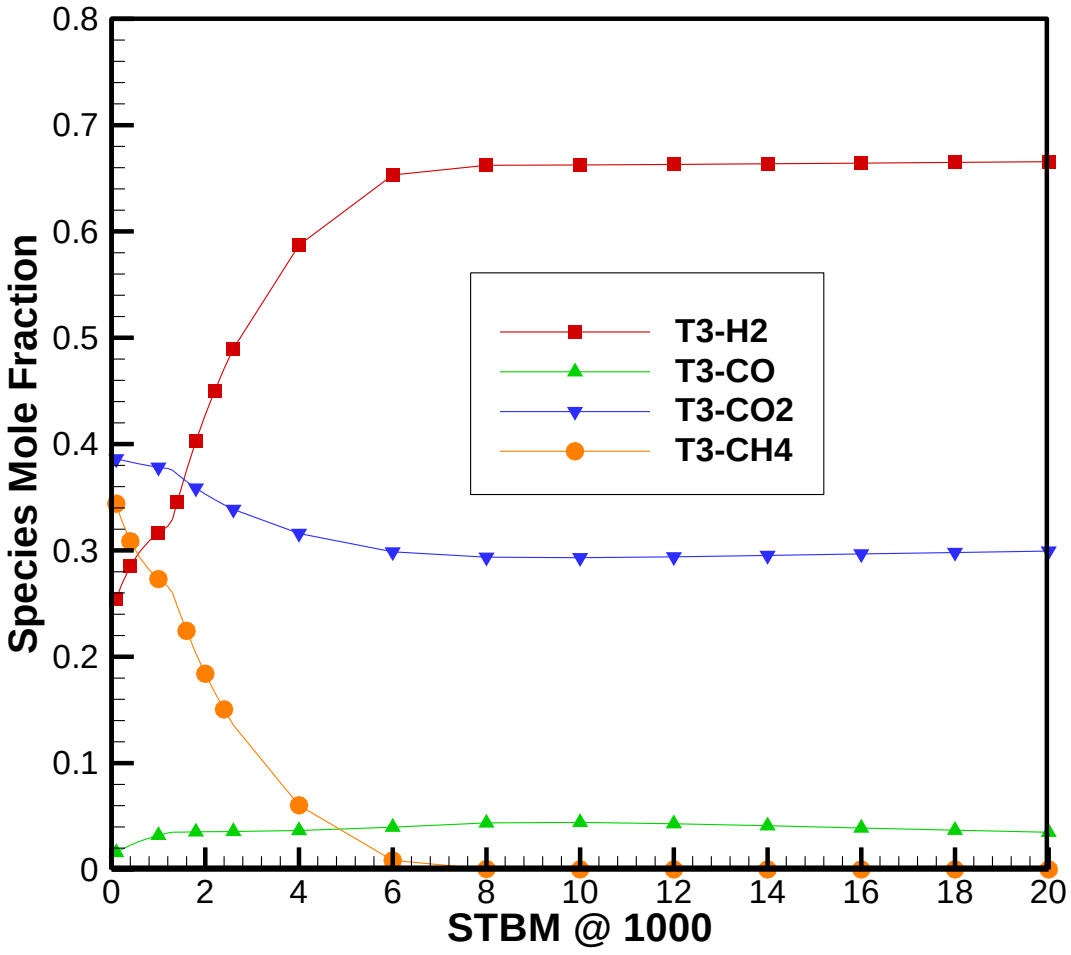

Figure 4-14. Syngas mole fractions predicted by equilibrium model at 1000°C steam inlet for feedstock $CH_{1.5}O_{0.67}$.

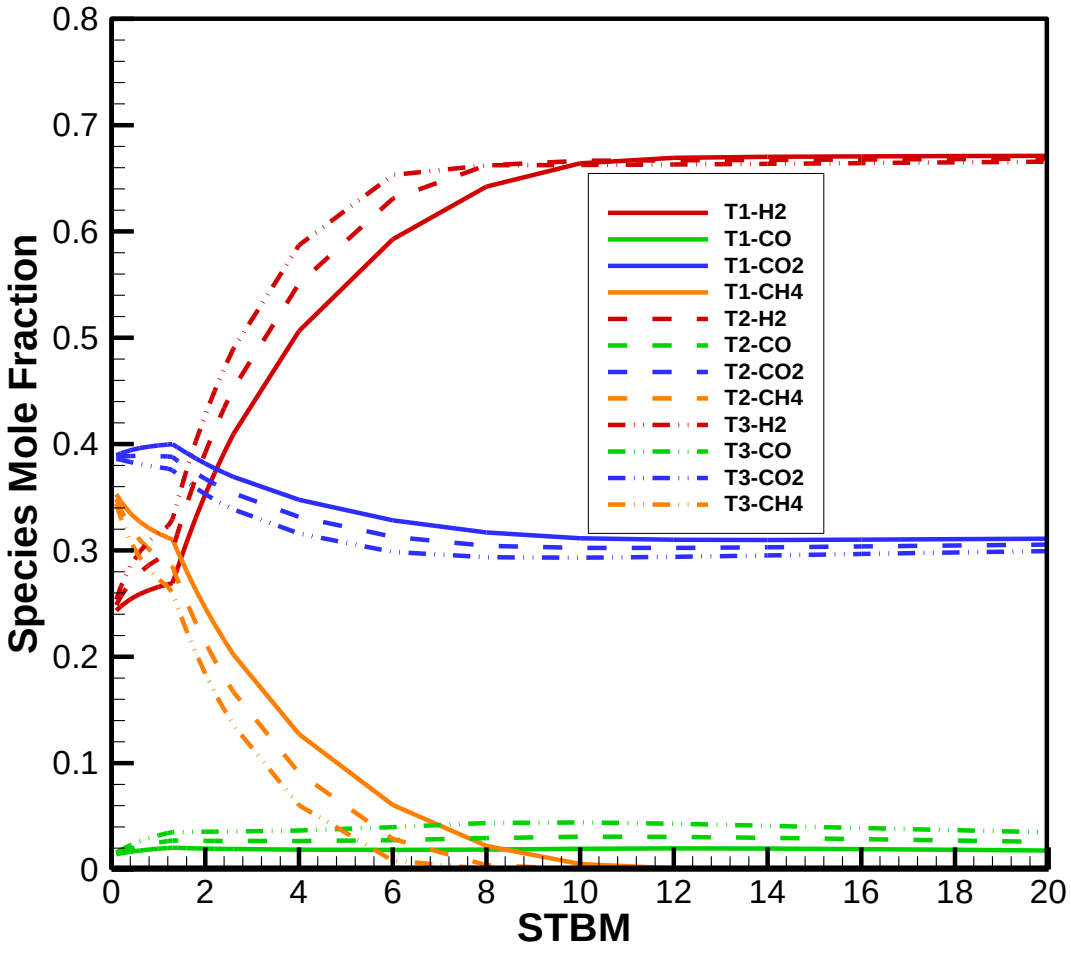

Figure 4-15. Syngas mole fractions predicted by equilibrium model at 800°C, 900°C and 1000°C steam inlet (T1, T2 and T3 respectively) – comparison, for feedstock $CH_{1.5}O_{0.67}$.

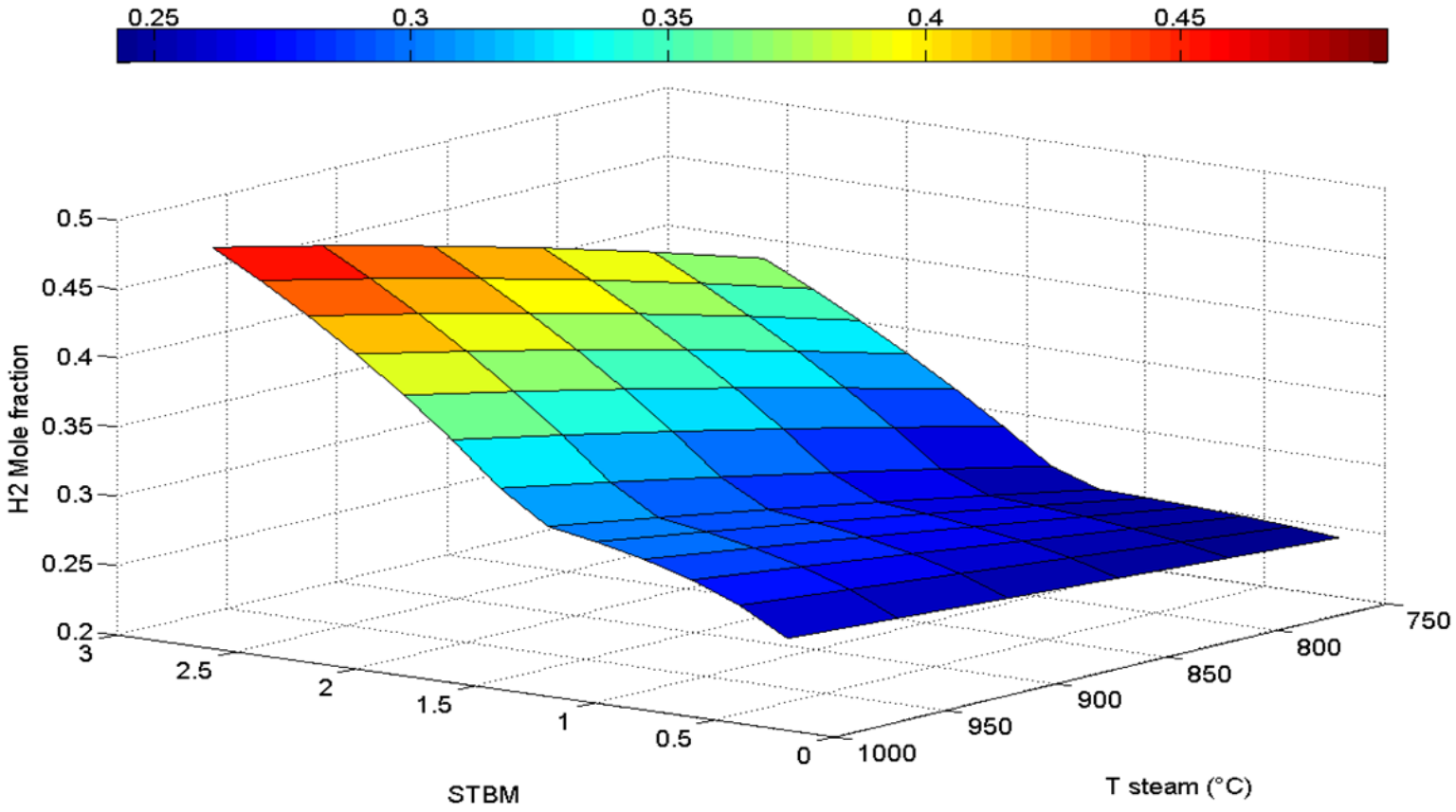

Figure 4-16. Surface plot of hydrogen mole fractions at varying STBM and steam temperatures from equilibrium model for feedstock $CH_{1.5}O_{0.67}$.

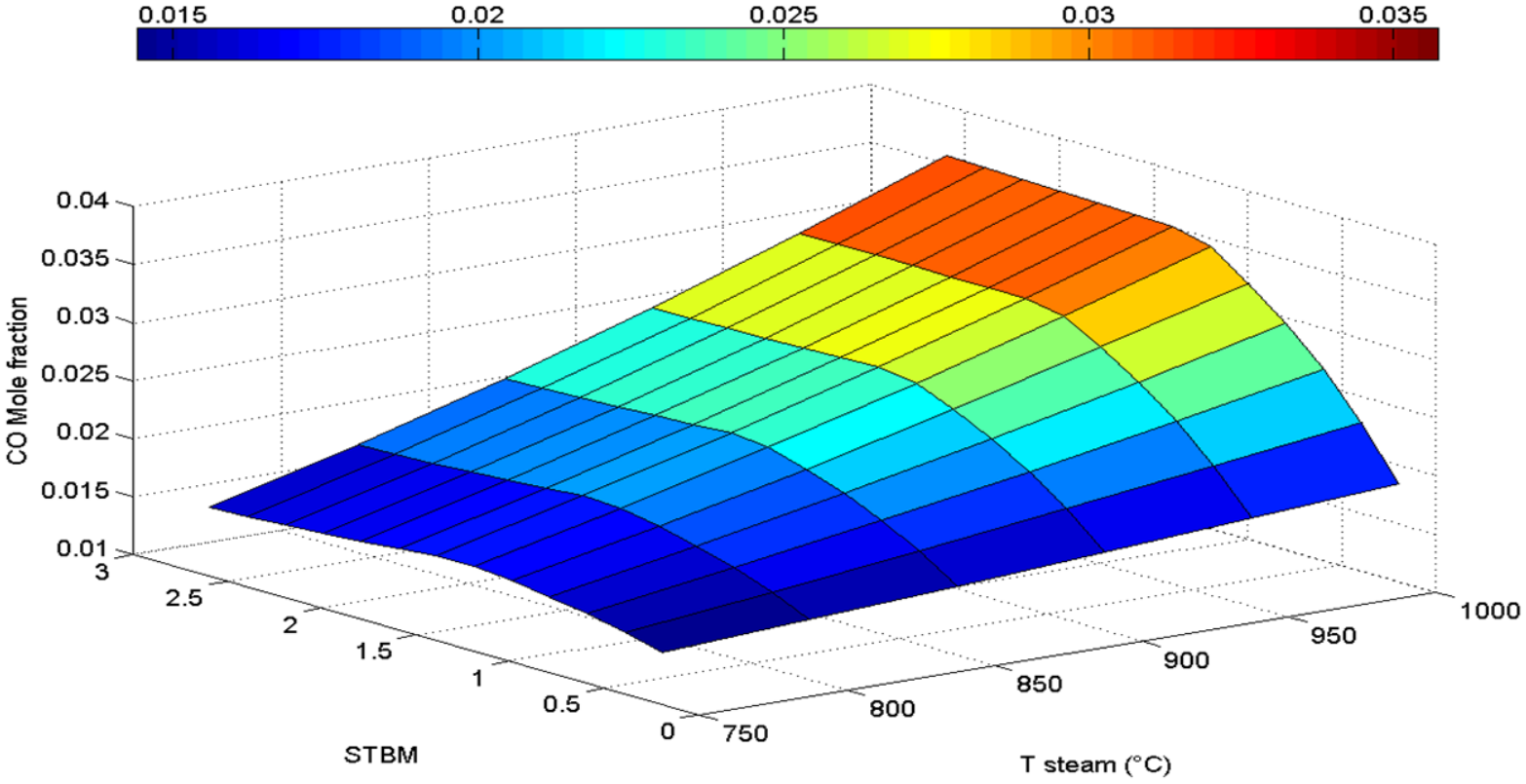

Figure 4-17. Surface plot of carbon monoxide mole fractions at varying STBM and steam temperatures from equilibrium model for feedstock $CH_{1.5}O_{0.67}$.

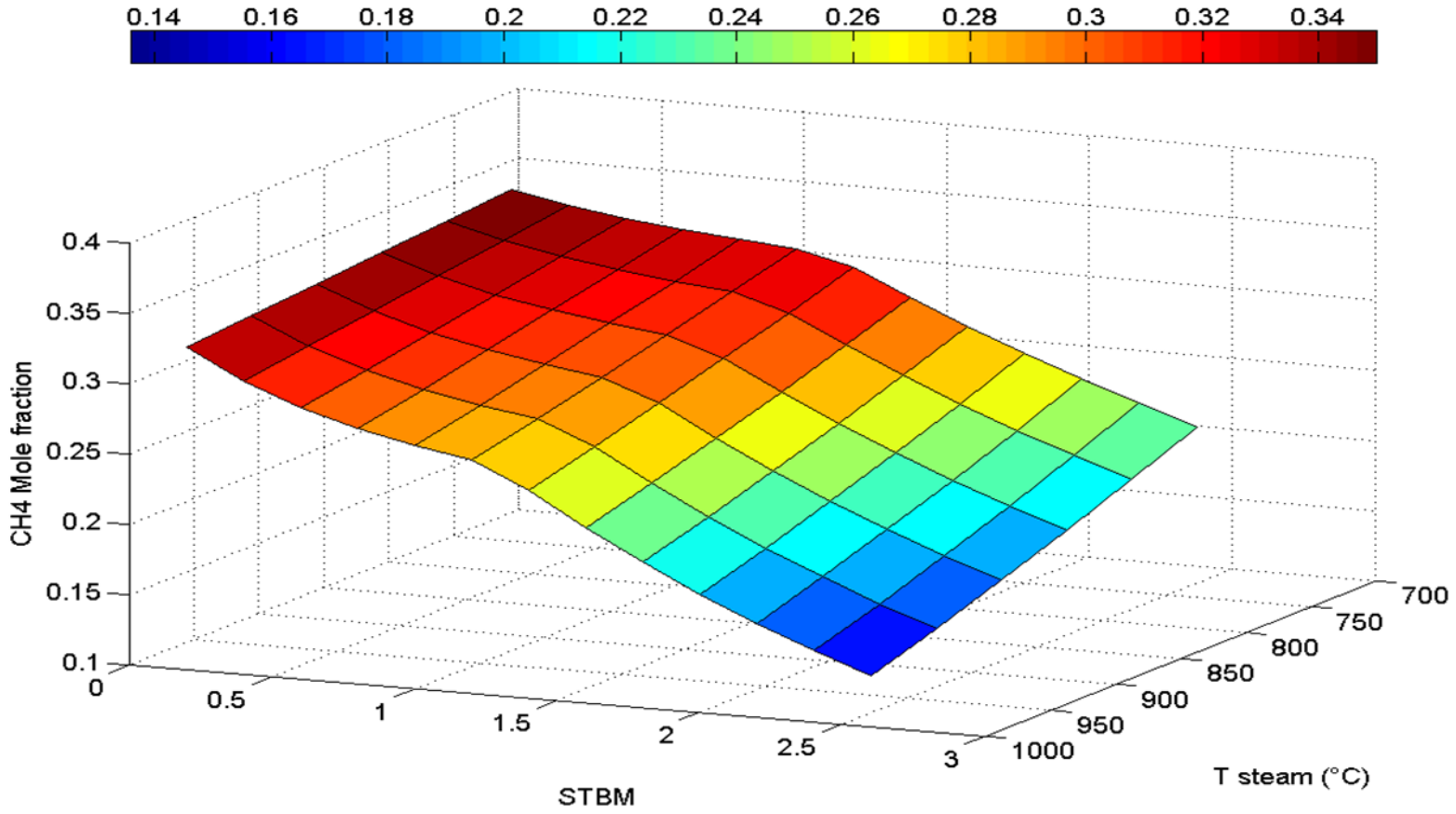

Figure 4-18. Surface plot of methane mole fractions at varying STBM and steam temperatures from equilibrium model for feedstock $CH_{1.5}O_{0.67}$.

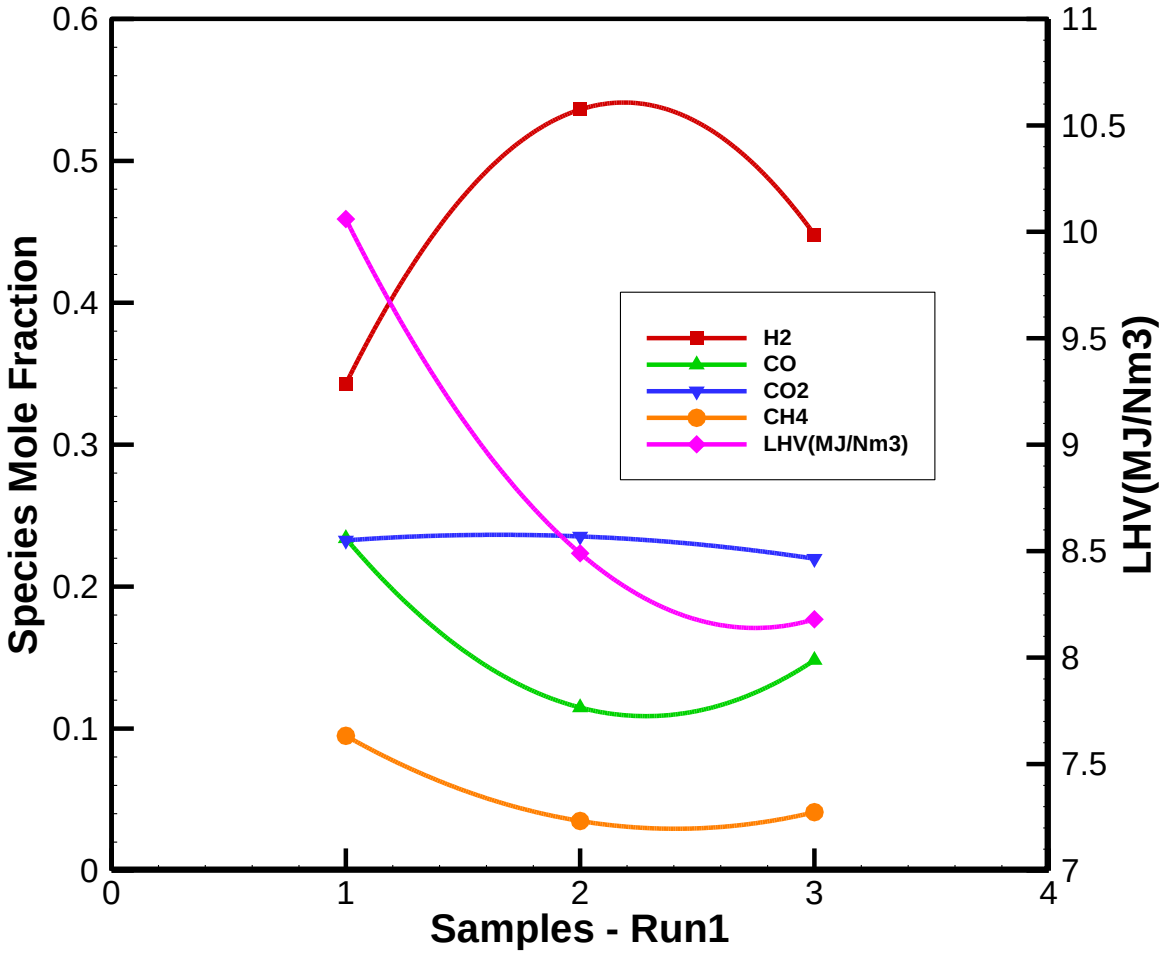

Figure 4-19. Mole fractions calculated from GC analysis, experimental 877°C steam run1

Table 4-2. Mole fractions from gas analysis run1

Run1 / Vol %	H_2	CO	CO_2	CH_4	LHV(MJ/Nm3)
1	0.3429	0.234	0.2326	0.0949	10.06
2	0.5362	0.1148	0.2354	0.0349	8.49
3	0.448	0.1482	0.2197	0.0411	8.18

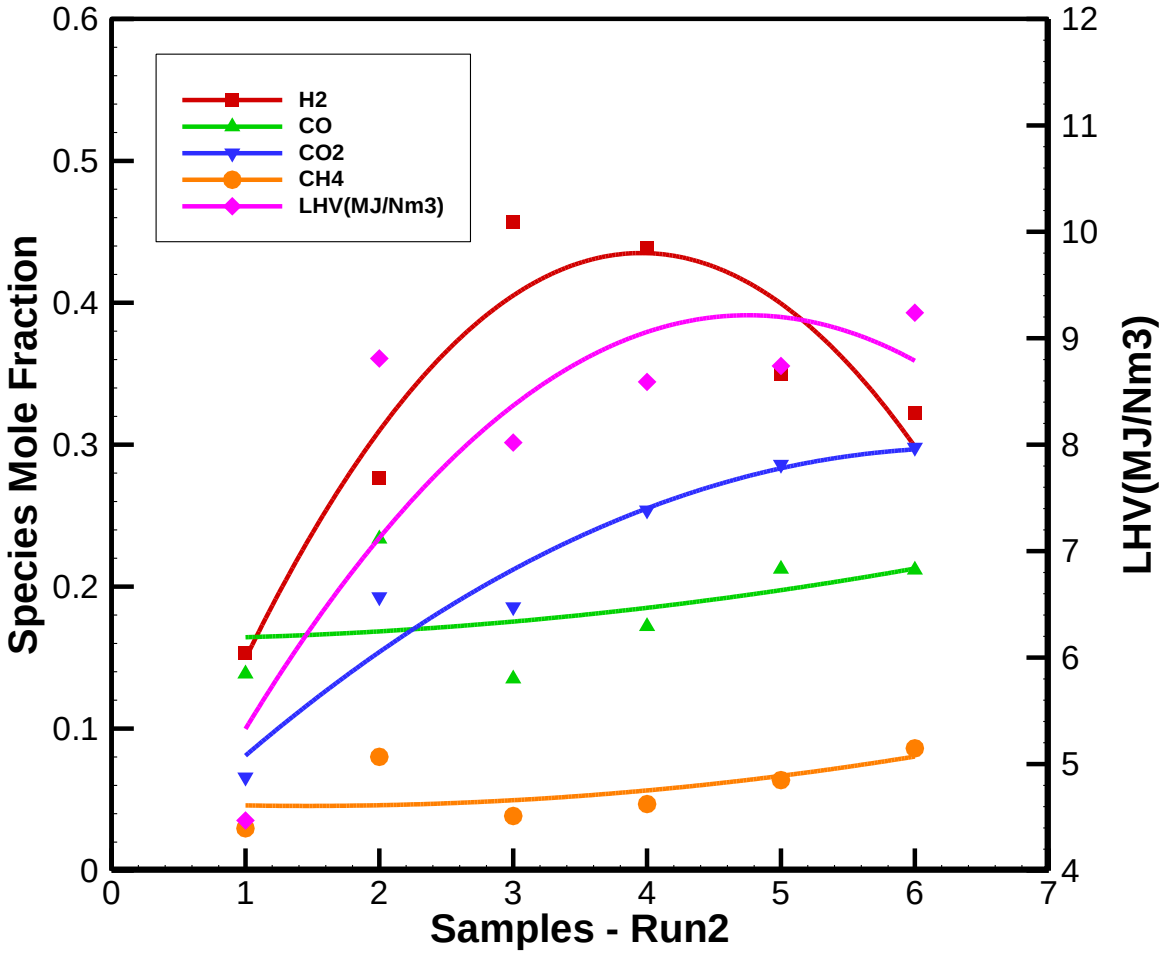

Figure 4-20. Mole fractions calculated from GC analysis, experimental 877°C steam run2

Table 4-3. Mole fractions from gas analysis run2

Run2 / Vol %	H_2	CO	CO_2	CH_4	LHV(MJ/Nm3)
1	0.1535	0.1386	0.0657	0.0297	4.47
2	0.2763	0.2337	0.1927	0.0801	8.81
3	0.4569	0.1351	0.1857	0.0384	8.02
4	0.4387	0.172	0.2539	0.0468	8.59
5	0.3498	0.2124	0.2861	0.0637	8.74
6	0.3222	0.2118	0.2981	0.0861	9.24

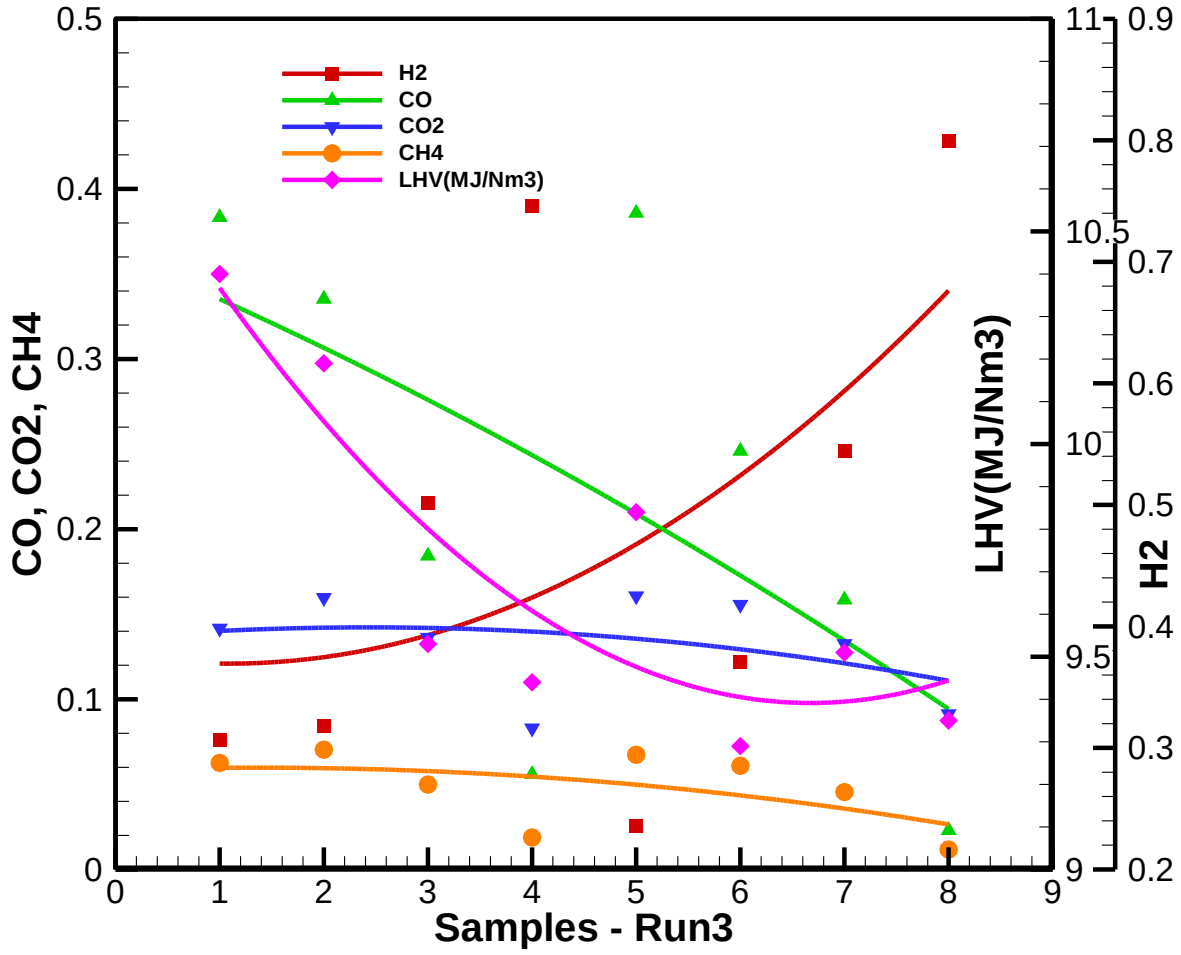

Figure 4-21. Mole fractions calculated from GC analysis, experimental 1000°C steam run3.

Table 4-4. Mole fractions from gas analysis run3

Run3 / Vol %	H_2	CO	CO_2	CH_4	LHV(MJ/Nm3)
1	0.3065	0.3833	0.1417	0.0626	10.4
2	0.3181	0.3353	0.1597	0.0704	10.19
3	0.5012	0.1843	0.1363	0.0499	9.53
4	0.7463	0.0559	0.083	0.0188	9.44
5	0.2359	0.3858	0.1607	0.0674	9.84
6	0.3704	0.2459	0.1557	0.0609	9.29
7	0.5444	0.1585	0.1326	0.0455	9.51
8	0.7998	0.023	0.0914	0.0117	9.35

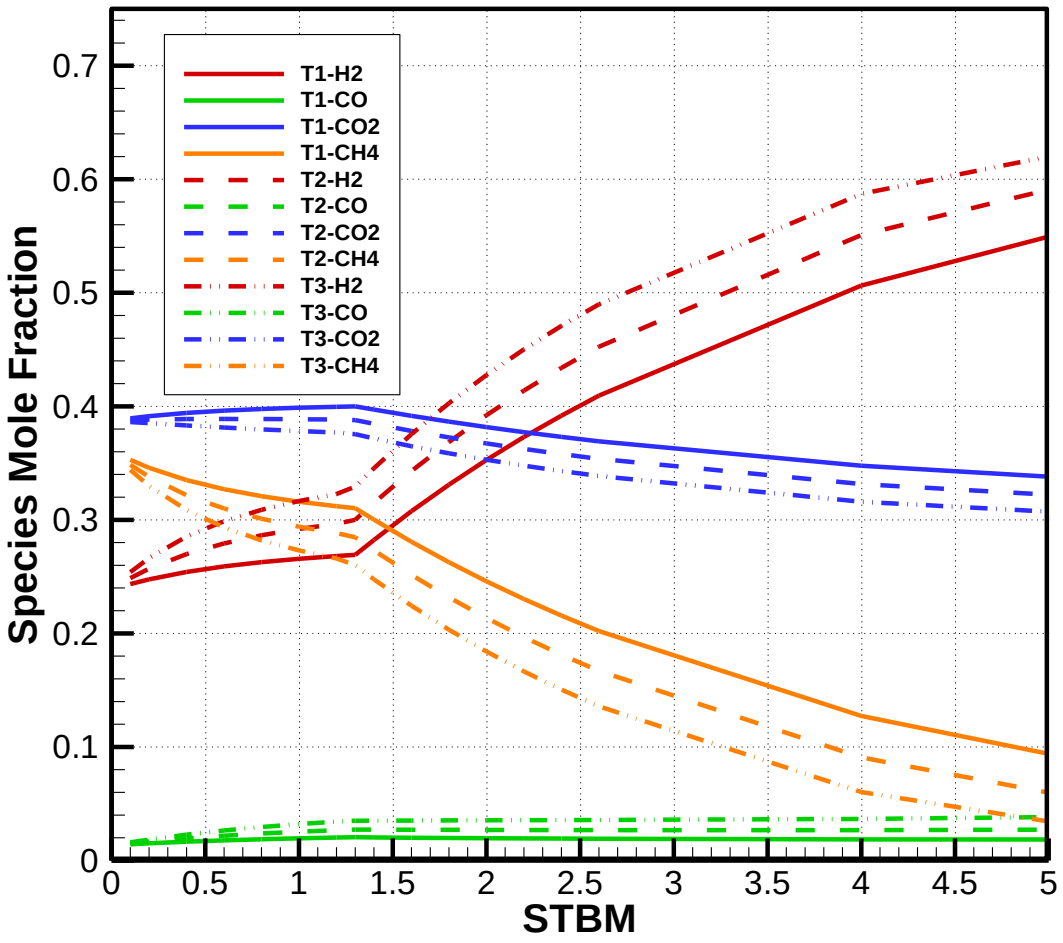

Figure 4-22. Mole fractions predicted by equilibrium model at lower STBM coincides well with the experimental data in the range of 4 to 6.

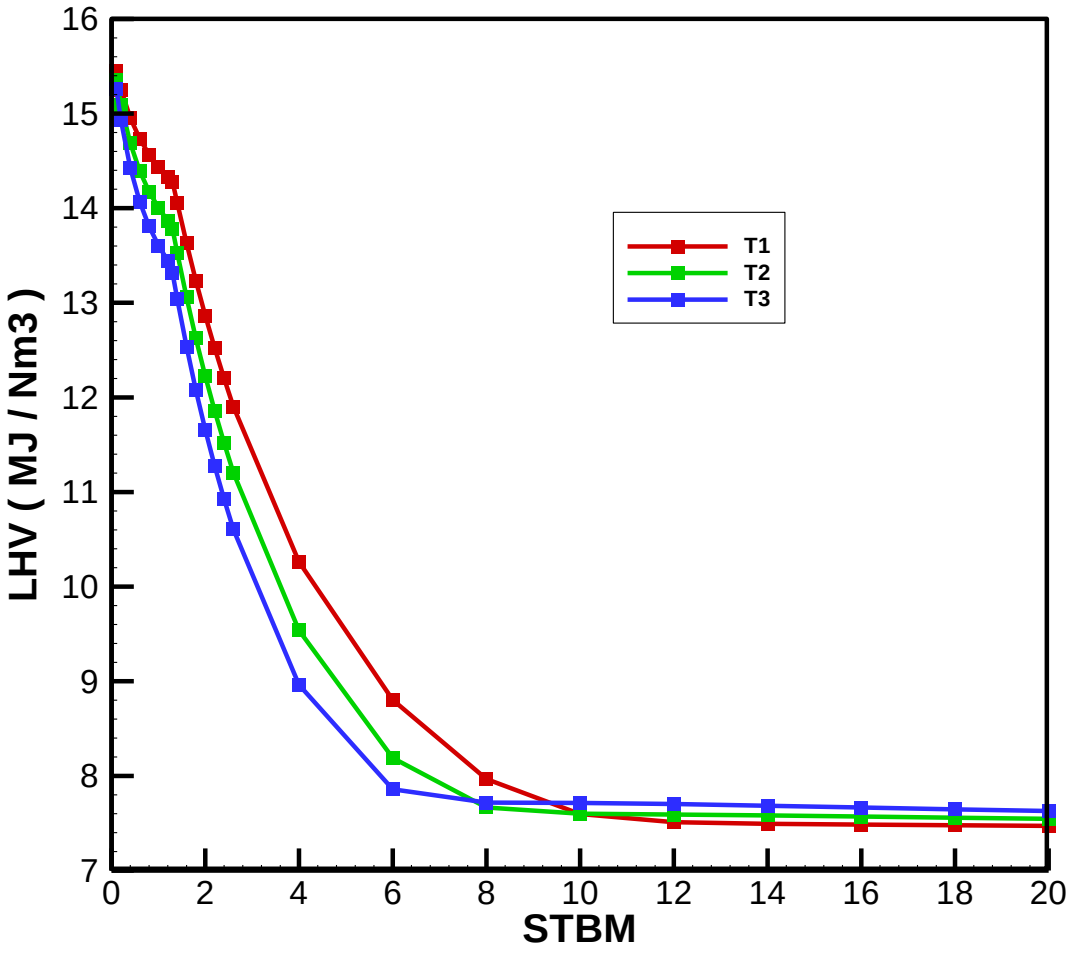

Figure 4-23. Heating value comparison for different steam inlet temperature, experimental and model data agree in the 4 to 6 STBM range similar to the mole fractions.

CHAPTER 5
MATERIAL SYNTHESIS AND FABRICATION OF NIO-SCZ82 SUPPORT TUBES AND SCZE721 THIN FILM MEMBRANES

5.1 Introduction

In this chapter the methods and type of processes used for synthesizing the materials required for making the material mixture (slurry) to fabricate the support structure and the thin film membranes are explained in detail. Further the coating and rolling technique used for preparing the thin film membrane and the support structures are also addressed.

5.2 SCZ82 ($SrCe_{0.8}Zr_{0.2}O_{3-\delta}$) and SCZE721 ($SrCe_{0.7}Zr_{0.2}Eu_{0.1}O_{3-\delta}$) Powder Synthesis

Traditional solid-state reaction method was used to prepare polycrystalline SCZ82 ($SrCe_{0.8}Zr_{0.2}O_{3-\delta}$) and SCZE721 ($SrCe_{0.}7Zr_{0.2}Eu_{0.1}O_{3-\delta}$) .The individual powder components used for making the mixture are $SrCO_3$ (99% purity), Ce $(NO_3)_3$ (99.5% purity), Sr $(NO_3)_2$ (99.97 % purity) and Eu $(NO_3)_2$ (99.9 % purity). All the powders mentioned were acquired from Alfa Aesar.

There are differences in the different batch of chemicals used, although the compound is the same there is significant variation in the surface chemistry of the ground powders. Hence there is no exact point for specifying the temperature and the hours required to create a fine mix, it rather depends on whether the original powder is finer or coarser than the previous batch used. Therefore the chemical mix usually operates in a favorable range of values instead of one specific set of values in terms of calcination and sintering temperatures.

The constituent mixtures were mixed in appropriate weight proportions determined from their molecular weight and then were mixed precisely to maintain

consistency in the final matrix. Table 5-1 explains the amount of powders used for synthesizing one mole of the respective final product.

The above table provides the amount of ingredients necessary for making 1 mole of the desired membrane support; the weights were calculated based on the no of moles of each element present in the compounds and the desired moles in the final product. This can be modified for various batch sizes by factoring the weight accordingly. Care was taken when adding Eu_2O_3 since it has 2 moles of Eu in it and must divide the weight by 2 to have the final 0.1.Once the respective powder mixtures were prepared they were transferred to a container suited for ball milling and ball media was also added accordingly to provide enough consistency. Then the two containers were filled with ethanol which makes the powder in to slurry and made it easy for mixing in the container. The two containers were then loaded on the ball mill for 24 hours and after that they were dried out separately to remove the ethanol, leaving just the dry products behind.

The contents were then transferred on to a crucible separate ones for the support and membrane powders. The powders were then calcined in a high temperature furnace at 1300°C for 10 hours. Once it cooled down the two set of powders can be used to make the slurry required for making the support and thin film membrane.

5.3 Support Tube Fabrication

The powder mix required for a typical batch of slurry to make the green tape is provided in Table 5-2.NiO was added to the mixture at a 46.7% weight ratio. The recipe for the preparation of the tubes and the thin film membranes were developed by a research group at FISE and was later tested for WGS [59].The base case for our tests would be to have permeation flux comparable to the previous runs. Stage one includes

adding ethanol and toluene for solvents and then solsperse is also added to the mix to avoid the fine particles from lumping together and settling in the slurry prepared. This mixture is put on ball mill for a day and then stage 2 constituents are added to the mixture. Plasticizers Polyethylene glycol (PEG) and Benzyl butyl phthalate (BBP) were added to make the tape easier to operate while rolling and shaping in the tape caster. While Polyvinyl butyral (PVB) was added to serve as the binder.

After adding stage 2 the mixture was further ball milled for a day and then it was treated in a vacuum pot shown in Figure 5-2 to retrieve any air molecules trapped in the slurry .This helps preventing bubble formations when the slurry is poured on the tape caster shown in Figure 5-3 and helped producing a consistent tape without any major imperfections. The green tape as it rolls out on the casting machine through the doctor blade gap is shown in Figure 5-4 and Figure 5-5 Once the tape dried out on the flat bed, it was taken out of the machine and cut in to desired lengths and was rolled in to circular tubes using 12 “ steel core teflon rods. Care was taken during rolling process to apply glue at the starting point so that it stuck to the rod for easy rolling and then at the end of each turn glue was applied to make sure the layers do not get separated since it was rolled 4 to 5 times. The glue was made up of 9:1 ethanol and toluene and then 5%of that weight PVB was added to the mixture and ball milled for a day to get consistency.

Then the end cap was made by cut pieces of the tape (3 pieces glued together) and was applied to one end of the tube and was polished further. Care was taken to remove the step inside the membrane tube before putting the end cap to avoid pin holes while coating. Figure 5-6 explains how the rolling process is done in steps.

The final step of tube preparation was to pre sinter the tubes at 1100°C for 4 hours which was preceded by a binder burnout phase of 400°C for 2 hours. Then the tube was cooled down and was ready to be coated with the membrane. Drying stations were made using foam material to protect the fragile tubes and for drying overnight along with circular supports for holding the tubes in place.

5.4 Thin Film Membrane Fabrication

The SCZE721 powder was prepared by mixing the appropriate proportions of the constituent elemental compounds and then they were mixed with ethanol and put on the ball mill for a day. Then the slurry was dried on a heating plate and the resultant dry powder was calcined at 1300°C for 10 hours. Once calcined the SCZE721 was used to make the thin film membrane by adding it with binder and anti-floccing agents to provide homogeneous membrane slurry and was put on the ball mill for a day before being used for coating the pre-sintered support tubes.

After ball milling, the pre-sintered tubes were coated on the inside with the membrane slurry and were air dried for a day. The numbers of coats usually govern the thickness of the coating. Once air dried the coated tubes were finally sintered at 1520°C for 5 hours. After this step the tubes can be used in the membrane reactor for testing.

The average thickness of the membrane coated on the tube was of the order of 30 microns. Figure 5-7 shows the different cross sectional view of the sintered tubed viewed under SEM (Scanning electron microscope). The SEM was used to inspect the cross section of the coated tubes for verifying the thickness of the membrane and also to check the surface for any cracks or pores, since that will be detrimental to the experiment by allowing gas species to leak rather than diffuse by means of ion transportation. So a sample from each batch was tested to make sure the coated tubes

were mechanically and chemically stable under the sintering temperatures. It was also used to detect any gaps in between the layers of green tape as it was rolled on to form the tape and to gauge the thickness of the “step” that was created due to initial contact point between the green tape and the roll bar at the start of the procedure. Since this uneven step would prevent coating the inner surface smoothly with the SCZE721 membrane slurry once the SCZ82 tubes were pre sintered.

Table 5-1. Powder proportions required

Element	A.W	SrCO3	CeO2	ZrO2	Eu2O3	SCZ.8.2	SCZE.7.2.1
Sr	87.62	1	0	0	0	1	1
Ce	140.116	0	1	0	0	0.8	0.7
Zr	91.224	0	0	1	0	0.2	0.2
C	12.0107	1	0	0	0	0	0
O	15.9994	3	2	2	3	3	3
Eu	151.964	0	0	0	2	0	0.1
Total		147.6289	172.1148	123.2228	351.9262	265.9558	267.1406

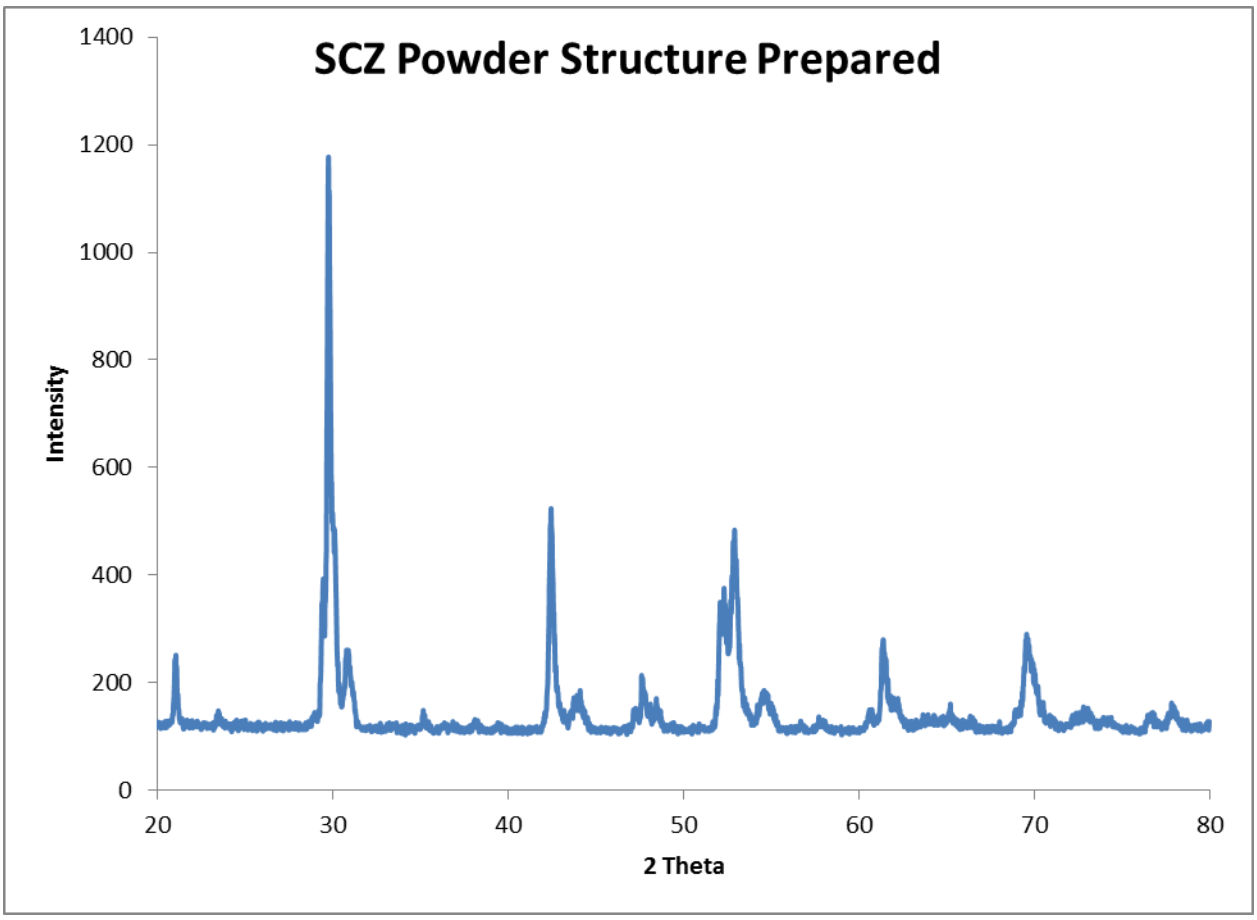

Figure 5-1. XRD (X-ray diffraction) peaks for support tube SCZ81 powder prepared after calcination.

Table 5-2. Support tube mixture

STAGE	Material	Quantity (gram)
Powder Recipe(1mol-SCZ82)	SrCO3	147.63
	CeO2	137.6982
	ZrO2	24.6448
Tape Slurry 1	Powder Wt%(53.3 SCZ82 / 46.7-NiO)	100
	Ethanol	22.25
	Toluene	22.25
	Solsperse	1
2	BBP	5
	PVB	7
	PEG-8000	2

Figure 5-2. Vacuum pot.to bubble out air in tape slurry Photo courtesy of Elango Balu.

Figure 5-3. Tape caster.at FISE lab used to fabricate support tube base. Photo courtesy of Elango Balu.

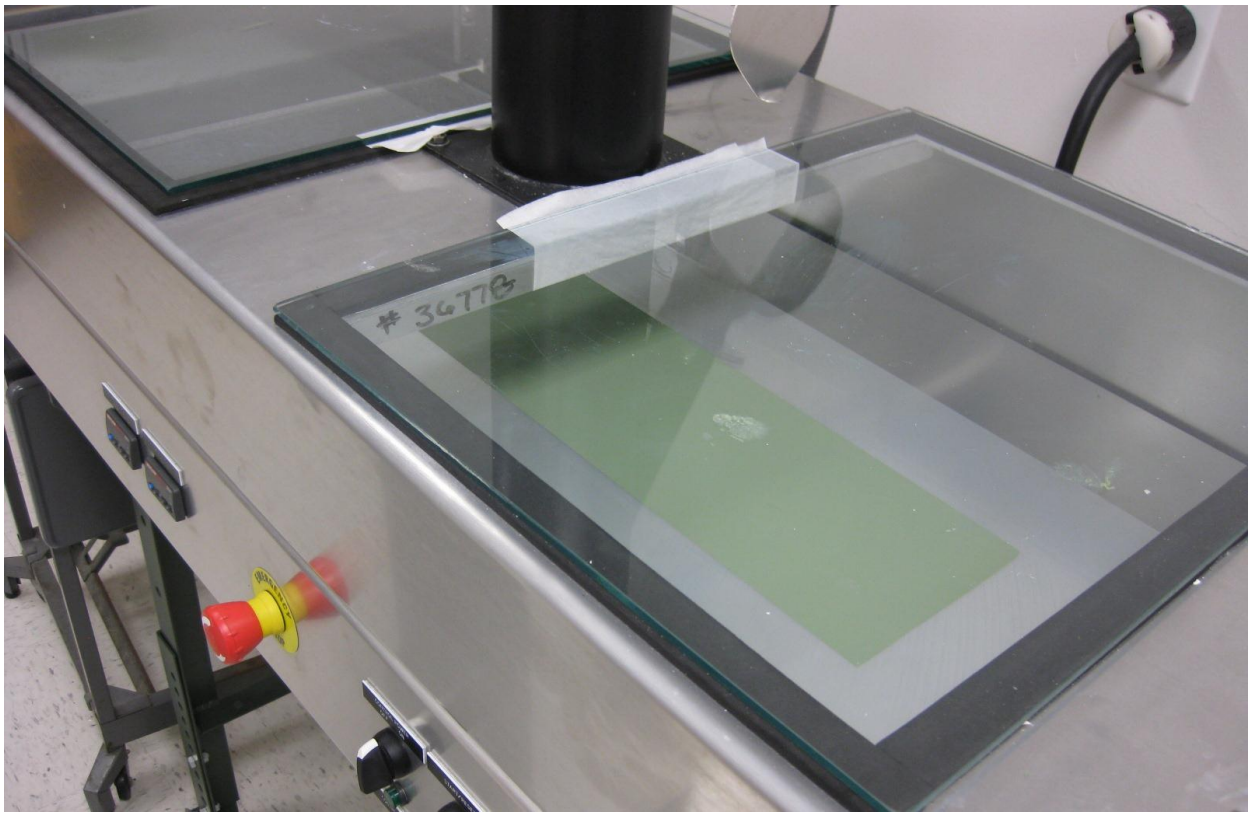

Figure 5-4. Finished support tape after tape casting. Photo courtesy of Elango Balu.

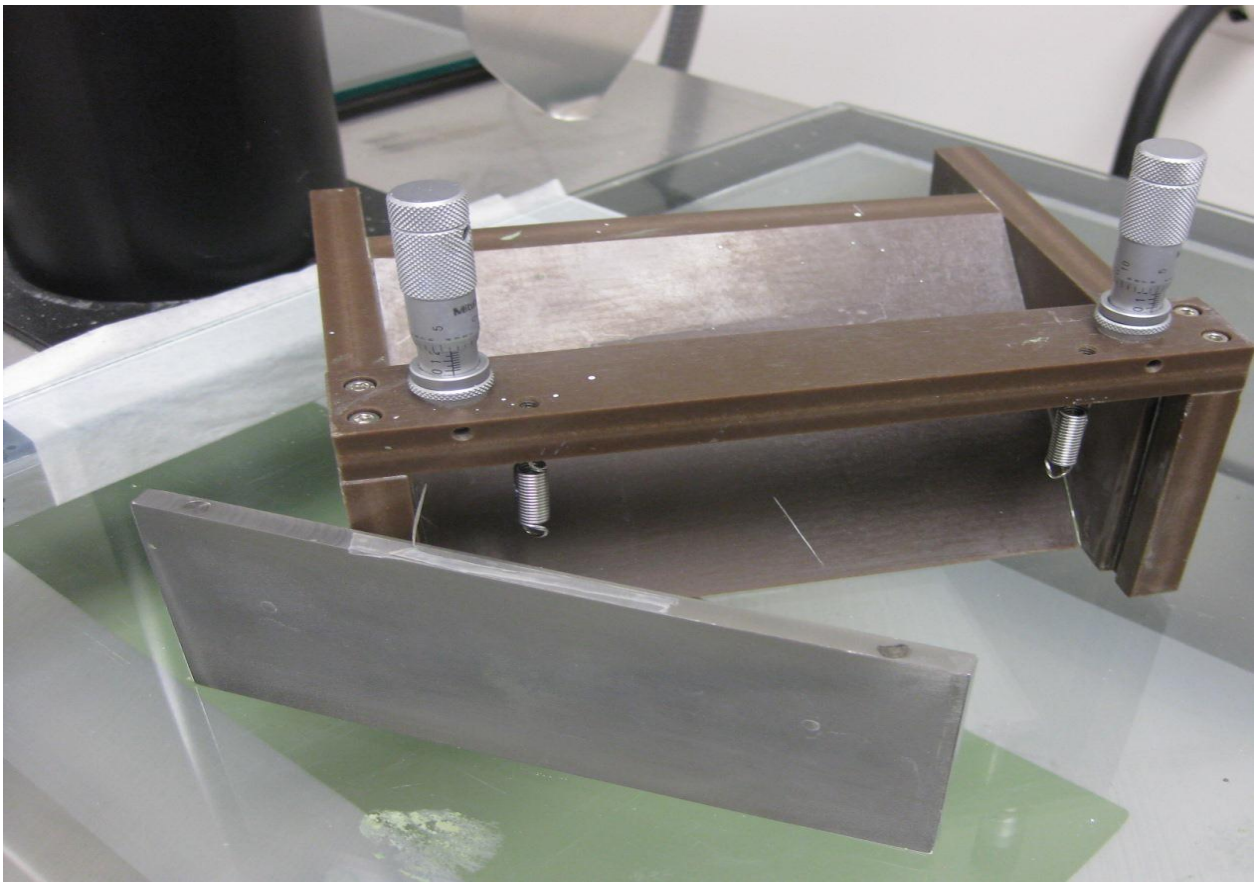

Figure 5-5. Doctor blade used for adjusting tape thickness. Photo courtesy of Elango Balu.

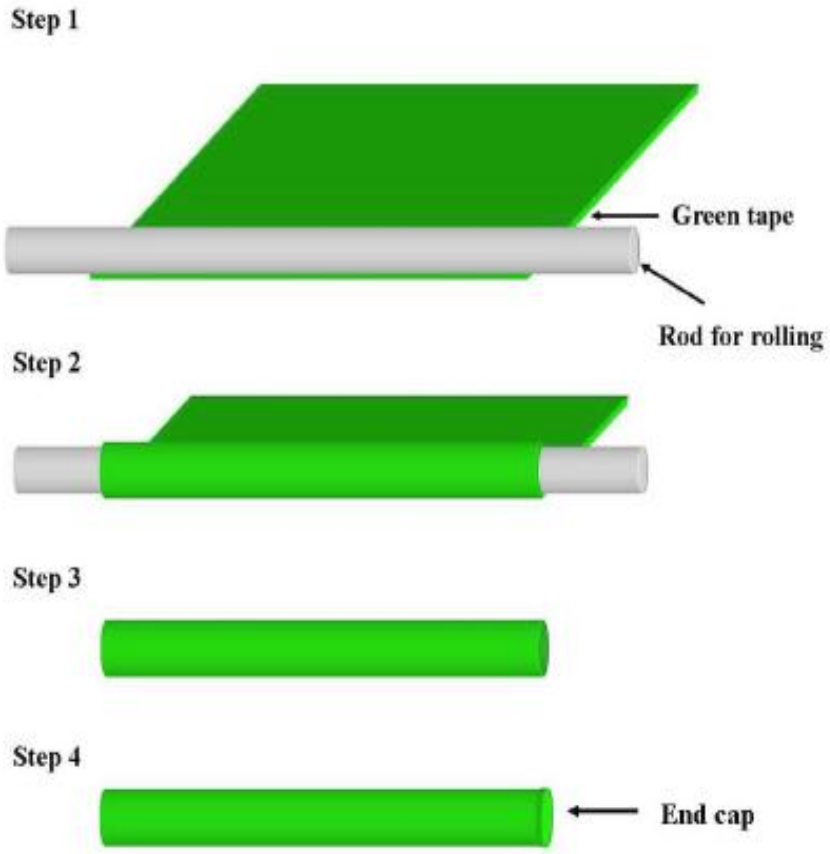

Figure 5-6. Schematic of tape rolling process developed by FISE [59]

Table 5-3. Thin Film membrane Mix

STAGE	Material	Quantity (gram)
Powder Recipe (1mol-SCZE721)	SrCO3	147.6289
	CeO2	120.48036
	ZrO2	24.64456
	Eu2O3	17.59631
Thin Film	Powder	10
	Ethanol	91
	Solsperse	0.1
	10 % wt PVB In ethanol	10

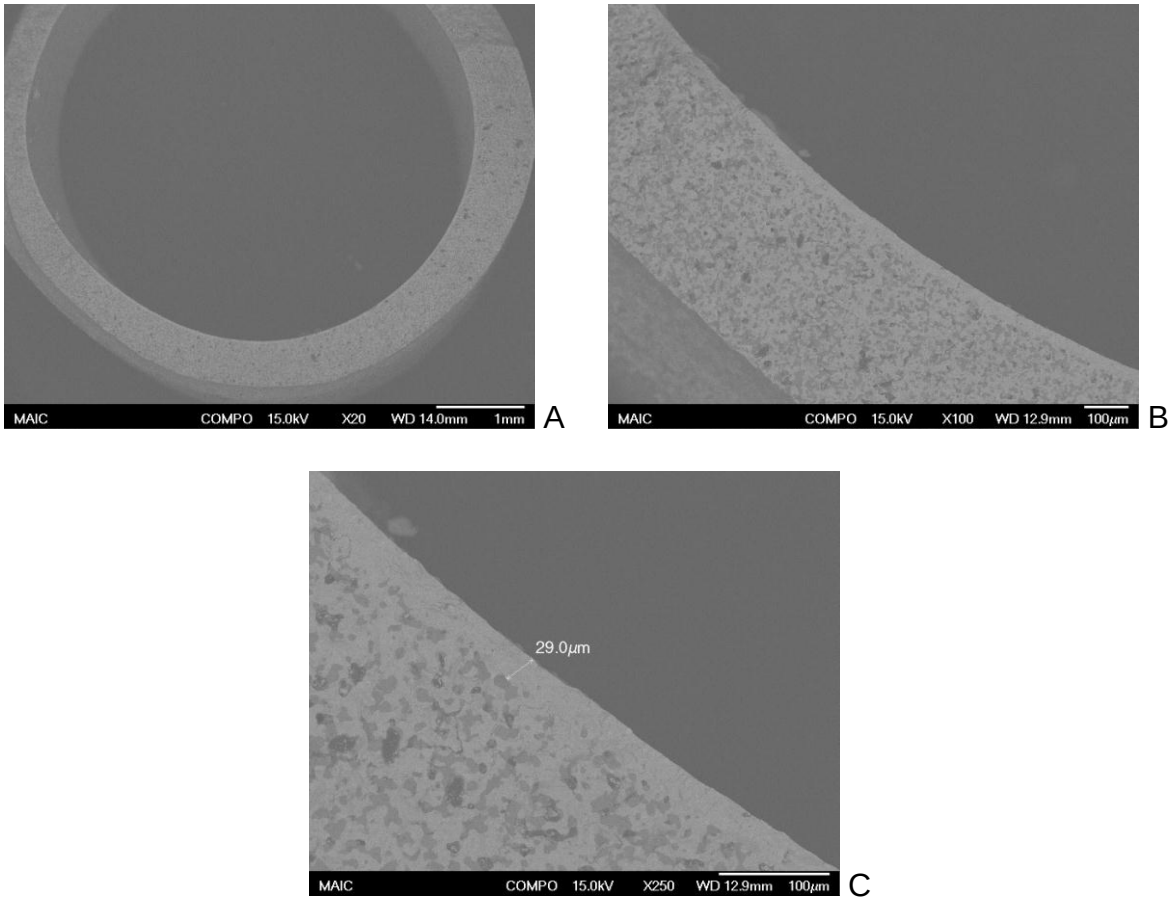

Figure 5-7. SEM of sintered tubes. A) Whole cross section B) Zoomed near the circular edge C) Dense membrane thickness measured

CHAPTER 6
EXPERIMENTAL STUDY OF MEMBRANE REACTOR

6.1 Membrane Reactor Design

The membrane reactor was designed to simulate the conditions of being operated alongside the exit gases from a steam gasifier and is designed to operate at high temperatures. The high temperatures allow the membrane tubes to carry out the WGS reaction using MIEC (Mixed Ionic Electronic Conductivity) properties. This coupled with the in-situ removal of H_2 helps in shifting the equilibrium to the right hand side of the WGS reaction, thus facilitating more H_2 production and conversion of CO. Li [59] conducted experiments to study hydrogen flux permeations using only CO + Steam. Since the syngas is a much more complex mixture of gases that include H_2+CO+CO_2+H_2O+CH_4. New experiments were conducted by modifying the water vapour content in the feed stream to match the concentrations to the order of exit gas compositions which has not been done in the literature.

The quartz chamber which serves as the housing for the membrane tubes was manufactured to fit the specifications of the vertical furnace, and was fabricated by as a special order by ARS scientific glass company. A 3D rendering of the quartz reactor model is shown in Figure 6-1. The two ends were capped with teflon caps with provisions to introduce the feed gas and thermocouple on one side and to introduce the membrane and collect the effluent/permeate on the other side. The O rings present in the teflon caps serve as gaskets providing a leak proof environment and to make sure that the O rings are not exposed to high temperatures, they are covered with glass wool to provide an extra layer of protection, even though they lie in the cold zone once placed in the furnace.

To further prevent any slipping of the stainless tubes that connect the gas lines to the glass reactor, brass housings were threaded in to the teflon caps as shown in Figure 6-2, with a slight taper. This allows a gas tight fit instead of sliding the stainless steel tubes directly in to the reactor. The reactor tube also has a provision for the insertion of a TC to monitor the temperature near the tip of the membrane tube; this prevents the TC tip from coming in contact with the wall when introduced from the top with an eccentric hole next to the feed gas inlet. The flow path of the feed and sweep gases are shown in Figure 6-3.

6.2 Experimental Setup of the Membrane Reactor

The setup consists mainly of the core reactor placed inside the furnace and because of the use of highly flammable gases like H_2 and CO, the entire setup is placed inside the glass hood with an exhaust vent on top. The other components include the mass spectrometer (MS) and the UHP (Ultra high purity) grade cylinders of individual gas components that are connected to mass flow controllers (MFC). Figure 6-4 shows the overall setup of the system.

Ultra-torr connections were used to house the tube inside the quartz reactor and this helps in providing air tight fitting without causing too much strain on the tubes. Helium was used as the zero gas for calibrating the MS and Argon was used as the sweep gas to carry the permeated H_2 inside the membrane tube. The gas cylinders used for calibration are ultra-high purity industrial grade mixes procured from Airgas. The membrane reactor setup along with the system components are shown in the block diagram below. The curly lines showed are heating tapes wrapped around the gas lines exiting the reactor and entering the MS. This was done to prevent condensation of

water in the exit gas lines, since it caused blockage of the inlet filters with bubbles and builds up back pressure in the system and also interfered with the gas analysis.

A 3-way valve is also used to make the process of calibration and testing easy. This allows the gas mixture to either flow through the bubbler or can be sent directly to MS to be analyzed as dry gas mixture. This also helps to test wet gas mixture in the MS without actually passing it through the membrane reactor during the calibration stages.

EXTREL MAX-300 LG was used for the analysis of the gas stream from the effluent and permeate side of the membrane reactor. The MS can handle only one process stream at a particular time and the lines were not switched to measure the effluent stream as it caused problems with the ionization chamber pressure and only the permeate side stream was measured in all the cases. The spider valve also has a heater plate at the entry which acts as a second line of defense against condensation which will clog the filters.

Concentration of watervapour in syngas from a steam gasifier is higher than 3% for most part, feed gases cannot be simply bubbled through water at room temperature to achieve higher concentrations. So this required heating up the water as per the Antoine equation to provide the adequate moisture content for the feed stream. So a special bubbler was designed that could accommodate a cartridge heater with specifically located hot zone and cold zone to prevent the O-ring from melting. The heater rod has an inbuilt thermocouple that was connected to a controller and monitors the water temperature. Once the set point was configured on the controller the heater was turned on automatically to provide the required rise in temperature and the temperature would overshoot for a couple of cycles and then stabilized to provide a

fairly constant water temperature that would help in adjusting the water vapour concentration used in the experiments.

Thin film membrane coated on the support tubes was used in the reactor to test its performance under WGS condition. Before actually exposing the tubes to CO, the outside support surface was heat treated overnight to reduce the nickel oxide so that the support tube was porous. This was done by fitting the tube inside the reactor and the furnace was heated up to 900 °C.Simultaneously the hydrogen is bubbled through water and is flown on the feed side of the tube diluted with Argon, whereas helium is flown inside the tube as sweep gas.

The permeate side was tested with the MS. Initially it would register only He peaks because of the oxidized surface. As time progressed and the temperature got higher the hydrogen peak started showing up in the permeate side, indicating the support surface was getting reduced and the hydrogen was permeated through the dense membrane. This also served as a step to check the integrity of the membrane. If there were huge helium peaks along with the smaller peaks of hydrogen and argon on the permeate then there was a significant crack or pin hole in the membrane tube and was deemed not suited for further testing. Figure 6-7 shows the reduced tube surface which changed color compared to the sintered tubes, which is green.

Once the heat treatment was done overnight, on the next day, tube was exposed to CO+Water vapour on the feed side and argon was used as the sweep gas. Owing to the availability of only one mass spec, it was decided to monitor the permeate side since the hydrogen flux permeation was the main focus of this study. The reactor was not allowed to cool down to prevent any cracks or stresses caused due to thermal

cycling. So after heat treatment the lines were switched to the appropriate gases, once the reading was confirmed the there was no significant leaks (crack/pinholes on membrane).

6.3 Results and Discussions

In this section the results from the preliminary test runs and as well as the results from the runs that were conducted to account for the failures during the initial runs are discussed in detail and the hydrogen permeation using higher concentrations of water vapour is also shown to further reinforce the potential of such membrane reactors in actual gasification applications to enhance the hydrogen concentration in the output syngas stream without having much concerns about the energy input.

Figure 6-7 shows the initial test setup that caused cracks in the tube near the cold/hot zone interface during continuous testing. Figure 6-8 shows the tube that was exposed to WGS conditions and it is very evident from the picture that the membrane was deteriorated during the process resulting in no selectivity and allowing the gases to pass through freely and also the tube was broken in to pieces at the interface. Another thing to notice was the slight traces of carbon deposits on the tube due to lower concentrations of watervapour ~3% in the feed stream To further confirm the damage caused to the membrane on a micro scale, the SEM image of the tube tested shown in Figure 6-9 was compared with another tube that was just taken out of the sintered block and the cracked surface of the tube exposed to WGS conditions stands out. So to prevent the tube from failing by such large cracks ,an insulation layer of glass wool was added to the inside of the reactor and was wrapped around the ulta-torr region and also over the interface to reduce the thermal/chemical stresses on the support tube. Figure 6-10 shows the housing inside the reactor covered with insulation and also the new

bubbler used for the experiment along with the temperature controller to adjust the temperature of the water to vary the vapour concentration in the feed stream.

Figure 6-11 shows the new bubbler designed specifically to accommodate the internal heater cartridge to provide better control over the temperature and concentration of watervapour in the feed stream. For the experimental runs the manufactured tubes were carefully sorted out based on defects and only the tubes that passed the initial screening were used. Figure 6-12 shows the different type of defects that were persistent throughout the research process and it was mainly due to the very complex interaction between the tape slurry viscosity, sintering temperature, powder particle size and many other factors. Since the original recipe was not reproducible exactly due to the change in one of the ingredients in terms of viscosity and particle size it was very difficult to produce a coherent batch of tubes with no defects. During the heat treatment process the tubes should hold the structural integrity and allow only the selective species to transfer but in the cases that were run, there was significant amount of tracer gases crossing the membrane layer and it was due to the defects in the tubes that could propagate the cracks during the heat treatment stage. Nonetheless the tubes still serve as a catalyst for the WGS reaction and further improvement to the recipe is needed to account for higher water vapour concentration so that it could also efficiently separate out the hydrogen without any selectivity issues. Figure 6-13 shows the tube inside the reactor after WGS testing and was not broken to pieces like the ones with no insulation around the interface of the hot/cold zone.

The experimental results clearly show that there is a clear production of hydrogen from the WGS reaction with no hydrogen being present in the feed stream

and the hydrogen recorded in the permeate stream could only be from the WGS reaction occurring on the tube surface and the hydrogen permeating through the thin film membrane. Antoine equation provided the concentration of watervapour available depending on the temperature of water and using that information and controlling the amount of CO in the feed stream bubbled through water, theoretically the amount of H_2 produced would be equal to the equal number of moles of CO and H_2O available but in experimental conditions this was not the case and more over the effluent side was not analyzed for any gas species to account for the H_2 that would have remained in the effluent stream and hence the total H_2 production was not measured.

Theoretically speaking based on the membrane performance all the hydrogen on the feed side permeates through the membrane to the inside of the tube but in experimental conditions there could be a fraction of total hydrogen that does not permeate and remain in the effluent stream. This also depends on the available surface area for adsorption, since the entire tube is not inside the hot zone, the permeated hydrogen concentration could be increased further by having more surface area available in the hot zone but it poses a huge challenge in terms of the temperature barrier for the ultra-torr. But, as it can be seen in Figure 6-14, there were a lot of challenges in terms of reducing the carbon deposition, which was a big problem in contaminating the gas flow path as well as the mass spectrometer as the filters to the mass spec can be easily clogged with solid phase particles and also these carbon deposits reduce the performance of the tubes.

Experimental results showed that the concentration of hydrogen that permeated through the membrane after WGS occurred on the surface of the tube. The values are

listed in table 6-1. This process of measuring permeated hydrogen was very intensive because of careful attention required in maintaining the vacuum pressure inside the ion chamber of the mass spec during measurements to get accurate readings. So, care was taken to adjust the flow valve to control this and the permeation also seemed to vary depending on the flow rate of the sweep gas as the passage was very narrow on the inside for the gases to escape out. As the water vapour concentration was increased by adjusting the temperature of the water column the permeated hydrogen increased from the previous settings only when there was a significant change in the sweep gas flow rate.

Using these values and the knowledge of the Antoine equation to predict the concentration of watervapour available for WGS, a detailed analysis was done to present the experimental data in a clear perspective. Here the 2 main varying factors were the WGS conversion and the hydrogen permeation through the membrane after WGS. So different cases of assumed membrane permeation levels and WGS conversions were plotted based on the availability of watervapour on the feed side. Different temperature settings in the water column enabled the prediction of maximum watervapour concentration available in the feed stream for WGS based on the partial pressure of the watervapour.

Further the CO conversion percentage was calculated based on the available CO and H_2 produced from WGS reaction inside the reactor. In all the cases presented below the hydrogen concentration on the permeate side and the conversion percentage remained consistent until 45 °C and then dropped drastically at 55°C, as seen in Figure 6-15 for a base case. To further understand the performance of the membrane reactor,

the collected data was compared with several cases of varying WGS conversion and H_2 permeation factor.

Figure 6-16 shows the experimental data measured using the mass spectrometer by analyzing the permeate stream from the membrane reactor plotted against varying permeation factors assumed, which were the maximum theoretical possible concentration of hydrogen that could be collected on the permeate side at that particular temperature with 100% WGS conversion depending on the permeation factor. In this case the data fell in the range of 40% permeation and it dropped off at 55°C because of the tube failure or membrane degradation.

Similarly the same data was plotted for 80%, 60%, 40% of assumed WGS conversion backdrops and the results are shown in Figure 6-17, Figure 6-18, and Figure 6-19 respectively. In all the four plots the following nomenclatures were used to identify each curve. P1 = 100% permeation + 0% effluent stream, P0.8 = 80% permeation + 20 % effluent stream, P0.6 = 60% permeation + 40 % effluent stream, P0.4 = 40% permeation + 60 % effluent stream. Where the effluent stream percentage indicates the percentage of hydrogen that did not permeate and remained in the effluent stream.

Figure 6-17 shows the competing effects of the permeation factor and the WGS conversion factor based on the assumed factors. As the WGS conversion is reduced in any reactor setup, the permeation factor has to go up to account for the loss of conversion and to maintain the performance. Here the same data was shifted towards a higher permeation factor line, which is above P0.4 and below P0.6, when compared to the 100% WGS conversion plot.

The same scenario could be seen in Figure 6-18 where the shift towards higher permeation factor lines occurs and in this case with a 60% WGS conversion factor, the data has shifted close to the P0.6 factor to compromise for the loss in the conversion efficiency.

Figure 6-19, indicates that this case might be highly unlikely in experimental conditions. Because in this case when the WGS efficiency was assumed to drop to 40% the data shifts towards the maximum possible permeation factor which is complete permeation of all the hydrogen produced from WGS on the feed side to the permeate side without any hydrogen left in the effluent side. Even though the perovskites have high selectivity for hydrogen this would be very difficult to achieve considering there is also reduction in surface area available for the WGS as time progresses.

Although the tubes did not break during operation before using insulation, there was a lot of carbon deposit on the tube as shown in Figure 6-14 and there were also blisters seen on the tube surface towards the cold side. This indicates that the area available for surface adsorption and for the hydrogen to permeate could be reduced a lot by clogging the pores with carbon deposits and also the tube could have also been damaged at the interface instead because of separated interlayers of the tube without breaking in to two pieces, and explains why the tubes broke while attempting to remove from the fittings. But the main aim of this research was to demonstrate the possibility of enhancing the hydrogen concentration in the exit syngas and separate it from the stream in one single step. Further tests should be done to make it feasible to withstand prolonged hours of operation and a consistent tape mixture recipe should be prepared based on the available ingredients. In that case it would be possible to see more

hydrogen being permeated and operating conditions greater than 15% of water vapour concentration.

Figure 6-1. 3-D rendering of quartz reactor

Figure 6-2. Membrane tube enclosed in reactor. Photo courtesy of Elango Balu.

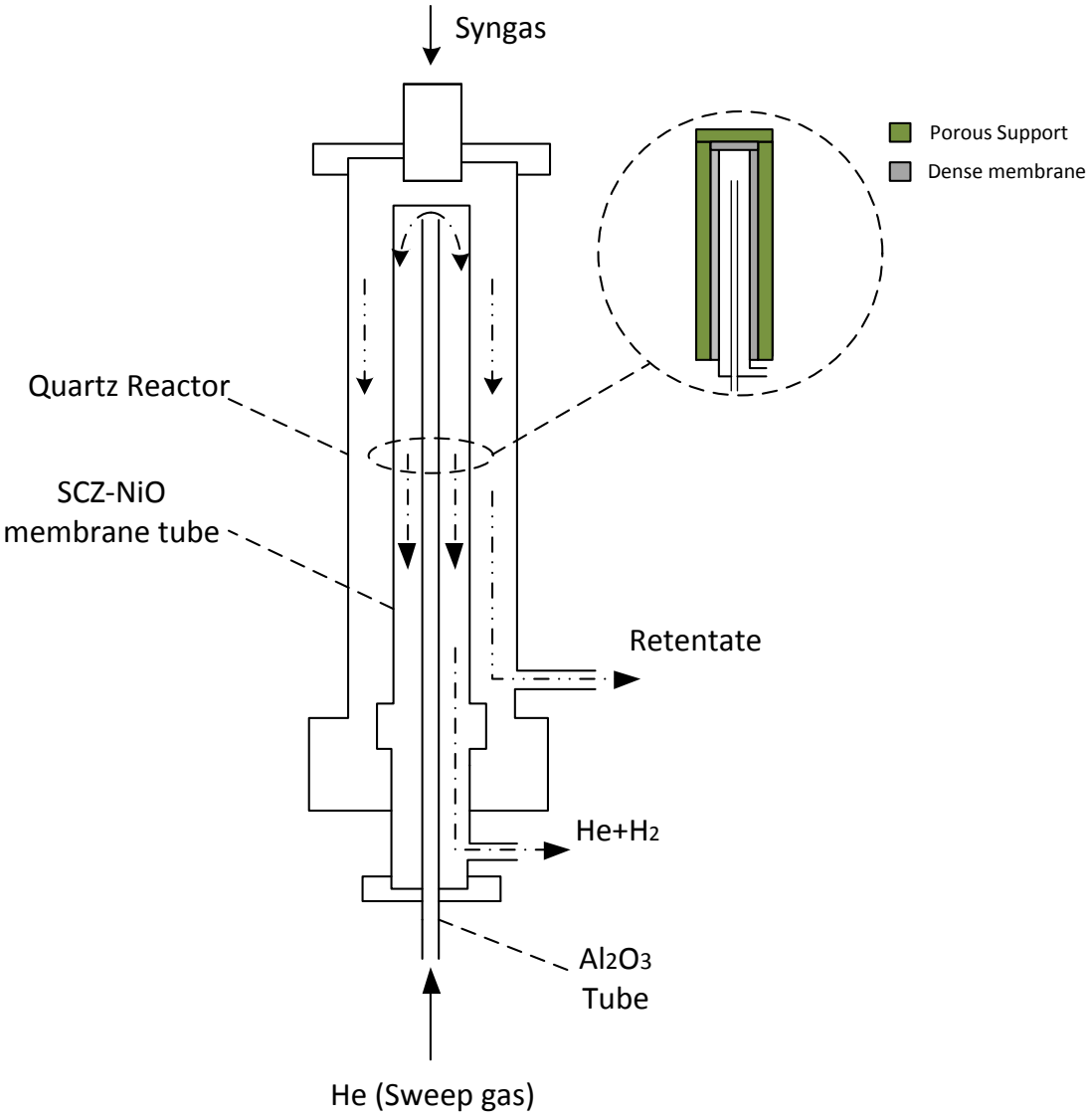

Figure 6-3. Schematic of reactor setup during operation

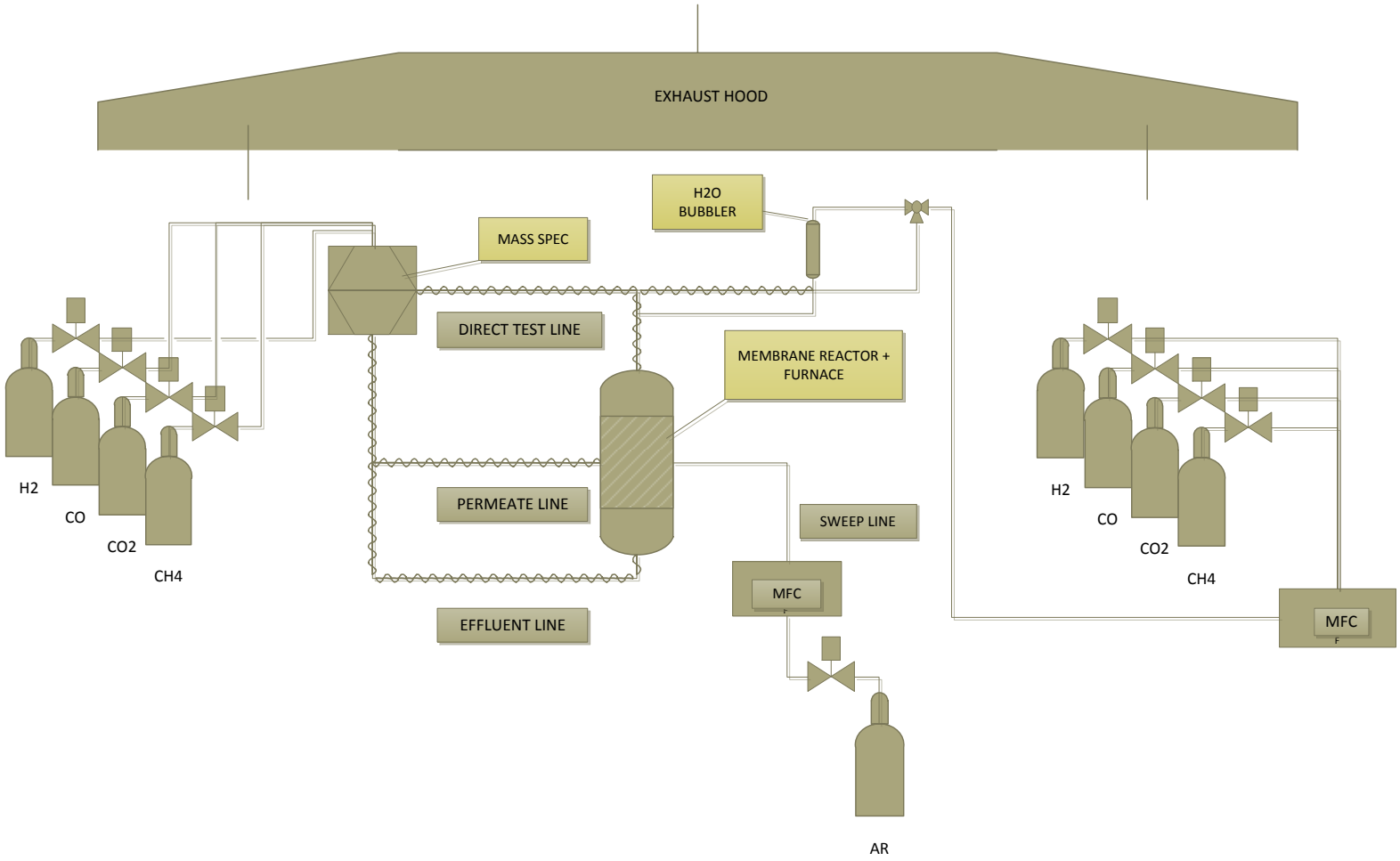

Figure 6-4. Overall system layout.

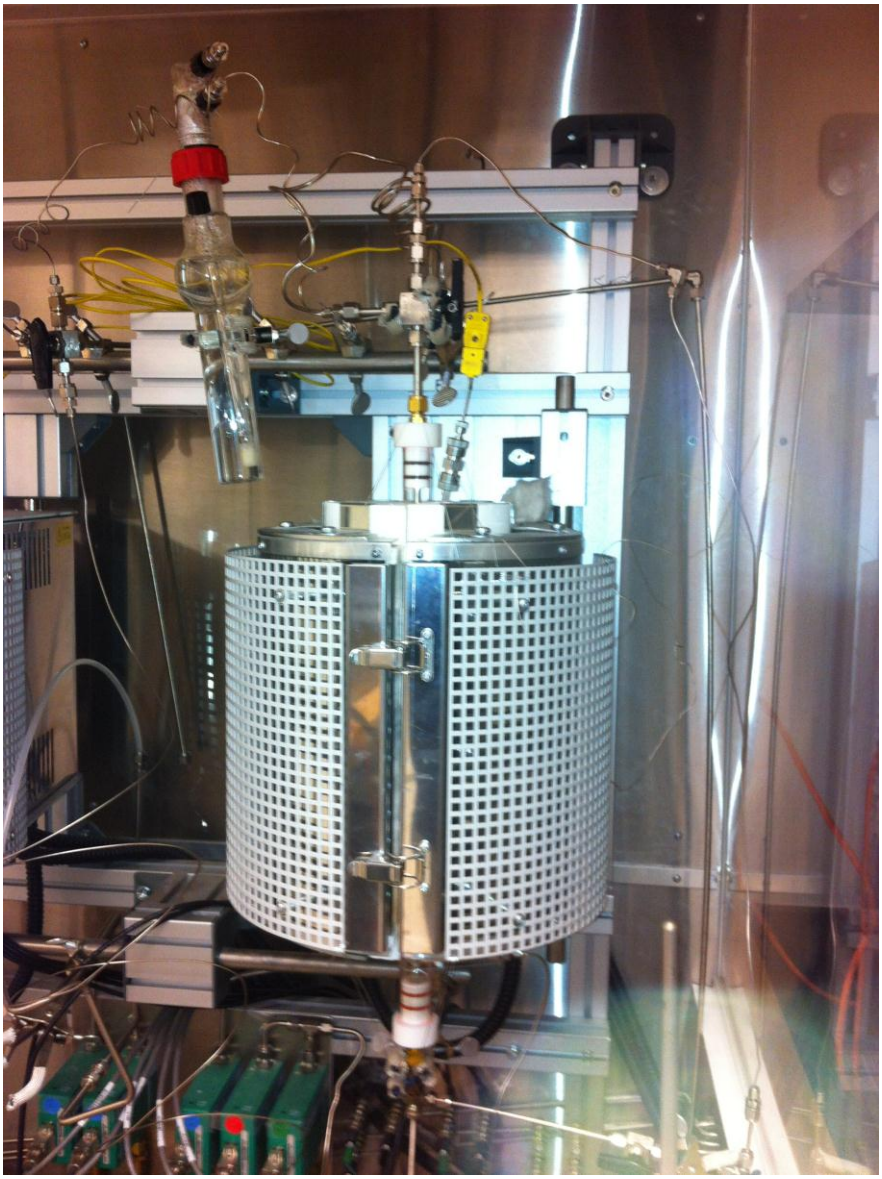

Figure 6-5. Reactor placed inside the furnace. Photo courtesy of Elango Balu.

Figure 6-6. Tube placement inside the reactor relative to heating coils with no insulation around interface. Photo courtesy of Elango Balu.

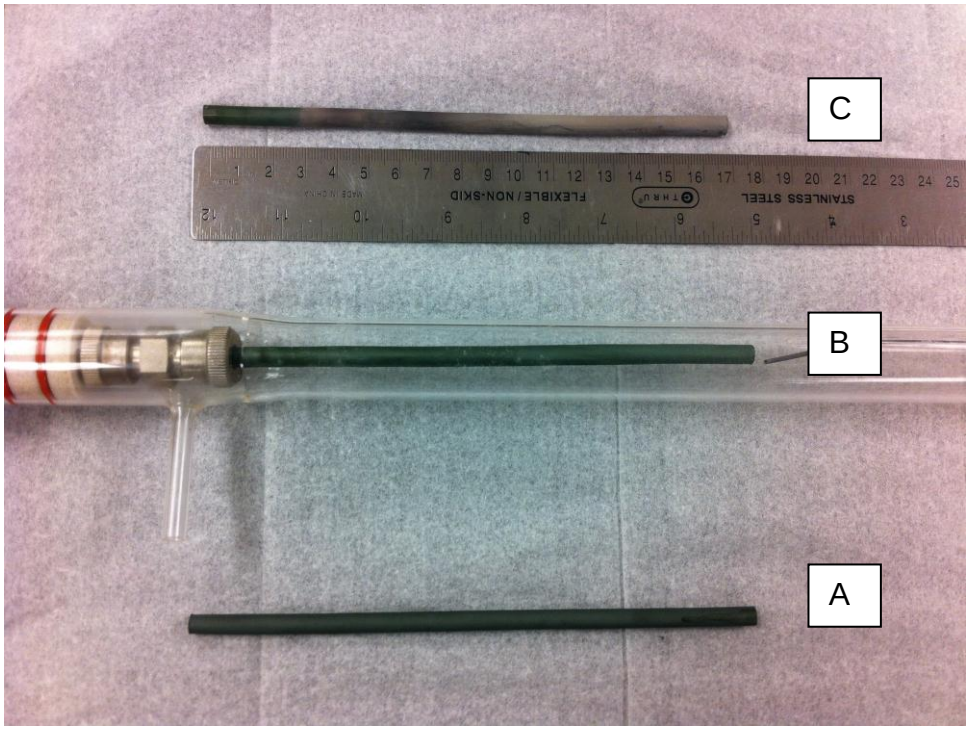

Figure 6-7. Membrane tubes Tested A) Sintered tube B) Tube inside reactor C) Tube after heat treatment (grey area). Photo courtesy of Elango Balu.

Figure 6-8. Membrane tube exposed to WGS conditons Photo courtesy of Elango Balu.

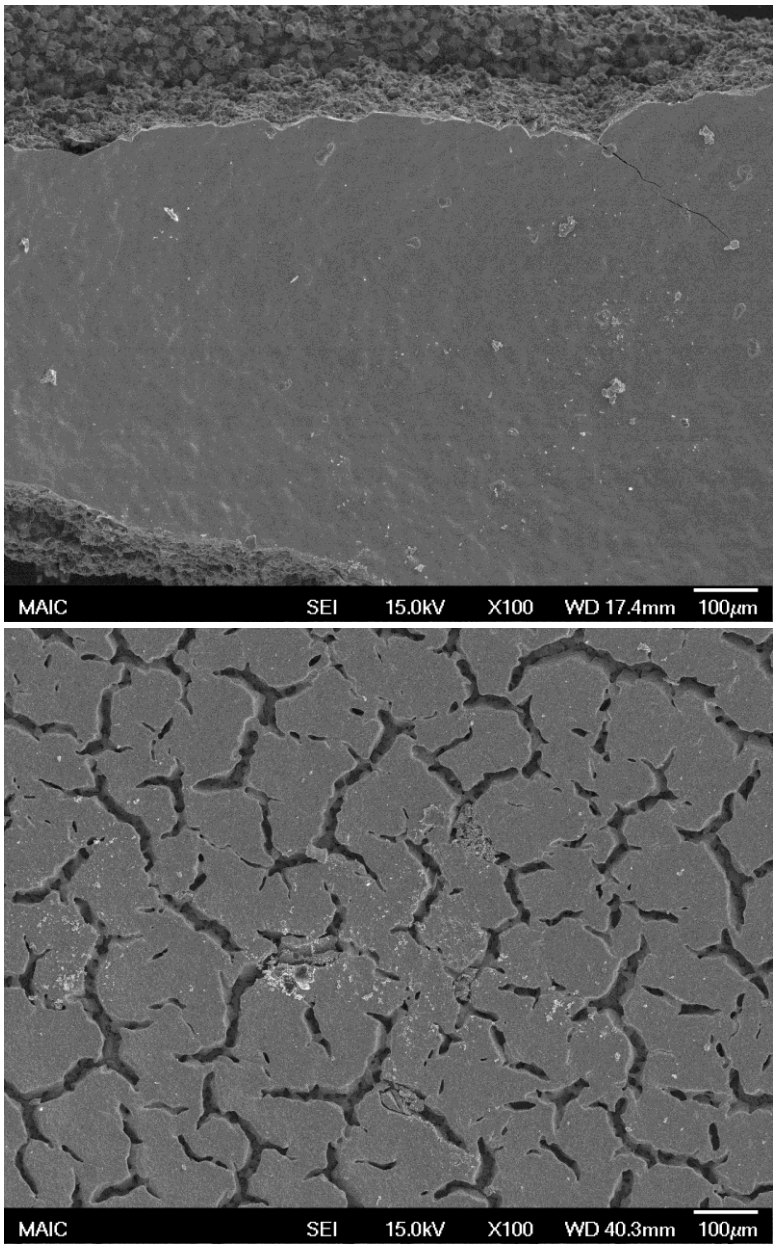

Figure 6-9. SEM Images of Tested Tubes A) Tube after sintering with membrane coat B) Exposed to WGS conditions

Figure 6-10. Setup with new bubbler with heating cartridge and temperature controller
Photo courtesy of Elango Balu

Figure 6-11. Modified bubbler design with heater cartridge down the middle and insulation jacket Photo courtesy of Elango Balu

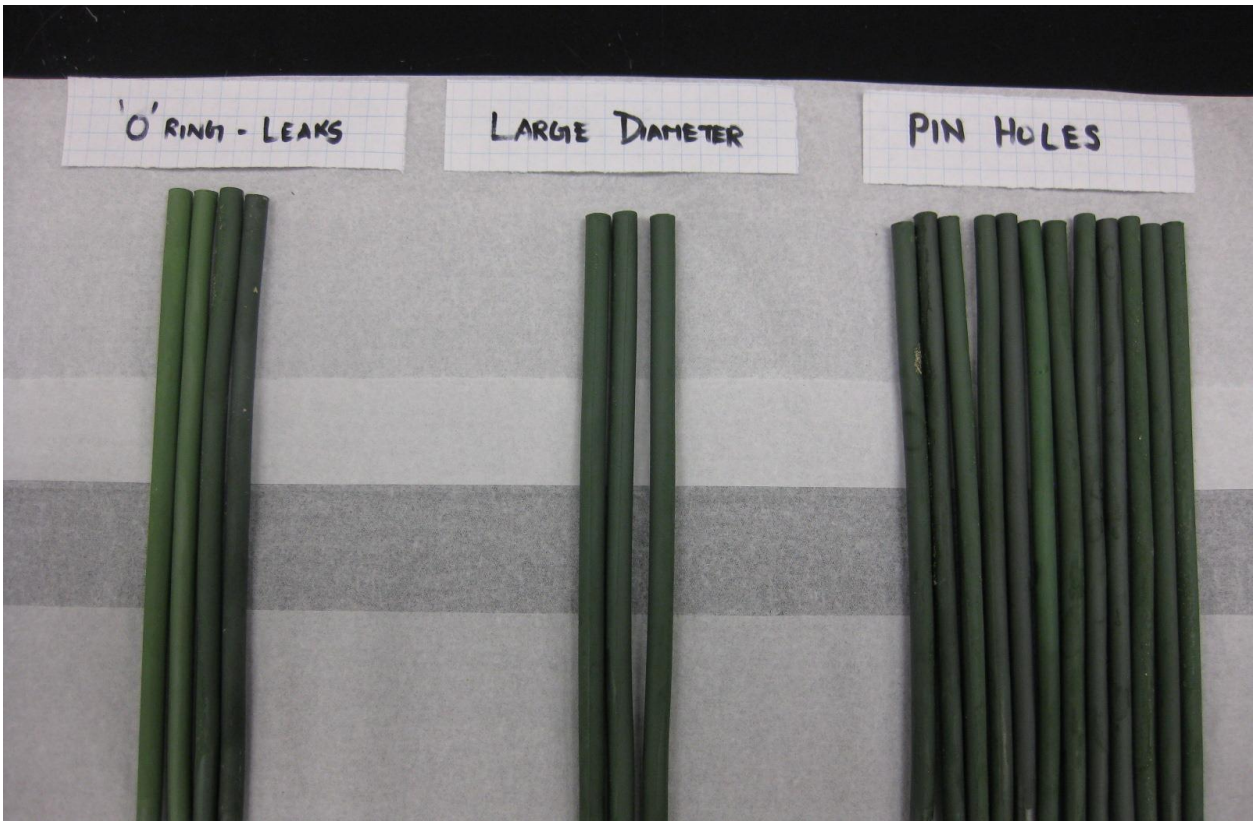

Figure 6-12. Sintered tubes tested for leaks and pinholes before being used for experiments Photo courtesy of Elango Balu

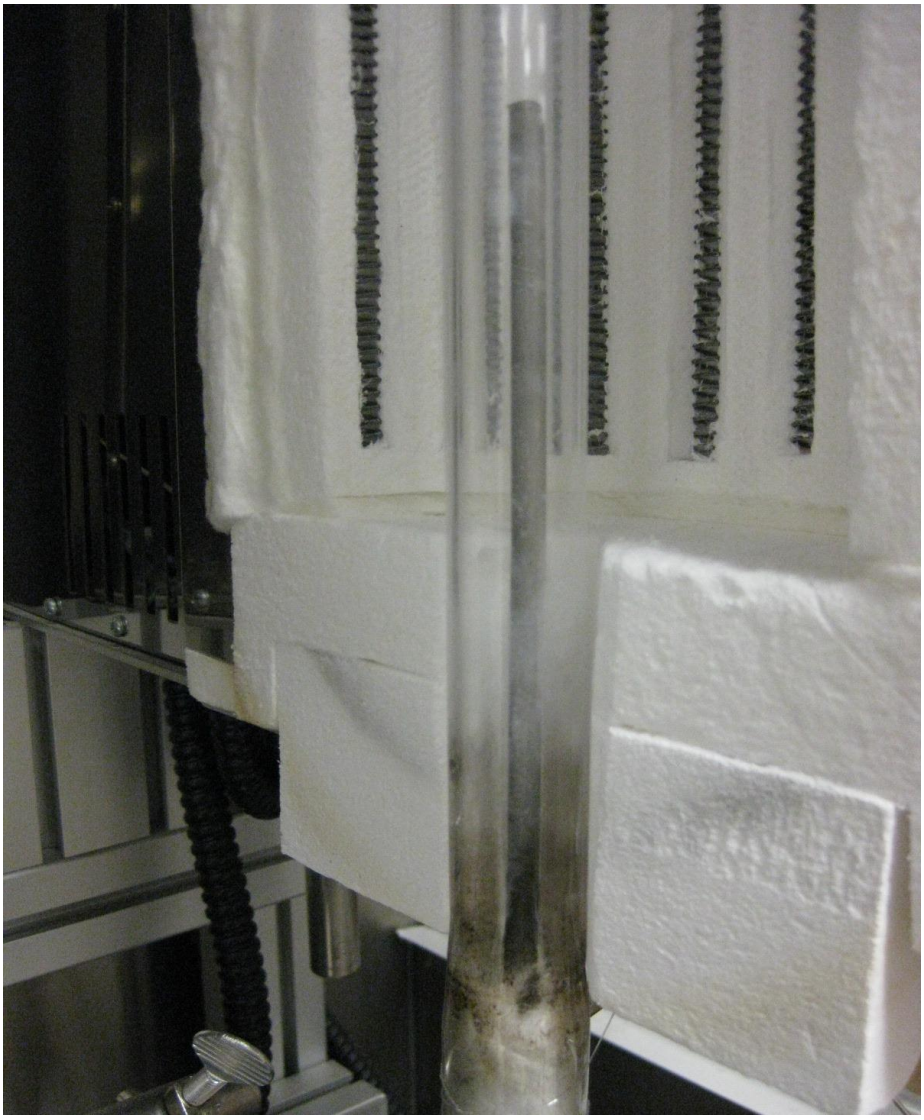

Figure 6-13. Tested tubes with no clear breakage at interface after using insulation inside Photo courtesy of Elango Balu

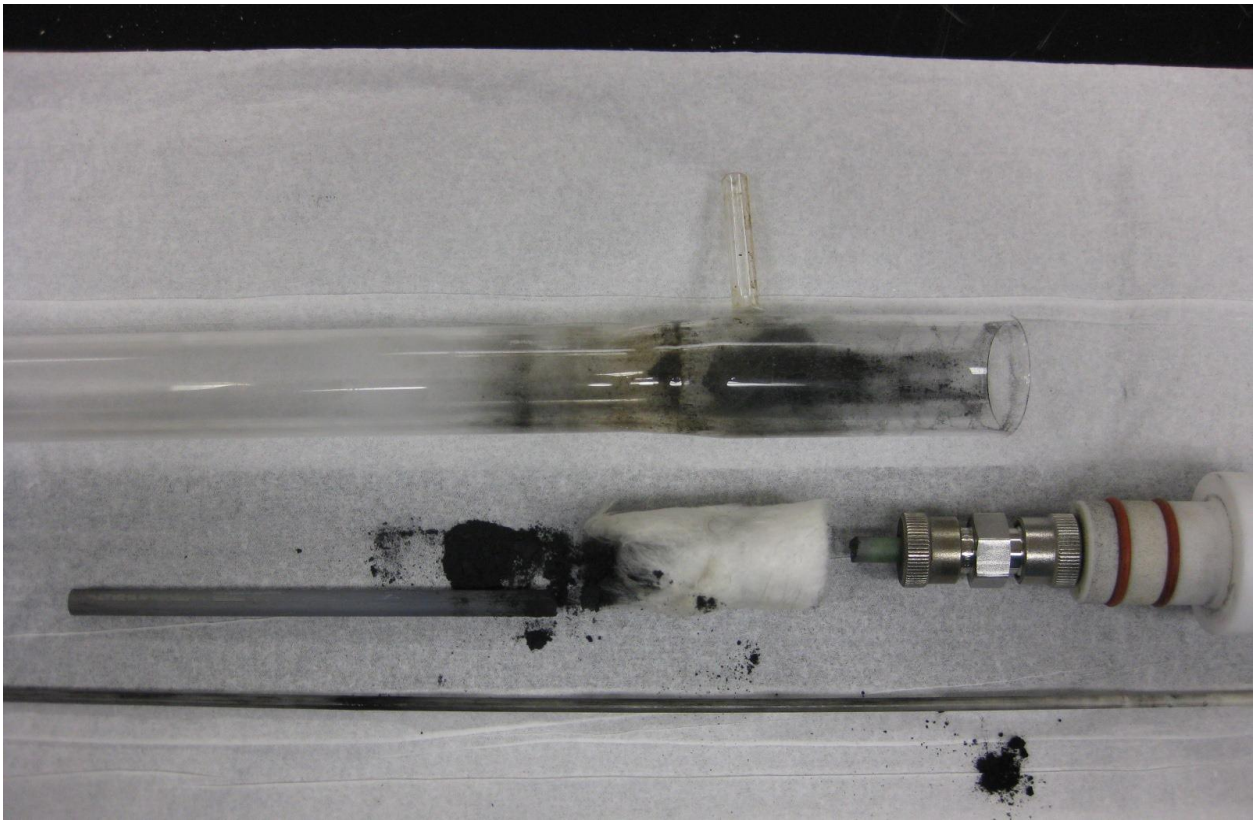

Figure 6-14. Tested tube with heavy carbon deposit at cold zone out of the heating coils after exposure to WGS atmosphere Photo courtesy of Elango Balu

Table 6-1. Permeated H_2 concentration vol% measured with mass spectrometer

Temperature(°C)	Antoine Eq	Experimental H2 permeation
22.3	2.63	0.8660±0.02
35	5.53	2.1008±0.04
38	6.52	2.6891±0.05
45	9.45	3.6610±0.07
55	15.53	2.8183±0.06

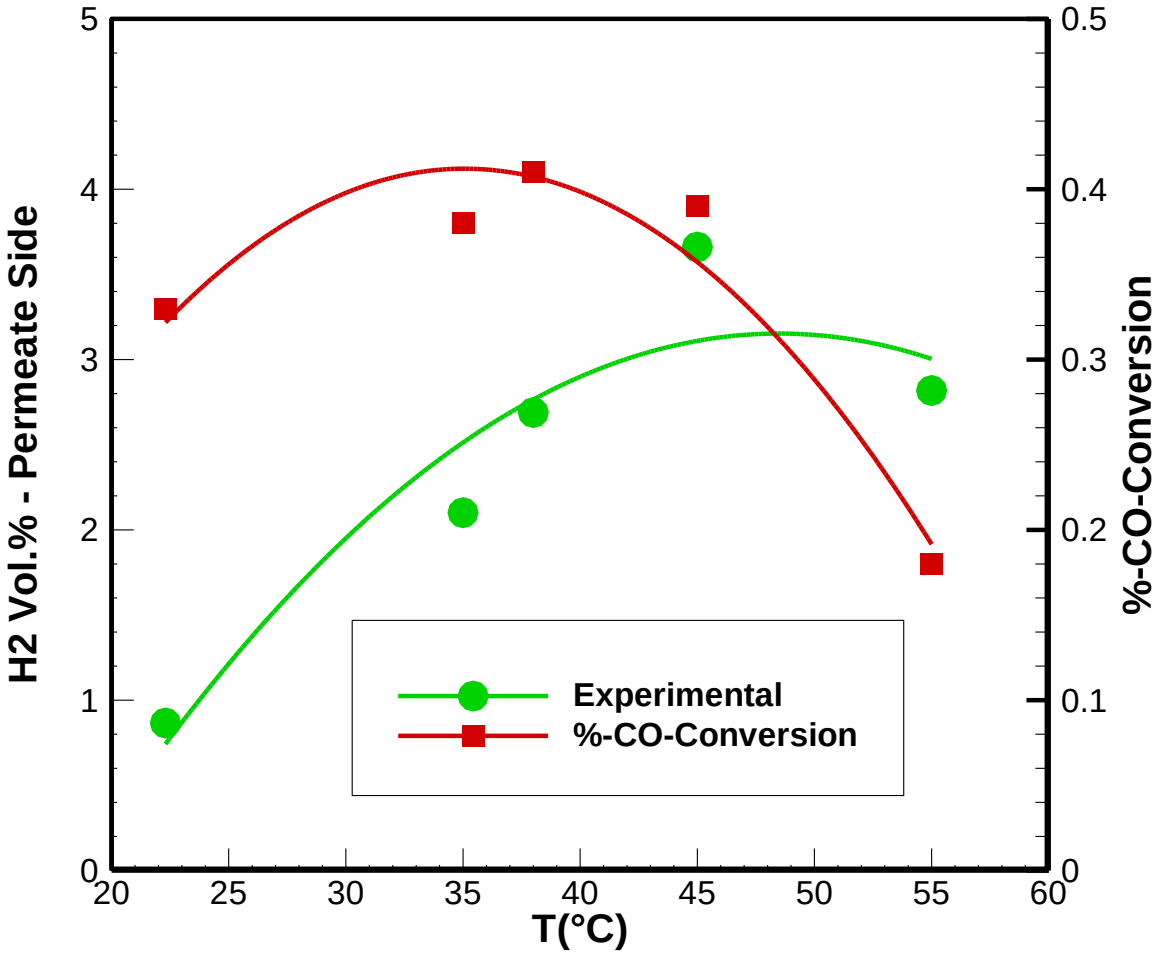

Figure 6-15. Conversion ratio calculated based on experimental data measured and Antoine equation.

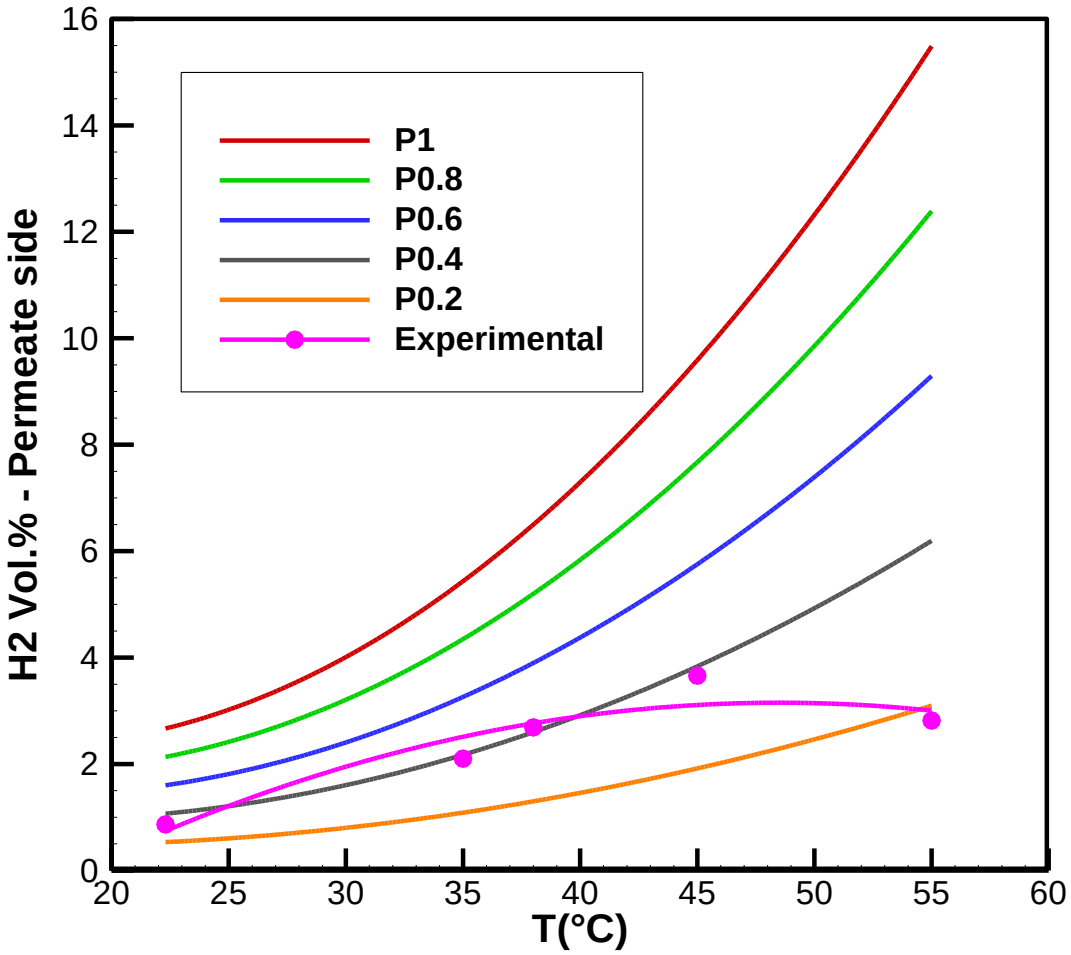

Figure 6-16. Experimental hydrogen concentration measured in comparison with different permeation factors at 100% WGS conversion. P1 = 100% permeation + 0% effluent stream, P0.8 = 80% permeation + 20 % effluent stream, P0.6 = 60% permeation + 40 % effluent stream, P0.4 = 40% permeation + 60 % effluent stream.

,

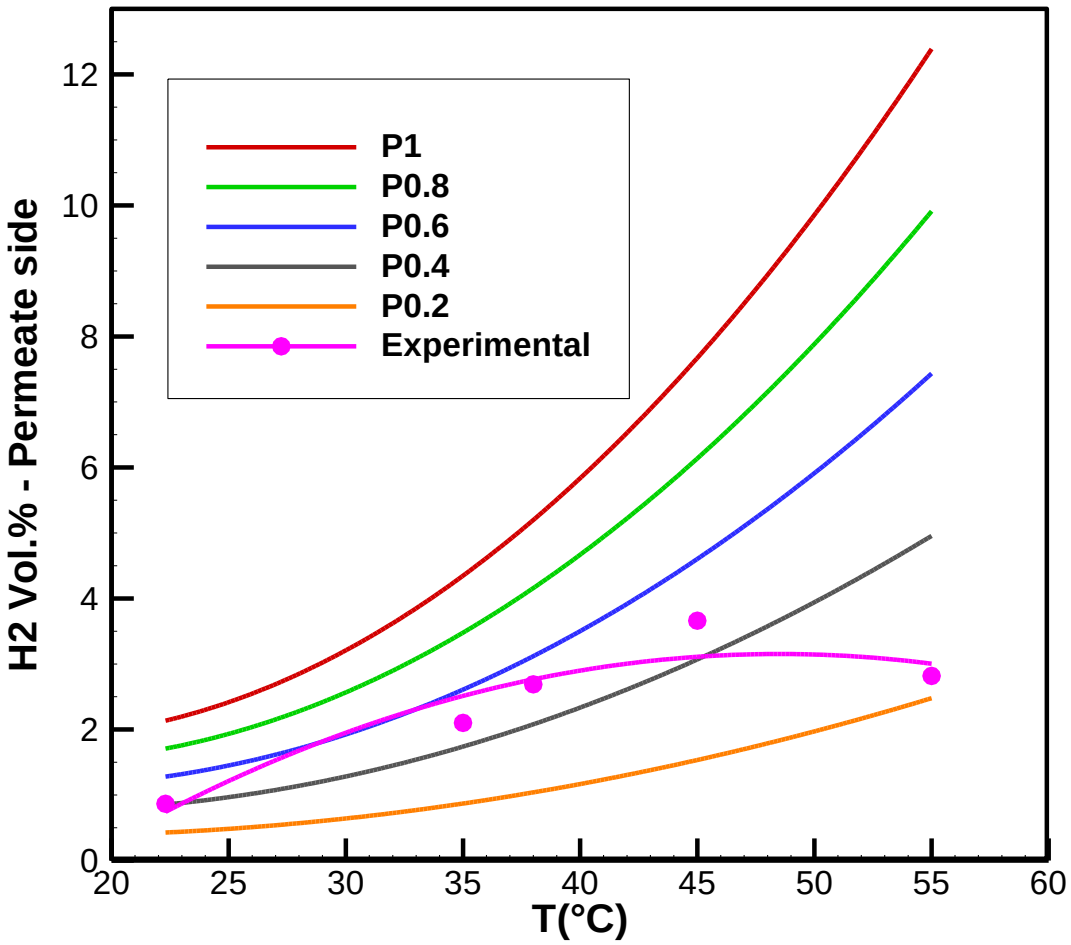

Figure 6-17. Experimental hydrogen concentration measured in comparison with different permeation factors at 80% WGS conversion. P1 = 100% permeation + 0% effluent stream, P0.8 = 80% permeation + 20 % effluent stream, P0.6 = 60% permeation + 40 % effluent stream, P0.4 = 40% permeation + 60 % effluent stream.

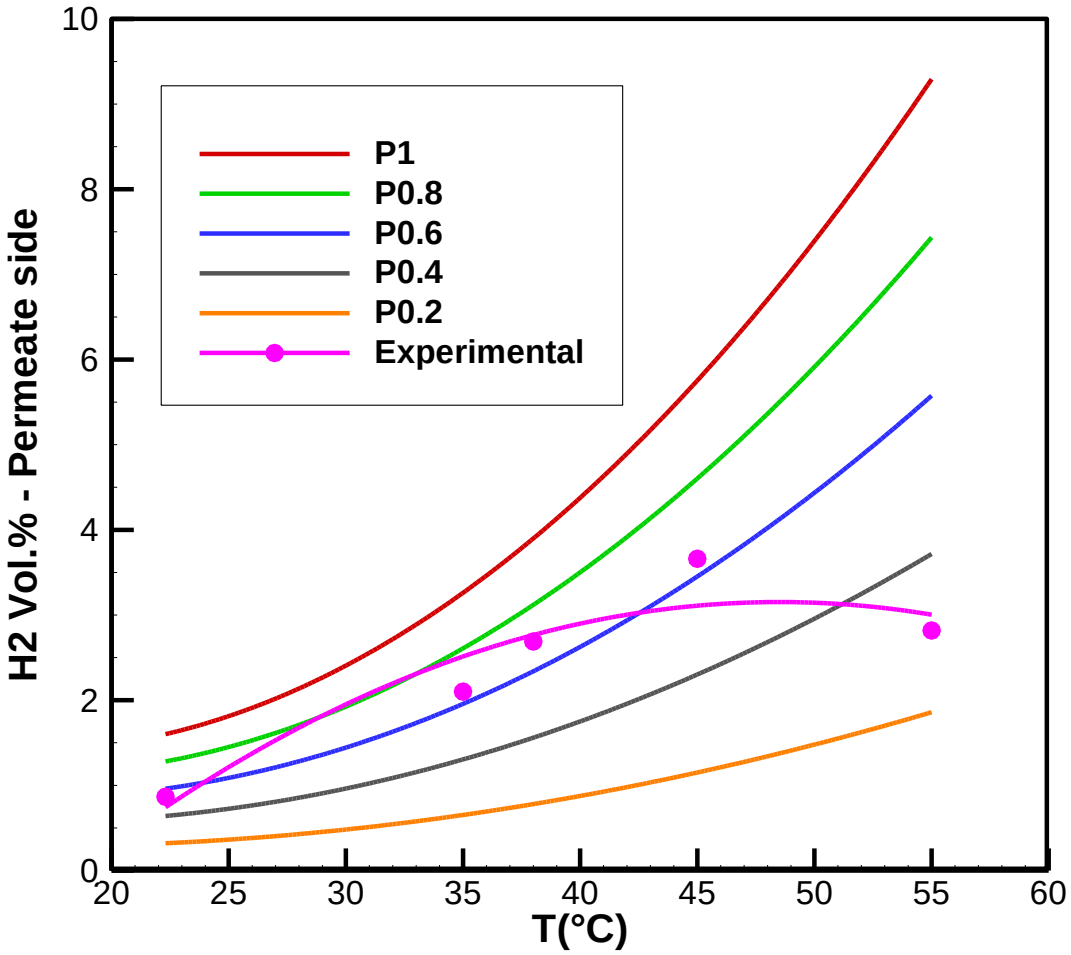

Figure 6-18. Experimental hydrogen concentration measured in comparison with different permeation factors at 60% WGS conversion. P1 = 100% permeation + 0% effluent stream, P0.8 = 80% permeation + 20 % effluent stream, P0.6 = 60% permeation + 40 % effluent stream, P0.4 = 40% permeation + 60 % effluent stream.

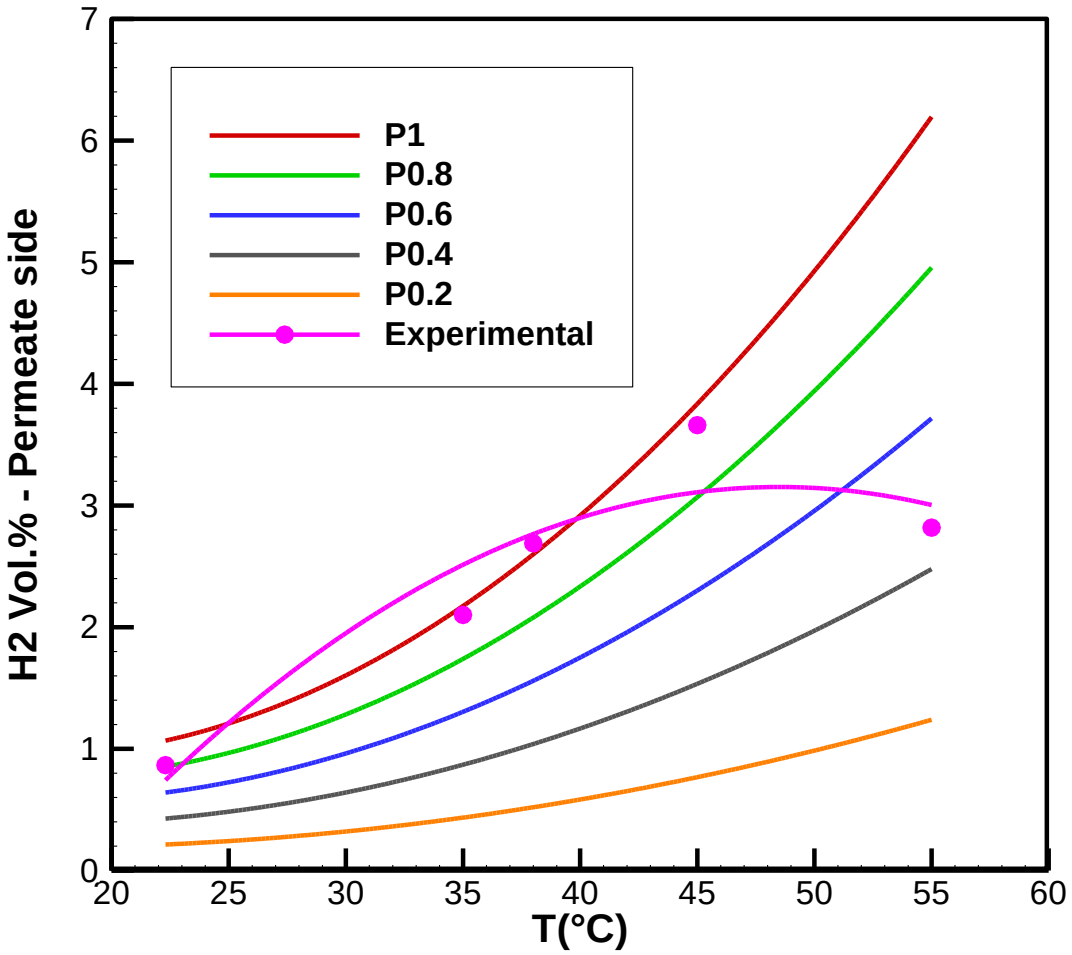

Figure 6-19. Experimental hydrogen concentration measured in comparison with different permeation factors at 40% WGS conversion. P1 = 100% permeation + 0% effluent stream, P0.8 = 80% permeation + 20 % effluent stream, P0.6 = 60% permeation + 40 % effluent stream, P0.4 = 40% permeation + 60 % effluent stream.

CHAPTER 7
CONCLUSIONS

Comprehensive testing and analysis were done using pilot scale and bench scale gasifier to study the potential of biomass as feedstock to provide sustainable product gas with calorific value high enough to run engine and the versatility of the gasifier was also established by using different types of feedstock based on the lignocellulosic structure and how the heating value could be a function of the species concentrations in the gasifier exit [62, 63, 64]. The methodology was to develop a consistent equilibrium model that could predict the product gas composition based on the operating temperature of the gasifier and also to validate the model by using the data collected during the experimental runs. Once this was done the model was also compared to other gasification models in the literature to further reinforce the consistency.

This helped establish the use of such downdraft gasifiers as standalone power generation units which could be essential at times of emergencies and they could also serve as distributed power sources located close to the feedstock rather than spending money and energy on transportation of the feedstock.

Further the steam gasification was also studied in detail and this time all the gas species were analyzed using gas chromatograph (GC) and the experimental results matches well with the equilibrium model. Model was used to predict the gas composition at higher temperatures that could not be replicated in laboratory conditions due to material limitations and time constraint. The goal was to show that the use of steam as a gasifying medium increases the calorific value of the exit syngas and as expected the value does go up by 2 to 3 times due to the absence of Nitrogen in the gasifier which dilutes the concentration and lowers the heating value in a traditional air gasification

system. Based on these test results, the idea of using steam gasification process as a part of a larger more self-sustained power generation system was envisioned and it was also coupled with the advancements in the membrane technology to further enhance the amount of hydrogen that is available for energy production.

To develop such a system there are immense challenges that has to be overcome so to work towards that goal, one aspect of this novel system which is the newly developed proton conducting membrane by FISE was tested under conditions replicating the gasifiers, to see if they could be incorporated in real world applications to enhance the hydrogen content and also to serve as a filter to produce pure hydrogen stream.

The process of successfully replicating the fabrication techniques used for developing the support tubes and membrane were hampered by several factors like base ingredients, furnace temperatures, particle sizes etc., preliminary results show that this mixed proton electron conducting membranes have a huge potential to augment the output of the gasifiers by utilizing the heat and steam concentration available in the exit gas.

Test results clearly show the capability of these membranes to facilitate the WGS reaction and produce more hydrogen by converting the available CO [59]. Though the conversion rates are not as high as expected, it could be attributed to the fact that the available surface area for reaction was reduced due to the limitations of the fittings and the partial pressure of H_2O that could be attained using the new bubbler design because of temperature overshoot at higher temperatures and boiling effects that compromise the seals. Further the tubes lose integrity along the process of heat

treatment and also facilitate the movement of the tracer gases in small concentrations. This should also be addressed in the future work to make sure there are no developing cracks in the tubes after heat treatment that allows such gas transfers.

More focus is needed on this area of developing the membrane to specifically operate under syngas environment. As the results show that there is a lot of coking in the reactor which deteriorates the membrane performance over the course of time. The presence of tracer gas on the permeate side indicates that ,even though the WGS is successfully taking place on the surface there are still issues with the stability of the membrane layer coated on the support structure. Further tests should be done using the membrane in the presence of syngas composition which already has significant amount of CO_2 in the stream and how that would affect the integrity of the tube and also the concentration of H_2 in the feed stream apart from the hydrogen produced during WGS. It would also be efficient to measure the gas composition of the effluent gas with another GC to provide a complete picture with respect to the total hydrogen in the gas exit (Permeate + effluent).

The original recipe has to be modified to suit the high concentration of water vapour concentration and partial pressure and also to account for the change in viscosity and particle size of the ingredients. And a further detailed study should be done to determine the right sintering temperature for the tubes to minimize warping and extreme stresses resulting in failure of the tubes through pinholes near the end caps and gaps between the layers.

Based on the promising results obtained from testing the membrane tubes the concept system was developed by assuming the membrane reactor to be fully

functional and with no short comings, to showcase huge potential of such systems by integrating the gasification and membrane separation technology in the future. The results from one such concept system is presented in this section to offer a peek in to the upside of this concept system.

The concept system includes the use of high-temperature steam as both the heat source and the gasification agent in an oxygen-starved (air free) environment [65, 66, 67].

Two cases as explained in previous chapter were run using this concept system to highlight the different path that could be chosen based on the requirements and they model results are presented below.

As shown in the Table 7-1 and Table 7-2 below, theoretically, the gasifier can reach more than 70% efficiency and the overall system efficiency ranges between 64% and 74% depending on the route chosen, either Hydrogen output or liquid fuel production. This is based on 100% conversion efficiency of the membrane reactor, but now that there is experimental data from the membrane reactor the same model was run at different conversion efficiency to see how this affects the overall efficiency of the system. Fig 7-2 clearly indicates the importance of the membrane reactor in determining the overall system efficiency, and at the current 40% rate it is not very feasible to have this system at expected level of operation, even with a multitude of simplifications and assumptions included in the model and the drop in efficiency of the overall system for both case with respect to the drop in membrane reactor efficiency is listed in Table 7-3. As it can be seen clearly that there is still a lot of improvements needed in the membrane reactor component to make this concept system a viable option. The drop in

efficiency of the reactor has been discussed in the previous chapter. In this section the various issues that need to be addressed to build a functional system with the proposed concept would be laid out in brief.

As it can be seen from the experimental results from testing the membrane reactor there is significant amount of carbon deposition near the lower end of the tube. This is because of the fact that the reactor currently designed and used is not able to place the whole membrane inside the heating coils because of the limitations of material properties. The Teflon cap at the ends of the reactor and the O-ring in the ultra torr cannot withstand high temperature. If this concept system is to be developed as a functional system, the issues with this high temperature seals must be addressed and also experiments should be run by placing the whole tube n the hot zone to provide more surface area for WGS. This would also help in avoiding the issues with cracks at the hot/cold zone interface since the whole tube is at uniform temperature. Also new recipes should be developed to fabricate tubes that can cope well with the syngas atmosphere, since the syngas inherently has CO_2 in it produced during the gasification process and additional CO_2 will also be produced from the WGS reaction occurring in the membrane reactor. This could deteriorate the performance of the membrane because of the stability issues of proton conducting materials in the presence of CO_2.

Further, alternative methods to sweep the permeated hydrogen from the tube inside must be developed and tested. As it is not feasible to use any inert gas on a regular basis and also further complicates the separation of pure hydrogen from this mixture once it is permeated. The possibility of using steam itself as a sweep gas sounds interesting as it would be easier to condense the steam and separate the pure

hydrogen once it is swept out. But this idea has to be tested to identify the operational constraints.

Finally, modules of stacked tubes should be tested to make sure that this technology is scalable to suit the high power generation systems. Since large gasifiers produce syngas at a very high flow rate and there must be enough surface area available for the gases to adsorb to, this can be done only by either making a large tube (issues with mechanical stability) or stacking up a lot of smaller tubes in bundle (issues with fittings/seals)connected to a common sweep inlet.

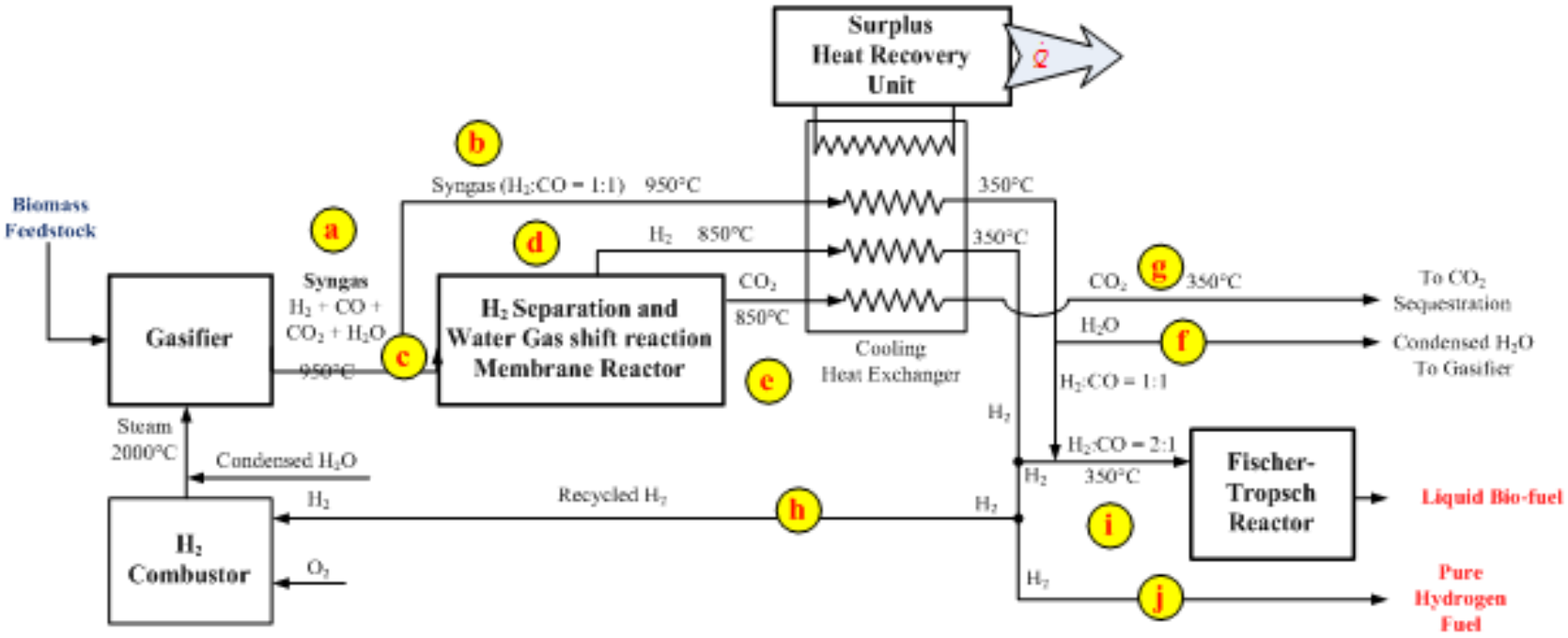

Figure 7-1. Schematic of a concept system with alternate path lines

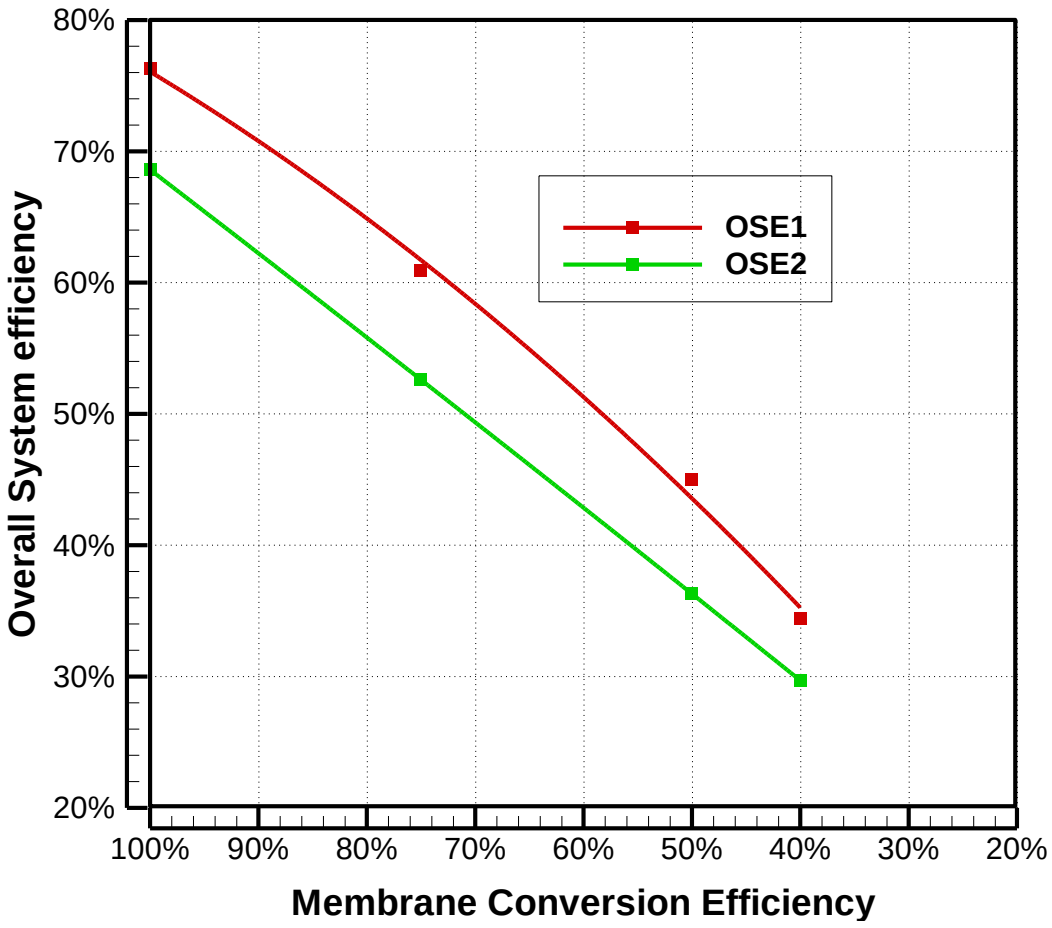

Figure 7-2. Effect of membrane reactor on overall system efficiency.

Table 7-1. Case1 with liquid fuel production only

Case 1	Supply / production rate (Kg/hr)	Gasifier efficiency	Overall system efficiency
Feedstock input	100		
Steam input	223		
Liquid fuel output	15.6	73%	64.40%
H_2 gas output	0		
CO_2 output	146		

Table 7-2. Case2 with hydrogen production only

Case 2	Supply / production rate (Kg/hr)	Gasifier efficiency	Overall system efficiency
Feedstock input	100		
Steam input	223		
Liquid fuel output	0	73%	72.10%
H_2 gas output	6.4		
CO_2 output	181.7		

Table 7-3. Effect of membrane reactor on overall system efficiency for both case 1 & 2

Membrane Conversion Efficiency %	Overall Efficiency C1	Overall Efficiency C2
100%	76.3%	68.6%
75%	60.9%	52.6%
50%	45%	36.3%
40%	34.4%	29.7%

LIST OF REFERENCES

[1] Huber GW. Breaking the chemical and engineering barriers to lignocellulosic biofuels: A research roadmap for making lignocellulosic biofuels a practical Reality, NSF, DOE and American Chemical Society Workshop 2007.

[2] Kırtay E. Recent advances in production of hydrogen from biomass. Energy Conversion and Management 2011;52:1778-89.

[3] Corradetti A, Desideri U. Should Biomass be Used for Power Generation or Hydrogen Production? J Eng Gas Turbines Power 2007;129:629-36.

[4] Green AES, Sadrameli SM. Analytical representations of experimental polyethylene pyrolysis yields. J Anal Appl Pyrolysis 2004;72:329-35.

[5] Sheehan J, Camobreco V, Duffield J, Graboski M, Shapouri H. Life Cycle Inventory of Biodiesel and Petroleum Diesel for Use in an Urban Bus. 1998;SR-580-24089:314.

[6] Sousa-Aguiar E, Noronha FB, Faro J, Arnaldo. The main catalytic challenges in GTL (gas-to-liquids) processes. Catal Sci Technol 2011;1:698-713.

[7] Damartzis T, Zabaniotou A. Thermochemical conversion of biomass to second generation biofuels through integrated process design—A review. Renewable and Sustainable Energy Reviews 2011;15:366-78.

[8] Barreto L, Makihira A, Riahi K. The hydrogen economy in the 21st century: a sustainable development scenario. Int J Hydrogen Energy 2003;28:267-84.

[9] Muradov NZ, Veziroğlu TN. From hydrocarbon to hydrogen–carbon to hydrogen economy. Int J Hydrogen Energy 2005;30:225-37.

[10] Tosti S. Supported and laminated Pd-based metallic membranes. Int J Hydrogen Energy 2003;28:1445-54.

[11] Carrara S. Small-scale biomass power generation. 2010.

[12] McKendry P. Energy production from biomass (part 3): gasification technologies. Bioresour Technol 2002;83:55-63.

[13] Higman C, Burgt , Maarten van der. Gasification. 2nd ed: Gulf Professional Publishing; 2008.

[14] Smoot LD, Smith PJ. Coal combustion and gasification. New York: Plenum Press, 1985.

[15] Bridgwater AV. The technical and economic feasibility of biomass gasification for power generation. Fuel 1995;74:631-53.

[16] Ruan R, Chen P, Hemmingsen R, Morey V, Tiffany D. Size matters: small distributed biomass energy production systems for economic viability, Int. J. Agric. & Biol. Eng 2008;1: 164－68

[17] Zainal ZA, Ali R, Lean CH, Seetharamu KN. Prediction of performance of a downdraft gasifier using equilibrium modeling for different biomass materials. Energy Conversion and Management 2001;42:1499-515.

[18] Zainal ZA, Rifau A, Quadir GA, Seetharamu KN. Experimental investigation of a downdraft biomass gasifier. Biomass Bioenergy 2002;23:283-9.

[19] Gautam G, Adhikari S, Bhavnani S. Estimation of Biomass Synthesis Gas Composition using Equilibrium Modeling. Energy Fuels 2010;24:2692-8.

[20] Jayah TH, Aye L, Fuller RJ, Stewart DF. Computer simulation of a downdraft wood gasifier for tea drying. Biomass Bioenergy 2003;25:459-69.

[21] Karmakar MK, Datta AB. Generation of hydrogen rich gas through fluidized bed gasification of biomass. Bioresour Technol 2011;102:1907-13

[22] Umeki K, Yamamoto K, Namioka T, Yoshikawa K. High temperature steam-only gasification of woody biomass. Appl Energy 2010;87:791-8.

[23] Umeki K, Namioka T, Yoshikawa K. Analysis of an updraft biomass gasifier with high temperature steam using a numerical model. Appl Energy 2012;90:38-45.

[24] Baratieri M, Baggio P, Fiori L, Grigiante M. Biomass as an energy source: Thermodynamic constraints on the performance of the conversion process. Bioresour Technol 2008;99:7063-73.

[25] Chang ACC, Chang H, Lin F, Lin K, Chen C. Biomass gasification for hydrogen production. Int J Hydrogen Energy 2011;36:14252-60.

[26] Olgun H, Ozdogan S, Yinesor G. Results with a bench scale downdraft biomass gasifier for agricultural and forestry residues. Biomass & Bioenergy 2011; 35: 572-80.

[27a] Sharma AK. Experimental study on 75 KW(th) downdraft (biomass) gasifier system. Renewable Energy 2009; 34: 1726-33.

[27b] Sharma AK. Experimental investigations on a 20 kWe, solid biomass gasification system. Biomass & Bioenergy 2011; 35: 421-8.

[28] Huang Y, Wang YD, Rezvani S, McIlveen-Wright DR, Anderson M, Hewitt NJ. Biomass fuelled trigeneration system in selected buildings. Energy Conversion and Management 2011; 52: 2448-54.

[29] Coronado CR, Yoshioka JT, Silveira JL. Electricity, hot water and cold water production from biomass. Energetic and economical analysis of the compact system of cogeneration run with woodgas from a small downdraft gasifier. Renewable Energy 2011; 36: 1861-8.

[30] Zabaniotou AA, Skoulou VK, Mertzis DP, Koufodimos GS, Samaras ZC. Mobile Gasification Units for Sustainable Electricity Production in Rural Areas: The SMARt-CHP Project. Ind Eng Chem Res 2011; 50: 602-8.

[31] Centeno F, Mahkamov K, Silva Lora EE, Andrade RV. Theoretical and experimental investigations of a downdraft biomass gasifier-spark ignition engine power system. Renewable Energy 2012; 37: 97-108.

[32] Mustafi NN, Miraglia YC, Raine RR, Bansal PK, Elder ST. Spark-ignition engine performance with 'Powergas' fuel (mixture of CO/H-2): A comparison with gasoline and natural gas. Fuel 2006; 85: 1605-12.

[33] Sahoo BB, Saha UK, Sahoo N. Theoretical performance limits of a syngas-diesel fueled compression ignition engine from second law analysis. Energy 2011; 36: 760-9.

[34] Lin JM. Combination of a biomass fired updraft gasifier and a stirling engine for power production. Journal of Energy Resources Technology-Transactions of the Asme 2007; 129: 66-70.

[35] Shah A, Srinivasan R, To SDF, Columbus EP. Performance and emissions of a spark-ignited engine driven generator on biomass based syngas. Bioresour Technol 2010; 101: 4656-61.

[36] Kluiters SCA. Status review on membrane systems for hydrogen separation. 2004;ECN-C--04-102.

[37] Scherban T, Nowick AS. Bulk protonic conduction in Yb-doped SrCeO3. Solid State Ionics 1989;35:189-94.

[38] Bonanos N. Transport properties and conduction mechanism in high-temperature protonic conductors. Solid State Ionics 1992;53–56, Part 2:967-74.

[39] Kreuer KD. Proton-Conducting Oxides-Annual Review of Materials Research. 2003;33:333-59.

[40] Iwahara H, Mori T, Hibino T. Electrochemical studies on ionic conduction in Ca-doped BaCeO3. Solid State Ionics 1995;79:177-82.

[41] Bonanos N. Transport properties and conduction mechanism in high-temperature protonic conductors. Solid State Ionics 1992; 53–56, Part 2: 967-74.

[42] Kuzmin AV, Gorelov VP, Melekh BT, Glerup M, Poulsen FW. Phase transitions in undoped BaCeO3. Solid State Ionics 2003;162–163:13-22.

[43] Ranlov J, Nielsen K. Crystal structure of the high-temperature protonic conductor SrCeO3. J Mater Chem 1994;4:867-8.

[44] Phair JW, Badwal SPS. Review of proton conductors for hydrogen separation Ionics 2006; 2006;12:103.

[45] Kreuer K, Rabenau A, Weppner W Vehicle Mechanism. A New Model for the Interpretation of the Conductivity of Fast Proton Conductors. Angewandte Chemie International Edition in English 1982;21:208-9.

[46] Liang KC, Du Y, Nowick AS. Fast high-temperature proton transport in nonstoichiometric mixed perovskites. Solid State Ionics 1994;69:117-20.

[47] Matsushita E, Tanase. A Theoretical approach for protonic conduction in perovskite-oxide ceramics. Solid State Ionics 1997;97:45-50.

[48] Reed TB, Das. A Handbook of Biomass Downdraft Gasifier Engine Systems. 1998;SERI/SP-271-3022.

[49] Lv P, Yuan Z, Ma L, Wu C, Chen Y, Zhu J. Hydrogen-rich gas production from biomass air and oxygen/steam gasification in a downdraft gasifier. Renewable Energy 2007;32:2173-85.

[50] NIST Chemistry WebBook. http://webbook.nist.gov/chemistry/.

[51] Mountouris A, Voutsas E, Tassios D. Solid waste plasma gasification: Equilibrium model development and exergy analysis. Energy Conversion and Management 2006;47:1723-37.

[52] Morley C GasEq. Chemical equilibria in perfect gases. Version 0.78,2005 www.gaseq.co.uk.

[53] Sandler SI ChemEq. Equilibrium model, In: Chemical and Engineering Thermodynamics,1999,3rd edition. John Wiley and Sons.

[54] Altafini, C.R., Wander, P.R., Barreto, R.M., 2003. Prediction of the working parameters of a wood waste gasifier through an equilibrium model, Energy Conversion and Management. 44, 2763-2777

[55] Yaws CL Chemical Properties Handbook. 1999.

[56] Daniel Martinez J, Mahkamov K, Andrade RV, Silva Lora EE. Syngas production in downdraft biomass gasifiers and its application using internal combustion engines. Renewable Energy 2012; 38: 1-9.

[57] Henriksen U, Ahrenfeldt J, Jensen T, Gobel B, Bentzen J, Hindsgaul C, et al. The design, construction and operation of a 75 kW two-stage gasifier. Energy 2006; 31: 1542-53.

[58] Balu E, Chung JN. System characteristics and performance evaluation of a trailer-scale downdraft gasifier with different feedstock. Bioresour Technol 2012; 108: 264-73.

[59] Jianlin Li . SrCeO3-based Protonic Conductors for Hydrogen Production and Separation by Water Gas Shift, Steam Reforming, and Carbon dioxide Reforming Reactions" ,PhD Thesis 2009.

[60] Lundgren E, Pettersson E. Combustion of horse manure for heat production, Bioresour Technology 2009. 100:3121–3126.

[61] Sorum L,Gronli MG, Hustad J.E. Pyrolysis characteristics and kinetics of municipal solid wastes. Fuel 80, 1217-1227.

[62] Demirbaş A. Calculation of higher heating values of biomass fuels. Fuel 1997; 76: 431-4.

[63] Friedl A, Padouvas E, Rotter H, Varmuza K. Prediction of heating values of biomass fuel from elemental composition. Anal Chim Acta 2005; 544: 191-8.

[64] Vassilev SV, Baxter D, Andersen LK, Vassileva CG. An overview of the chemical composition of biomass. Fuel 2010; 89: 913-33.

[65] Howaniec N, Smoliński A. Steam gasification of energy crops of high cultivation potential in Poland to hydrogen-rich gas. Int J Hydrogen Energy 2011; 36: 2038-43.

[66] Smoliński A, Stańczyk K, Howaniec N. Steam gasification of selected energy crops in a fixed bed reactor. Renewable Energy 2010; 35: 397-404.

[67] Kalinci Y, Hepbasli A, Dincer I. Biomass-based hydrogen production: A review and analysis. Int J Hydrogen Energy 2009; 34: 8799-817.

BIOGRAPHICAL SKETCH

Elango Balu was born in Trichy, India in 1986. Elango did his schooling at Trichy and graduated with a higher secondary certificate from K.A.P. Higher Secondary School. He attended the Sardar Vallabhbhai National Institute of Technology and graduated with a Bachelor of Technology degree in mechanical engineering in 2007. In fall 2007, he enrolled at University of Florida for his master's program. After finishing his M.S in the fall of 2008, he joined the biomass research group at the Department of Mechanical Engineering headed by Dr. Jacob Chung in spring 2009 and started working towards his PhD in the field of biomass gasification and hydrogen production using mixed proton electron conducting membranes developed by FISE.